PERGAMON

Progress in Energy and Combustion Science 25 (1999) 1–53

PROGRESS IN ENERGY AND COMBUSTION SCIENCE

Light scattering for particle characterization

A.R. Jones

Department Chemical Engineering, Imperial College, London SW7 2BY, U.K.

Abstract

Light scattering has proved to be one of the most powerful techniques for probing the properties of particulate systems. The purpose of this paper is to review the status of elastic light scattering. The emphasis is on recent developments, rather than being over-repetitive of earlier reviews, but considerable background is included with the aim of making the paper self-contained. There is an extensive summary of theoretical treatments, including both historical work and new. On the experimental side, while there is some discussion of well-tried methods, the emphasis is on recent techniques for measuring other properties as well as size. This includes, among others, the fractal treatment of agglomerates, determination of particle shape and measurement of refractive index. The discussion is broad rather than deep to provide a wide-ranging review of an extremely active field.

Contents

0360-1285/99/$ - see front matter
PII: S0360-1285(98)00017-3

Nomenclature

Roman letters

a_n	expansion coefficient in series for field
A	cross-sectional area (m^2)
$\tilde{A}(\theta, \phi)$	dimensionless vector amplitude
b_n	expansion coefficient in series for field
c	speed of light ($m\,s^{-1}$); mass concentration ($kg\,m^{-3}$)
C	cross-section (m^2)
D	diameter (m)
D_f	diffusion coefficient ($m^2\,s^{-1}$); fractal dimension
$\vec{E}$	vector electric field ($V\,m^{-1}$)
f_v	volume fraction
$F(\theta, \phi)$	dimensionless scattering function
$G(\vec{r}, \vec{r}')$	scalar Greens function
h	height of ray above axis (m)
$h_n^{(1)}$	spherical Hankel function of first kind of order n
H	affinity exponent
$H_n^{(1)}$	cylindrical Hankel function of first kind of order n
$\vec{H}$	vector magnetic field ($A\,m^{-1}$)
i	$\sqrt{-1}$
I	irradience ($W\,m^{-2}$)
I	identity tensor
$\Im$	intensity ($W\,m^{-2}\,ster^{-1}$)
Im	imaginary part
j_n	spherical Bessel function of order n
J_n	cylindrical Bessel function of order n
k	wavenumber ($2\pi/\lambda$) (m^{-1}); Boltzmann's constant ($J\,K^{-1}$)
K	coefficient (m^{-1}); Kubelka–Munk absorption coefficient (m^{-1})
K_f	premultiplier in fractal expression for agglomerate
l_{co}	cut-off of Gegenbauer spectrum
L	length (m)
m	refractive index
M_{ij}	element of Stokes matrix
M_2	second moment of size distribution
$n(D)$	number of particles per unit volume in elemental size interval dD (m^{-4})
$\hat{n}$	unit vector in the direction of n
N	number of particles per unit volume (m^{-3}); number of particles in fractal agglomerate
$p(\theta, \phi)$	normalized phase function
P	power (W)
$P_{sca,N}$	scattered power per unit volume ($W\,m^{-3}$)
q	scalar flux ($W\,m^{-2}$); $2k\sin(\theta/2)$ (m^{-1})
Q	efficiency
r_0	radius of individual sphere in agglomeration
$\vec{r}$	radial position
$\vec{r}'$	radial position at internal point
R	radius ($D/2$) (m)
R_1, R_2	Fresnel reflection coefficients
R_g	radius of gyration (m)
S	element of amplitude scattering matrix; Kubelka–Munk scattering coefficient (m^{-1})
$\vec{S}$	Poynting vector or radiative flux ($W\,m^{-2}$)
t	time (s)
T	temperature (K); transmissivity
T_n	Chebyshev polynomial
$[T]$	T matrix
u	particle velocity ($m\,s^{-1}$)
v	gas velocity ($m\,s^{-1}$)
V	volume (m^3); visibility
W	width (m)
W_0	beamwidth (m)
x	particle size parameter ($\pi D/\lambda$)

Greek letters

ε_0	permittivity of free space ($F\,m^{-1}$)
$\varepsilon(\vec{r})$	relative permittivity of particle
η	$\cos(\theta)$

θ	scattering angle
Θ_n	angular position of nth rainbow
λ	wavelength (m)
λ_f	fringe spacing (m)
μ	viscosity (N s m^{-2})
μ_0	permeability of free space (H m^{-1})
ν	frequency (s^{-1})
ξ	characteristic cluster size
ρ	density (kg m^{-3})
ρ_V, ρ_H	depolarization ratios
τ	turbidity (KL)
ϕ	azimuthal scattering angle; phase
ψ	scalar field
Ψ	shape factor
ω_0	albedo
Θ	solid angle (ster)

Subscripts

0	original or incident
abs	absorbed
ae	aerodynamic
diff	diffracted
eff	effective
ext	extinction
geom	geometrical optics
inc	incident
pr	radiation pressure
sca	scattered
t	transmitted
ve	volume equivalent

Superscript

*	complex conjugate

1. Introduction

In numerous cases there is the need to understand the nature of multi-phase systems. These occur in combustion, for example, whether particles are burning, being formed or are added as tracers. However, liquid drops and solid particles have practical implications in very many industrial and everyday situations.

In order to determine the properties of particulate systems and understand their behaviour it is necessary to acquire diagnostic tools. Paramount among these is electromagnetic radiation since it can be used remotely and, at the intensities normally used, does not interfere with the system under test. The advantages of visible wavelengths are not only that the radiation can be seen, but the wavelength is small (≈ 0.5 μm) yielding excellent resolving power.

When light interacts with a phase boundary a number of processes can occur, including reflection, refraction and diffraction. When the boundary encloses a discrete volume or when it has structure within itself, these processes are often lumped together under the title "scattering". Analysis of the scattered light reveals the properties of the structure.

The study of light scattering by small particles has a long and honourable history. The books by van de Hulst [1] and Kerker [2] are classical reviews of the subject. More recent general works include the paper by Jones [3] and the books by Bohren and Huffman [4] and Bayvel and Jones [5]. Laser-based techniques for industrial applications have recently been discussed by Black et al. [6] Instrumentation, with particular emphasis on combustion applications, was reviewed by Jones [7].

The purpose of this paper is to consider recent developments in the theoretical treatment of scattering and its use for particle characterization. The intention is to be general without being too repetitive of the earlier reviews. Thus, instrumentation is not discussed unless it has some particular novelty. However, while the aim is to emphasize recent work, an attempt is made to make the paper self-contained and it is hoped that sufficient background material is provided to make it understandable.

The review begins with a definition of the basic variables used in describing light scattering, and then moves on to general theoretical treatments. These are of two types: those which may be considered as "rigorous" in the sense that, in principle, they can be calculated to any desired accuracy and those which are approximate. The former includes both analytical and numerical techniques which are limited only by computer power. The latter covers a wide range of theories, each of which is valid only over a limited range of parameters but which provide easy means of calculation and much insight. The review of theoretical methods concludes with a discussion of multiple scattering which occurs in dense media.

Experimental methods for the measurement of particle properties are described in the second half of the paper. These cover techniques applied both to clouds of particles and to individual particles to measure parameters as diverse as size, concentration, refractive index, shape, structure and velocity.

2. Basic definitions of scattering variables

2.1. Individual particles

When light is incident on a particle two processes can occur: it can be deflected or absorbed. For particles that are large compared with the wavelength of the radiation, the deflection processes are commonly described by reflection, refraction and diffraction, though these will not describe certain phenomena such as the glory which arises from waves in the surface of the particle. For particles that are of the order of the wavelength in size or smaller, we cannot distinguish these processes and can only refer to "scattering". However, in general we group all the

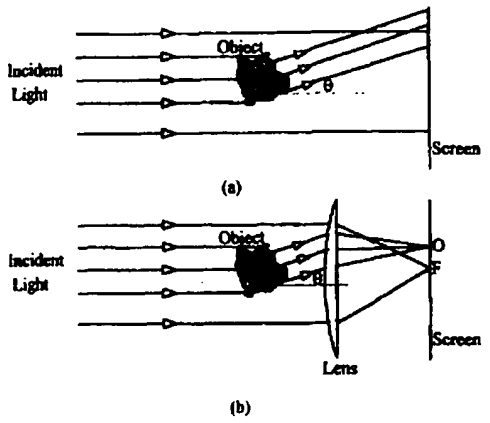

Fig. 1. Diffraction by an object: (a) Fresnel diffraction; (b) Fraunhofer diffraction.

deflection phenomena and absorption under the heading of scattering.

Diffraction and scattering are often used synonymously and it is worth spending a little time to show how they differ and to what extent they are the same. We recognize that diffraction is usually divided into two classes, as indicated in Fig. 1. The first, as in Fig. 1(a), is Fresnel or "near-field" diffraction. In this scattered light interferes at the observation plane with that unscattered. Clearly, the scattered and diffracted light patterns are not the same.

In the second, the observation screen is moved to a distance far from the scatterer—ideally to infinity. This is Fraunhofer or "far-field" diffraction as illustrated in Fig. 1(b). Since parallel lines meet at infinity, the situation can be simulated by observation in the focal plane of a lens. Here the incident light is focused to a spot at F, whereas the light scattered through some angle θ is focused at some other point such as O. The scattered and incident light waves are quite separate and do not interfere with each other. It follows that the diffracted and scattered light patterns are identical.

Thus in the case of Fraunhofer diffraction the difference is only one of terminology. However, "diffraction" is usually used for an approximation valid for large particles in which a scalar wave interacts with their cross-section. The term "scattering" is reserved for vector wave interaction with the body of a particle.

We now consider a single particle illuminated by radiation with irradience (incident intensity) I_0 (W m^{-2}). In all that follows we shall assume that the incident radiation has the form of an infinite plane wave. Practically this implies that the amplitude and phase must be sensibly constant across the particle. Certain of the results, such as the optical theorem (see below), can become invalid for shaped beams when the particle size is a significant fraction of the beam-width. This is an important aspect of the Gaussian output from lasers, for example.

The total scattered power P_{sca} is proportional to I_0, the constant having the dimensions of area, i.e.

$$P_{sca} = C_{sca} I_0$$

where C_{sca} is the scattering cross-section. Similarly, for absorption

$$P_{abs} = C_{abs} I_0$$

C_{abs} being the absorption cross-section. Both of these processes remove power from the incident radiation, and their combined effect is extinction. The power extinguished is

$$P_{ext} = P_{sca} + P_{abs}$$

and

$$C_{ext} = C_{sca} + C_{abs}$$

is the extinction cross-section.

The power incident on the particle is

$$P_{inc} = A I_0$$

where A is the cross-sectional area. The ratio of scattered to incident power is

$$\frac{P_{sca}}{P_{inc}} = \frac{C_{sca}}{A} = Q_{sca}$$

where Q_{sca} is the scattering efficiency. It follows that

$$Q_{ext} = Q_{sca} + Q_{abs}$$

The light scattered by a particle diverges over the surface of a sphere and its propagation must satisfy the wave equation in spherical coordinates. In free space far from the particle the scattered electric field has the form of an outgoing spherical wave with an angular modulation. We write

$$\vec{E}_{sca} = \frac{e^{ik_0 r}}{k_0 r} E_0 \vec{A}(\theta, \phi)$$

Since the field must remain transverse to the direction of propagation, which in this case is $\hat{r}$, $\vec{E}_{sca}$ can only have terms in A_θ and A_ϕ. Thus

$$\vec{E} = E_\theta \hat{\theta} + E_\phi \hat{\phi}$$

From Maxwell's equations it can be shown that the magnetic field is

$$\vec{H} = -\left(\frac{\varepsilon_0}{\mu_0}\right)^{1/2} \left(E_\phi \hat{\theta} - E_\theta \hat{\phi}\right)$$

The Poynting vector, which determines the energy flux in the wave, is

$$\vec{S} = \frac{1}{2} \mathrm{Re}\left(\vec{E} \times \vec{H}^*\right)$$

which becomes

$$\vec{S}_{sca} = \frac{1}{2}\left(\frac{\varepsilon_0}{\mu_0}\right)^{1/2} \frac{E_0^2}{k_0^2 r^2} \left|\vec{A}(\theta, \phi)\right|^2 \hat{r} = \frac{I_0}{k_0^2 r^2} F(\theta, \phi) \hat{r}$$

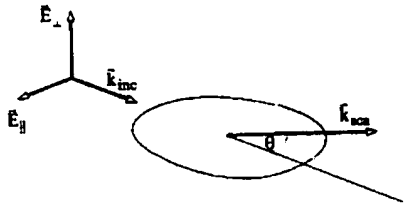

Fig. 2. Polarization states relative to the scattering plane.

where $F(\theta,\phi) = |\vec{A}(\theta,\phi)|^2$ is the dimensionless scattering function. Since $\hat{r}\cdot\hat{r} = 1$, the scattered power is given by integration over a sphere at radius r as

$$P_{sca} = \frac{I_0}{k_0^2}\int_0^{2\pi}\int_0^{\pi} F(\theta,\phi)\sin\theta\,d\theta\,d\phi$$

and the scattering cross-section is

$$C_{sca} = \frac{1}{k_0^2}\int_0^{2\pi}\int_0^{\pi} F(\theta,\phi)\sin\theta\,d\theta\,d\phi$$

We note that

$$\mathfrak{I}_{sca} = \frac{I_0}{k_0^2 r^2}F(\theta,\phi)$$

is the scattered intensity (W m^{-2} ster^{-1}).

If the scattering is isotropic, in the sense that it is independent of angle, then

$$C_{sca} = \frac{4\pi F}{k_0^2}$$

Using this we define the normalized scattering function, or phase function, by

$$p(\theta,\phi) = \frac{4\pi F(\theta,\phi)}{k_0^2 C_{sca}}$$

so that

$$\frac{1}{4\pi}\int_0^{2\pi}\int_0^{\pi} p(\theta,\phi)\sin\theta\,d\theta\,d\phi = 1$$

The extinction cross-section is obtained from the optical theorem [1, 2]

$$C_{ext} = \frac{4\pi}{k_0^2}\,\mathrm{Im}\left(\hat{z}\cdot\vec{A}\right)_{\theta=0}$$

When measuring scattered light, it is usual to allow the detector to rotate around the scattering centre in a plane as shown in Fig. 2. It is convenient to describe the incident and scattered light such that the polarization is resolved into components parallel and perpendicular to this plane. The fields are related through

$$\begin{pmatrix} E_{\parallel,sca} \\ E_{\perp,sca} \end{pmatrix} = \frac{e^{ik_0 r}}{k_0 r}\begin{pmatrix} S_2 & S_3 \\ S_4 & S_1 \end{pmatrix}\begin{pmatrix} E_{\parallel,inc} \\ E_{\perp,inc} \end{pmatrix}$$

which defines the amplitude scattering matrix. We note that for an isotropic particle, such as a sphere, no cross-polarization is introduced and $S_3 = S_4 = 0$. Also, for any particle there can be no indication of the azimuth angle ϕ at $\theta = 0°$. Then it also follows that, at $\theta = 0°$, $S_3 = S_4 = 0$ and that $S_1 = S_2 = S(0)$. Thus

$$\vec{E}_{sca} = \frac{e^{ik_0 r}}{k_0 r}S(0)\vec{E}_{inc}$$

and $\vec{A} = S(0)\hat{z}$. Finally,

$$C_{ext} = \frac{4\pi}{k_0^2}\,\mathrm{Im}[S(0)]$$

There is one other cross-section which should be mentioned in passing, namely that for radiation pressure, C_{pr}. The rate of momentum of a light wave is given by $(P/c)\hat{z}$. For light scattered through the angle θ the rate of momentum in the original direction of propagation is changed to $(P_{sca}/c)\hat{r}$. Thus there is a force on the particle given by

$$\vec{F} = \frac{P_{sca}}{c}(1 - \overline{\cos\theta})\hat{z}$$

where $\overline{\cos\theta}$ is the average of $\cos\theta$ obtained by integration of the scattered intensity over all values of θ. In addition, any power the particle absorbs stops the radiation and contributes a force given by $(P_{abs}/c)\hat{z}$. The total force is

$$\vec{F} = \left[\frac{P_{ext}}{c} - \overline{\cos\theta}\frac{P_{sca}}{c}\right]\hat{z}$$

Thus the force per unit irradiance is

$$\frac{\vec{F}}{I_0} = \frac{1}{c}[C_{ext} - \overline{\cos\theta}C_{sca}]\hat{z}$$

By analogy with the previous definitions we define C_{pr} as

$$C_{pr} = C_{ext} - \overline{\cos\theta}C_{sca}$$

Since pressure is force per unit area, the radiation pressure is given by Q_{pr}/c.

Another property of the amplitude scattering is that if the incident and scattering directions are interchanged then

$$\begin{pmatrix} E_{\parallel,sca} \\ E_{\perp,sca} \end{pmatrix} = \frac{e^{ik_0 r}}{k_0 r}\begin{pmatrix} S_2 & -S_4 \\ -S_3 & S_1 \end{pmatrix}\begin{pmatrix} E_{\parallel,inc} \\ E_{\perp,inc} \end{pmatrix}$$

which is the reciprocity theorem. This important relationship has been derived, for example, by Saxon [8].

When we examine scattered intensity we need a means of describing all the polarization states and their relationships. This is achieved through the Stokes' matrix which relates

four "intensities", defined by

$$I = E_\parallel E_\parallel^* + E_\perp E_\perp^*$$

$$Q = E_\parallel E_\parallel^* - E_\perp E_\perp^*$$

$$U = E_\parallel E_\perp^* + E_\perp E_\parallel^*$$

$$V = E_\parallel E_\perp^* - E_\perp E_\parallel^*$$

through

$$\begin{pmatrix} I_{sca} \\ Q_{sca} \\ U_{sca} \\ V_{sca} \end{pmatrix} = \frac{1}{k_0^2 r^2} \begin{pmatrix} M_{11} & M_{12} & M_{13} & M_{14} \\ M_{21} & M_{22} & M_{23} & M_{24} \\ M_{31} & M_{32} & M_{33} & M_{34} \\ M_{41} & M_{42} & M_{43} & M_{44} \end{pmatrix} \begin{pmatrix} I_0 \\ Q_0 \\ U_0 \\ V_0 \end{pmatrix}$$

The M_{ij} form the elements of the Stokes' matrix. They are given in terms of the S_i of the amplitude scattering matrix by Bohren and Huffman [4], for example.

There are various symmetry relationships between the elements M_{ij}. In particular it can be shown that, for a cloud of randomly aligned particles [1, 9],

$$M = \begin{pmatrix} M_{11} & M_{12} & 0 & 0 \\ M_{12} & M_{22} & 0 & 0 \\ 0 & 0 & M_{33} & M_{34} \\ 0 & 0 & -M_{34} & M_{44} \end{pmatrix}$$

For isotropic particles, $M_{11} = M_{12}$ and $M_{33} = M_{44}$. If either of these inequalities is unsatisfied anisotropy is present.

2.2. Particle clouds

Particles very rarely, if ever, exist singly. They exist in clouds containing very large numbers. The actual number of interest to light scattering depends upon the circumstances, such as the volume of the test space as seen by the detector. Thus at low concentrations and with a small volume we may be *looking* at a single particle, but the presence of the others cannot be ignored in all cases. For larger volumes and concentrations we may be looking at many millions of particles. As we shall see later, measurement techniques naturally fall into these two classes: single-particle counting or cloud methods.

The extension of single scattering theory to clouds can be performed at two levels, the simplest being at low concentration. The complications arise at high concentrations where multiple scattering and particle interaction effects become significant.

For very low concentration the simple definitions of the previous section can be extended to a cloud in a straightforward manner provided three conditions are met:

1. The particles are randomly positioned and are of sufficient number that incoherent superposition may be applied. The random positioning means that the phases of the scattered waves arriving at the detector are also random. If the number is sufficiently large that the phases sum to zero, then intensities can be added directly.
2. There is negligible multiple scattering. This means that a photon once scattered has a very high probability of leaving the cloud without encountering another particle. We shall examine the requirements for this shortly, but, approximately, it means that the transmission by the cloud must be greater than 60%.
3. There is no interactive scattering. This implies that the electric fields should not interact directly. If this happens then there is a coherent structure to the multiple scattering and the particles tend to behave to some extent as an assembly. In the limit they are touching and they behave as a single particle or agglomerate. To avoid interactive scattering the evidence is that a separation of three diameters is thought to be sufficient [2]. The implications in terms of particle size and concentration are shown in Table 1. The maximum volume fraction that can be occupied by particles of any size is approximately 3%.

Table 1
Maximum concentration of particulates to avoid direct interaction effects

Particle radius (μm)	Concentration (m^{-3})
0.1	10^{19}
1.0	10^{16}
10.0	10^{13}
100.0	10^{10}
1000.0	10^{7}

If all three conditions apply we simply add intensities. Thus, if there are N particles per unit volume all having the same size D, the total scattered power per unit volume of space is

$$P_{sca,N} = NP_{sca}$$

and, on dividing by the irradience,

$$\frac{P_{sca,N}}{I_0} = N\frac{P_{sca}}{I_0} = NC_{sca} = K_{sca}$$

where K_{sca} is the scattering coefficient. The absorption may

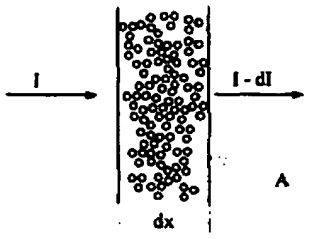

Fig. 3. Transmission through a slab.

be similarly defined, and the extinction coefficient is

$$K_{ext} = K_{sca} + K_{abs}$$

More usually, there will be a distribution of particle sizes. We allow there to be $n(D)\,dD$ particles per unit volume in the size range D to $D + dD$. Then

$$N = \int_0^\infty n(D)\,dD$$

and

$$K_{sca} = \int_0^\infty C_{sca} n(D)\,dD$$

and so on.

We now consider transmission through a slab containing particles, as in Fig. 3. The volume of a section of length dx is $A\,dx$, so that the power lost is

$$-dP_{ext} = IK_{ext}A\,dx$$

or the loss of irradiant flux is

$$-dI = IK_{ext}\,dx$$

On integration

$$I_t = I_0 \exp\left(-\int_0^L K_{ext}\,dx\right)$$

If the cloud is uniform throughout the length, then

$$I_t = I_0 \exp(-K_{ext}L)$$

The product $K_{ext}L$ is called the turbidity, τ.

The optical mean free path (the average distance a photon will travel between scattering events) is $1/K_{ext}$. This suggests that to avoid multiple scattering requires

$$I_t/I_0 = e^{-1} = 0.368$$

The actual value will depend upon the particle type. For example, if a particle is very heavily absorbing, so that scattering is relatively small, multiple scattering may not occur until interactive effects become appreciable.

To have some idea of the limits to concentration we may examine large spheres. As we shall see later, for large particles $Q_{ext} \approx 2$ so that

$$K_{ext}L \approx 2N\frac{\pi D^2}{4}L$$

Thus, for example, 10 μm particles will require $NL < 1.6 \times 10^{10}\,m^{-2}$. 100 μm particles require $NL < 1.6 \times 10^{8}\,m^{-2}$. These concentrations are quite modest, and multiple scattering is very common.

A brief discussion of the treatment of multiple scattering is given in Section 4.

3. General scattering theory

We now briefly summarize means for calculating the expected scattering from particles. Fundamentally, there are two approaches. In the first, expansions are written down for the incident, internal and scattered waves and a solution is found for the expansion coefficients by applying the electromagnetic boundary conditions. In the second, the solution is found from an integral over the volume of the scatterer. In both cases there are limitations and complications.

3.1. Boundary condition method

To obtain an analytical solution by this method, the fields are expanded in a coordinate system in which the tangential components of the field are readily obtainable. Thus for a sphere, for example, spherical coordinates are chosen. The tangential fields then lie in the θ and ϕ directions.

In order to obtain a form for the expansion the wave equation must be separable in the chosen coordinate system. Further, there must exist orthogonality relations to enable calculation of the expansion coefficients. These requirements limit the number of possible solutions to six coordinate systems: rectangular Cartesian; circular, elliptical and parabolic cylindrical; spherical; and conical [10, 11].

The infinite cylinder has been studied in some detail as it is the most straightforward geometry. The solution for the case of normal incidence was first obtained by Lord Rayleigh [12]. The more general case of oblique incidence was solved by Wait [13], and is discussed by Kerker [2] and Bohren and Huffman [4]. Other solutions for radially stratified cylinders and cylinders with inhomogeneous shells are reviewed by Kerker [2]. By considering the limits as the step in thickness and refractive index to go to zero, Kai and d'Alessio [14] were able to consider very large numbers of shells with high computational efficiency. Their program could easily accommodate up to 80 000 shells.

A suggested scheme for the treatment of a finite cylinder was given by van de Hulst [1]. In this, the result for the infinite case was multiplied by the diffraction pattern of a slit of length equal to that of the cylinder. More recently, this approach was revisited by Wang and van de Hulst [15]. They claim good agreement in comparison with microwave measurements on models.

The more useful, and most widely applied, solution is that for a sphere. This can be applied to real particles, though it must be emphasized that most particles are non-spherical.

The solution for the sphere was first derived by Lorenz [16] and later independently by Mie [17]. It is discussed in detail by van de Hulst [1], Kerker [2] and Bohren and Huffman [4], among others. The elements of the amplitude scattering matrix are given by

$$S_1(\theta) = \sum_{n=1}^{\infty} \frac{2n+1}{n(n+1)}\left[a_n \pi_n + b_n \tau_n\right]$$

$$S_2(\theta) = \sum_{n=1}^{\infty} \frac{2n+1}{n(n+1)}\left[a_n \tau_n + b_n \pi_n\right]$$

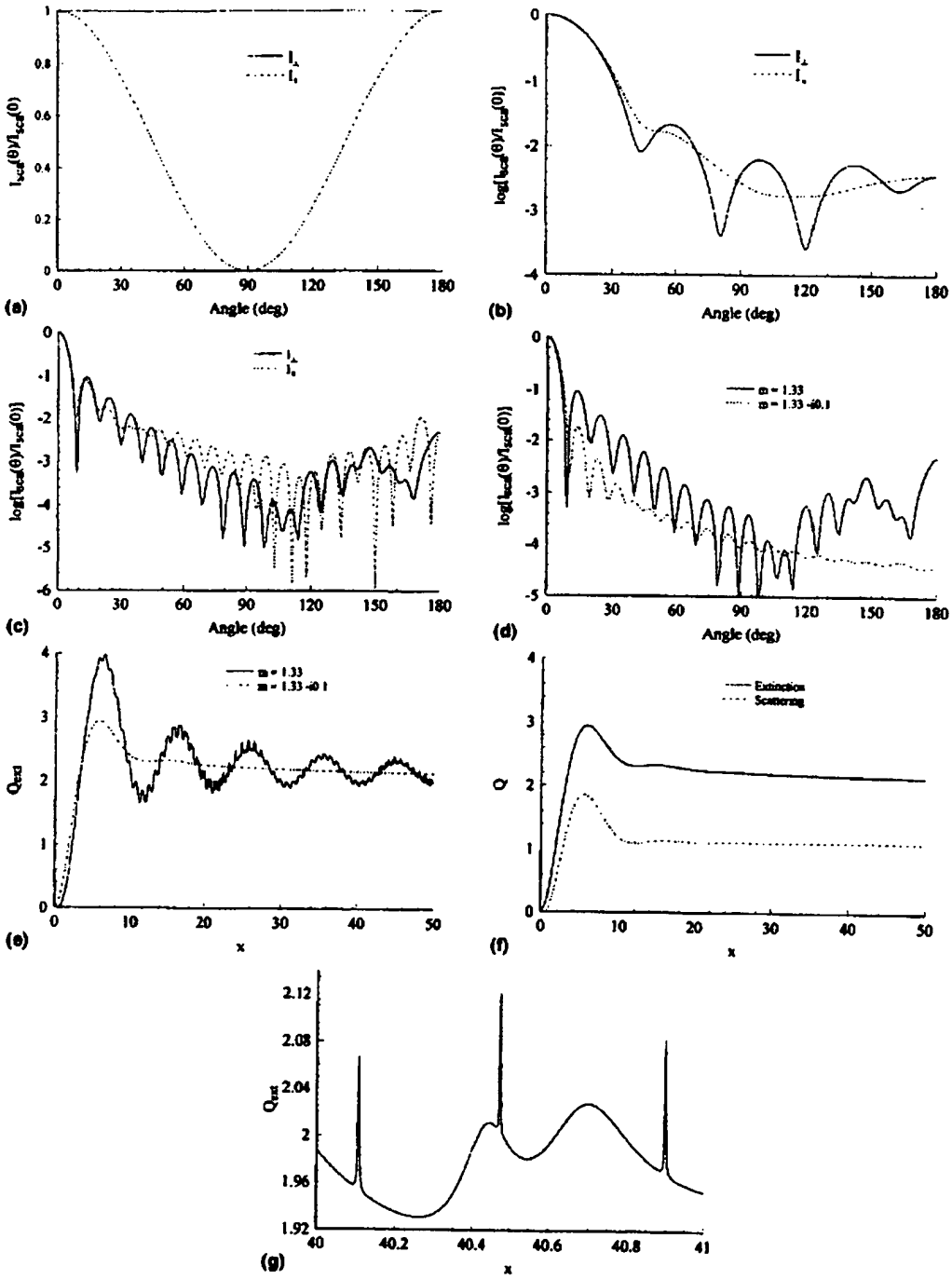

Fig. 4. Scattering diagrams and efficiency factors: (a) intensity versus angle for $x = 0.01$ and $m = 1.33$; (b) intensity versus angle for $x = 5$ and $m = 1.33$; (c) intensity versus angle for $x = 20$ and $m = 1.33$; (d) intensity versus angle for $x = 20$ and perpendicular polarization, showing the effect of absorption; (e) extinction efficiency showing the effect of absorption; (f) efficiency factors for absorbing particles; (g) extinction efficiency in detail, illustrating the presence of singularities for $m = 1.33$.

The coefficients a_n and b_n for a non-magnetic homogeneous particle have the form

$$a_n = \frac{m\psi_n(mx)\psi_n'(x) - \psi_n'(mx)\psi_n(x)}{m\psi_n(mx)\xi_n'(x) - \psi_n'(mx)\xi_n(x)}$$

$$b_n = \frac{\psi_n(mx)\psi_n'(x) - m\psi_n'(mx)\psi_n(x)}{\psi_n(mx)\xi_n'(x) - m\psi_n'(mx)\xi_n(x)}$$

where $x = k_0R$. $\psi_n(z) = zj_n(z)$ and $\xi_n(z) = zh_n^{(1)}(z)$ are Riccati–Bessel functions.

Also

$$\pi_n(\cos\theta) = \frac{1}{\sin\theta}P_n^1(\cos\theta)$$

$$\tau_n(\cos\theta) = -\sin\theta\frac{P_n^1(\cos\theta)}{d(\cos\theta)}$$

The scattering and extinction efficiency factors are

$$Q_{sca} = \frac{2}{x^2}\sum_{n=1}^{\infty}(2n+1)\left[|a_n|^2+|b_n|^2\right]$$

$$Q_{ext} = \frac{2}{x^2}\,\mathrm{Re}\sum_{n=1}^{\infty}(2n+1)[a_n+b_n]$$

There are several algorithms for the calculation of a_n and b_n. These are discussed by, for example, Bayvel and Jones [5] and Bohren and Huffman [4]. A FORTRAN program is listed in the back of Bohren and Huffman's book. It is found that the series are convergent and can be terminated after a certain number of terms, N. Bohren and Huffman use

$$N = x + 4x^{1/3} + 2$$

It is evident that as the particles become larger more terms are required and, eventually, the computer time becomes excessive. Ultimately it becomes more efficient to use geometrical optics.

Some typical results for scattered intensity and the efficiency factors are shown in Fig. 4. There are a number of typical points. For a very small particle with $x \ll 1$ (Fig. 4(a)) the scattering pattern is that of a simple dipole. For polarization perpendicular to the plane of measurement the scattered intensity is independent of angle and the scattering is isotropic. For polarization parallel to this plane there is a $\cos^2\theta$ variation. As the particle becomes larger, forward scattering increases more rapidly than that at other angles and quickly becomes dominant. The shape of this lobe for large particles ($\geq 4\,\mu$m at visible wavelengths) is well described by Fraunhofer diffraction theory. This shows that the height of the forward lobe is proportional to D^4 and its width to $1/D$. The scattering pattern also becomes convoluted with a complicated lobe structure. The number of lobes is of the order $x|m|$. Absorption by the particle damps the lobe structure away from the forward direction. Again, for large particles where Fraunhofer diffraction holds, calculation shows that the forward scattering is not sensitive to refractive index. This is very important in practice to particle sizing if refractive index is not known.

The efficiencies initially rise rapidly with particle size, but then peak and go asymptotically to a constant with a decaying oscillation. Lock and Yang [18] have demonstrated that the oscillations are caused by interference between near forward transmission and diffraction.

For the extinction efficiency the value of the constant is two. This would suggest that the particle will block off twice the light falling upon it, an effect called the "extinction anomaly". The explanation lies in the fact that two processes are occurring: diffraction and the geometrical optics effects of reflection, refraction and absorption. The efficiency for each of these processes is one, so that

$$Q_{ext}' = Q_{diff} + Q_{geom} = 2$$

For very large particles the diffraction pattern is very narrow. All real detectors, including the eye, collect light over a finite angular range. Thus the diffracted light is collected and is not measured as a loss. The measurement yields

$$Q_{ext}' = Q_{geom} = 1\ .$$

as would be expected. In order to ensure that the true extinction efficiency is measured, it is necessary to restrict the angular collection range of the detector to be much less than the width of the forward lobe. Thus a measure of transmissivity is not necessarily the same as a measure of extinction, and great care is required.

If the efficiencies are calculated in fine detail, with very small steps in x, a number of extremely sharp peaks and troughs are observed. These are scattering resonances associated with the zeros of the denominator in the expressions for a_n and b_n. The expansion coefficients become infinite at these points.

The extension to radially stratified spheres is quite straightforward and is discussed, for example, by Kerker [2]. A FORTRAN program to calculate scattering from two concentric spheres is listed by Bohren and Huffman [4]. Multiple concentric spheres have been considered by, for example, Johnson [19] and the application to radially inhomogeneous spheres has been discussed by a number of authors (e.g. Perelman [20]).

Kai and Massoli [21] considered the limits as the steps in size and refractive index go to zero and obtained a simple and speedy algorithm. This method has enabled a very large number of shells to be considered and various aspects of radial inhomogeneity have been investigated. An example is the influence of a radial variation of refractive index on the resonances in Q_{ext}. Kai and d'Alessio [22, 23] and Kai et al. [24] concluded that their location depends primarily on the average value of the refractive index near to the surface. If the refractive index only changes in a thin layer near the surface, then an equivalent homogeneous sphere can be found.

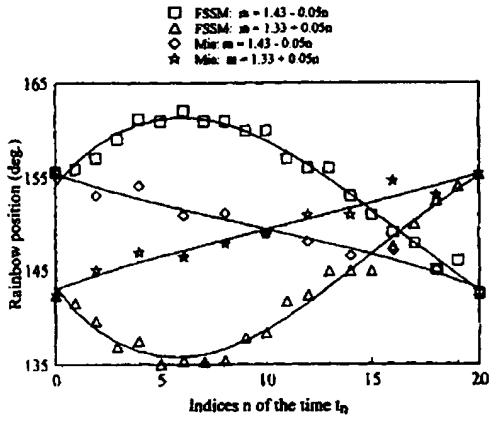

Fig. 5. Primary rainbow angles for 10 μm droplets during heating ($m = 1.43 - 0.05n$) and cooling ($m = 1.33 + 0.05n$). FSSM refers to a parabolic profile of refractive index using the finely stratified sphere model. The Mie theory results are for homogeneous spheres. (After Kai et al. [25].)

Another area of interest to potential diagnostics is the position of the rainbow. Kai et al. [25] used the stratified sphere model to indicate the ways in which this position fluctuates. Figure 5 compares the variation of the rainbow angle from a homogeneous sphere with one having a variable profile of refractive index. In this case a homogeneous drop with a refractive index of 1.43 enters a hot environment. As the drop heats up a temperature profile develops. Initially only the outer edge is heated but then the higher temperature penetrates further until, eventually, the drop is once again homogeneous at the final temperature where the refractive index is 1.33. As the drop cools the process is reversed. In the stratified sphere model the refractive index is allowed to vary over a given shell of increasing thickness with a parabolic profile. In the Mie calculations the sphere is homogeneous with a linear variation of refractive index. It is evident that there is considerable difference between the two models and that significant error could be introduced by the assumption of homogeneity.

The detection of inhomogeneity via measurements of the scattering matrix was investigated by Bhanti et al. [26] They used a stratified sphere model to predict elements of the matrix for coatings of soot on both water drops and coal particles.

The case of a sphere containing an eccentric inclusion has been considered by Borghese et al. [27, 28] and Videen et al. [29] In a similar approach, Fuller [30, 31] considered the coated sphere in terms of multiple scattering with a view to developing a model for spheres with multiple inclusions. Not only does the presence of an inclusion affect the absorption cross-section very considerably, but it is strongly dependent upon the position and orientation relative to the incident wave. This is illustrated in Fig. 6.

Videen et al. [32] and Chýlek et al. [33] also looked at the case of carbon particles enclosed within water drops because of the relevance to absorption of radiation in the atmosphere. The former authors suggested the use of effective medium predictions and concluded that the extended methods for the calculation of equivalent refractive index removed any restriction on the size of the internal grains.

The Lorenz–Mie theory can also be used to calculate the internal fields of spheres. This has become of interest particularly because of studies in laser heating, and also because of interests in radiation pressure. Examples of such studies are the papers of Lock and Hovenac [34] and Lai et al. [35]

Notable among solutions for other shapes is that for the spheroid due to Asano and Yamamoto [36]. This theory is complicated and computationally expensive. To date scattering has only been calculated for quite small spheroids. A recent advance due to Kurtz and Salib [37] has modified the formulation of the boundary conditions to yield a more convergent form. Another approach due to Martin [38] is to apply a perturbation to Mie theory for the case of slightly deformed spheres. Coated spheroids have been considered by Farafonov et al. [39] and Voshchinnikov [40].

As mentioned earlier, the theory outlined above is for infinite plane waves. However, with the advent of the laser, attention has been drawn to scattering out of Gaussian beams. Early work in this area was due to Tam and Corriveau [41]. This problem has been vigorously pursued by Gouesbet and co-workers in recent years. Although the general problem is very complex, they have been able to develop a quite simple form for sufficiently large particles on the beam axis by employing van de Hulst's "localization principle" [1, 42–45]. A rigorous justification of the localization principle for both on-axis and off-axis beams has been propounded by Lock and Gouesbet [46, 47]. Ren et al. [48] have discussed the evaluation of the beam shape

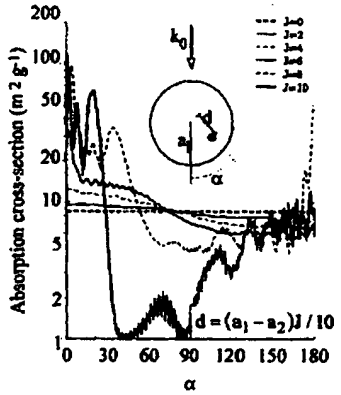

Fig. 6. Specific absorption cross-sections for a 0.1 μm carbon sphere eccentrically located in a water drop of diameter 5 μm. The refractive indices are 1.5 − i0.5 and 1.33, respectively. a_1 and a_2 are the radii of the water drop and the inclusion, and d is the radial distance of the inclusion. The cross-sections have been averaged over polarization. (After Fuller [31].)

coefficients for laser sheets. Lock [49] and Ren et al. [50] have proposed improved algorithms for scattering by a sphere out of a Gaussian beam, and Gouesbet [51] has examined scattering by an arbitrarily located and oriented infinite cylinder. The validity of this generalized Mie theory has been demonstrated by Guilloteau et al. [52] by observing light scattering by particles levitated on laser beams.

Interesting new developments occur when this theory is applied to situations where the beamwidth is of the order or less than the diameter of the particles. For example, Lock [53] demonstrated that a narrow Gaussian beam incident near the edge of a particle can produce rainbows up to ninth order. Also, Hodges et al. [54] find that diffraction theory fails if the beamwidth is less than the diameter. Beam confinement also affects extinction and this has been explored by Gouesbet et al. [55], who found that additional terms were needed in the optical theorem. Lock [56] has shown that when the beamwidth approaches infinity, $Q_{ext} \rightarrow 2$ in agreement with current knowledge. However, when the beamwidth approaches zero, $Q_{ext} \rightarrow 1$ because of the loss of the diffraction term.

Attention is now being given to beam shapes of a more general nature [57–59]. Lock and Hodges [60] have investigated scattering of an off-axis non-Gaussian beam by a sphere, and Onofri et al. [61] have performed similar calculations for a multi-layered sphere.

Most particles in nature are not spherical. Indeed most particles have shapes which cannot be strictly treated by the boundary condition method. When faced with this situation we have to be pragmatic and accept that an analytical solution is not possible. There are two routes we can take. We can either approximate or we can use a numerical method. The latter is not an approximation in so far as the calculation can, in principle, be continued to any desired accuracy. The only limitations are computer time and space and numerical precision. Nonetheless, certain assumptions are often made in setting up the numerical scheme which can make it only approximate, or limit its application within certain bounds.

There is a set of numerical schemes based on the boundary condition method. The principle here is to presume that the fields can be expanded in terms of some basis functions which enable them to be written down and matched at the boundary. Perhaps the simplest is the point matching method in which it is assumed that the series can be terminated after N terms. The consequence is that there are then $2N$ unknown coefficients. Selection of a sufficient number of points on the surface enables a set of simultaneous equations to be written down which can be solved for the unknowns.

The question is that, if it is this straightforward, why is it not more widely used? The problem lies with the assumption that the series is convergent. Of course, it is if the matching takes place over the surface of a simple shape for which a series solution is known, but it is not necessarily so for other shapes. There has been considerable discussion on this over the years (e.g. Lewin [62]).

Joo and Iskander [63] modified the point matching method by expanding the field using spherical harmonics at various points along the axis of an extended object. In each zone they used point matching but, additionally, ensured that the fields in different regions agreed where they overlapped. They also used a least-squares fit for the coefficients and claimed considerable reductions in computer time.

A similar concept is the multipole technique (e.g. Ludwig [64]) which uses a set of point sources within the particle, the total field of which approximates the true field. A linear combination of such points is found which satisfies the boundary conditions, and matching at a discrete number of points reduces the problem to a matrix inversion. The matrix can be over-determined and the method of least squares applied. Generally, this avoids the problem of ill-conditioning of the matrix. A further extension of this idea is mode matching [65]. A generalized multipole technique has been developed by Al-Rizzo and Tranquilla [66] which enabled them to examine quite large elongated and composite objects.

An attempt to avoid the convergence difficulty lies with the extended boundary condition method (EBCM). Waterman [67] considered a wave incident on a perfect conductor. This generates electric currents in the surface which cancel the internal field. By the use of analytical continuation it was shown that the field cancellation held throughout the particle's interior. The scattered field is obtained from an integral of these currents over the particle surface. The method has been extended to dielectric particles by, for example, Barber and Yeh [68].

The number of terms, N, of the series expansion required for convergence increases with size and refractive index, but also with deviation from spherical shape. For any particle it is possible to draw inscribed and exscribed spheres of radii r_i and r_e. The spherical harmonic expansion can be shown to be convergent at radii $r < r_i$ and $r > r_e$. The Rayleigh hypothesis is that the series is also convergent within $r_i < r < r_e$. It is this assumption which is dubious. The EBCM, which was supposed to be exact, makes a similar assumption and suffers from the same kind of defects. Lewin [62] showed that this is due to hypersensitivity to minute errors of the field on the matching circle. If the true shape differs significantly from a sphere then difficulties will arise with convergence. This can make the method very time-consuming for all but the smallest, only slightly perturbed sphere.

Numerous calculations have been made for small particles where the shape is essentially spherical with a small perturbation. Most popularly, the shape is described by an expansion in Chebyshev polynomials such that

$$r = R[1 + \delta T_n(\cos\theta)]$$

and δ is small. For example, Wiscombe and Mugnai [69] compared Chebyshev particles and spheres. They found reasonable agreement between the two types for particle size parameter, x, less than three to five. After that the differences grow rapidly. A universal feature was that the

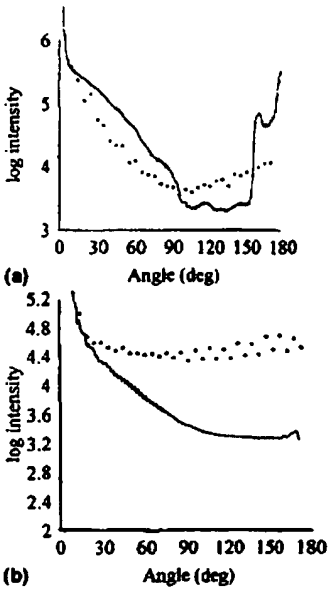

Fig. 7. Light scattering polar diagrams of irregular particles. The solid line is for an ideal sphere of the same size. (a) A rough and slightly elongated glass sphere (50 μm). (b) A fly ash particle (15 μm, $m = 1.55 + i0.01$). (After Killinger and Zerull [70].)

lobe structure in the scattering pattern became averaged out for the non-spheres. They also found that particles with concavities scattered substantially more than totally convex ones. Differences in intensity could be summarized as below:

Angular range (deg)	*Non-sphere*	*Sphere*
0–10		≥
10–80		<
80–150		≫
150–180		< ($x \leq 8$ to 12)
		> ($x > 8$ to 12)

An example is shown in Fig. 7(a). This was measured experimentally by Killinger and Zerull [70] for a randomly oriented, slightly irregular, 50 μm diameter glass sphere. Very small deviations from spherical shape cause distinct differences in the scattering properties. The conclusions are largely in agreement with those of Wiscombe and Mugnai. They are not universal, however, as witnessed by Fig. 7(b) which Killinger and Zerull obtained for an absorbing fly ash particle of 15 μm diameter.

Later, Mugnai and Wiscombe [71] attempted to represent scattering from irregular particles by that from a size distribution of spheres, which has the similar effect of averaging out the lobe pattern. However, the results were not easy to interpret universally. The authors commented that even after many hours on a Cray supercomputer they did not have sufficient results to come to any firm conclusions.

There have been several attempts to combine the EBCM with other methods to improve speed and convergence. For example, Iskander et al. [72] proposed an iterative procedure starting with a known approximate solution. They claim that this approach is more stable and quicker, and used it to study elongated particles, such as spheroids [73, 74]. For this, the fields were expressed as expansions in spherical harmonics about several points along the axis of the particle. The EBCM has also been applied to ellipsoids by Schneider and Peden [75] and to finite cylinders by Ruppin [76] and Kuik et al. [77] The latter authors comment that for random orientation the solution does not converge to that of an infinite cylinder as the axial ratio increases, though it does for single aligned cylinders. They also state that ellipsoids do not model finite cylinders well because of the sharp edges. Barton [78] has studied layered Chebyshev particles illuminated with focused Gaussian beams.

The EBCM is usually combined with the T-matrix method and the two terms are used interchangeably. The T-matrix simply relates the expansion coefficients of the scattered field to those of the incident field, i.e.

$$\begin{pmatrix} a_{\nu,\mathrm{sca}} \\ b_{\nu,\mathrm{sca}} \end{pmatrix} = -[T]\begin{pmatrix} a_{\nu,\mathrm{inc}} \\ b_{\nu,\mathrm{inc}} \end{pmatrix}$$

where EBCM is used to compute the elements of $[T]$. This matrix contains all the information about the scatterer, such as size, shape and refractive index. Rotation of the scatterer can be allowed for simply by rotating the incident field, which changes $a_{\nu,\mathrm{inc}}$ and $b_{\nu,\mathrm{inc}}$. A discussion of this method and of its use for the determination of particle shape has been give, for example, by Barber and Hill [79].

Because of the intensive computational requirements coupled with the influence of rounding errors on the ill-conditioned matrix which has to be inverted, there has been an upper limit to the particle size parameter that can be calculated, of the order 25. Mishchenko and Travis [80] have managed to extend this by up to 2.7 times by the use of extended precision computing.

Mishchenko [81, 82] has considered the problem of light scattering by randomly oriented particles with axial symmetry. A method is described to generate the components of the Stokes' matrix directly for assemblies of such particles which avoids the need to perform many individual calculations. Storage requirements are reduced and it is claimed that computation times can be reduced by a factor of up to 20. Contour plots of elements of the scattering matrix for polydispersions of randomly oriented spheroids have been provided by Mischchenko and Travis [83]. Orientational averaging in the T-matrix method has also been discussed by Khlebtsov [84]. In a further paper by Mishchenko [85], simplifications are discussed for the calculation of Q_{ext} for ellipses.

A general review of the application of the T-matrix method to non-spherical particles has been provided by Mishchenko et al. [86].

An extension of numerical techniques to non-spherical particles illuminated by a Gaussian beam is discussed by Barton and Alexander [87]. They provide a numerical scheme for solving the boundary conditions, and the results are expressed in terms of expansions in spherical harmonics. The method was tested for off-axis spheres and ellipsoids. Khaled et al. [88, 89] have treated the same problem by expanding the Gaussian beam as a spectrum of plane waves.

Recent work has concerned the extension of the T-matrix method to interactive and multiple scattering [90–93].

3.2. Integral equation methods

The alternative numerical methods are based on the integral formulation of the scattering problem. It has been shown by various authors that a solution of the scalar wave equation is given by

$$\psi(\vec{r}) = \psi_{\text{inc}}(\vec{r}) + k_0^2 \int_{V'} [\varepsilon(\vec{r}') - 1]\psi(\vec{r}')G(\vec{r}, \vec{r}')\, \mathrm{d}V'$$

where $\vec{r}$ and $\vec{r}'$ are two points in space. $G(\vec{r}, \vec{r}')$ is the appropriate Greens function. In infinite cylindrical coordinates

$$G(\vec{r}, \vec{r}') = \frac{1}{4} H_0^{(1)}(k_0|\vec{r} - \vec{r}'|)$$

In spherical coordinates

$$G(\vec{r}, \vec{r}') = \frac{\mathrm{e}^{\mathrm{i}k_0|\vec{r}-\vec{r}'|}}{4\pi|\vec{r} - \vec{r}'|}$$

$\psi_{\text{inc}}(\vec{r})$ is the incident field at $\vec{r}$. The boundary conditions are automatically taken into account and the radiation condition is satisfied.

If $\vec{r}$ is a point internal to the particle, the integral equation can be used to calculate the internal field. If $\vec{r}$ is an external point, then it can be used to calculate the scattered field

$$\psi_{\text{scu}}(\vec{r}) = k_0^2 \int_{V'} [\varepsilon(\vec{r}') - 1]\psi(\vec{r}')G(\vec{r}, \vec{r}')\, \mathrm{d}V'$$

External to the particle, it is usual for practical purposes that $|\vec{r}| \gg |\vec{r}'|$ and the far-field approximation to the Greens function may be used. For spherical coordinates this is

$$G(\vec{r}, \vec{r}') \cong \frac{\mathrm{e}^{\mathrm{i}k_0 r}}{4\pi r} \mathrm{e}^{-\mathrm{i}k_0 r' \cos\beta}$$

where

$$\cos\beta = \cos\theta\cos\theta' + \sin\theta\sin\theta'\cos(\phi - \phi')$$

It can be seen that there are two difficulties with these equations. The first is that the unknown field appears inside the integral. The second is that there is a singularity in the Greens function when $|\vec{r} - \vec{r}'| = 0$.

Despite these difficulties the integral formulation has formed the basis of a number of calculation methods for the scattered field. Some of these are approximations where a form is assumed for the internal field. This is the subject of the next section, but the most commonly used assumption is that

$$\psi(\vec{r}') = \psi_{\text{inc}}(\vec{r})$$

which is the Born approximation. Once the internal field is given, the scattered field can be calculated without the problem of the singularity arising.

Another possibility is to expand the internal field by a known set of functions (commonly spherical harmonics) with unknown expansion coefficients. Then an attempt is made to match the coefficients, perhaps by some method such as least squares.

The most common numerical method is to subdivide the internal volume into a number of much smaller volumes. An assumption is then made about the nature of the field within each sub-volume. Typically, if the sub-volume is sufficiently small, the internal field is taken to be an unknown constant. Then we have

$$\psi(\vec{r}_i) = \psi_{\text{inc}}(\vec{r}_i) + k_0^2 \sum_{j=1}^{N} \psi(\vec{r}_j) \int_{V'} \left[\varepsilon(\vec{r}_j) - 1\right] G(\vec{r}_i, \vec{r}_j)\, \mathrm{d}V_j$$

The problem then reduces to solving N linear simultaneous equations. There is still, however, the problem of the singularity. This can be tackled in two ways. One is to draw an exclusion zone around the point and leave this small volume out of the problem. This zone is then made successively smaller and the solution is found in the limit as the volume of the zone tends to zero. This is equivalent to taking the principal part of the integral.

The other way out is to let the volume around the point be a sphere. Since we assume that the field is constant, we may restrict the calculation such that $\vec{r}_i$ is at the centre of the small volume. It can be shown that on integration the singularity disappears. The assumption of spherical shape for this one small volume should contribute very small error. The accuracy can be improved if the singularity is removed by using an expansion in Taylor's series to two terms [94].

For the purposes of electromagnetic scattering the vector equation is needed. This is [95]

$$\vec{E}(\vec{r}) = \vec{E}_{\text{inc}}(\vec{r}) + k_0^2 \int_{V'} [\varepsilon(\vec{r}') - 1]\vec{E}(\vec{r}') \times \left(\mathbf{I} + \frac{1}{k_0^2}\vec{\nabla}'\vec{\nabla}'\right) G(\vec{r}, \vec{r}')\, \mathrm{d}V'$$

where $\mathbf{I}$ is the identity tensor. An alternative form is given by Saxon [96] which in some ways is more tractable. This is

$$\vec{E}(\vec{r}) = \vec{E}_{\text{inc}}(\vec{r}) + k_0^2 \int_{V'} [\varepsilon(\vec{r}') - 1]\vec{E}(\vec{r}')G(\vec{r}, \vec{r}')\, \mathrm{d}V' + \int_{V'} \vec{\nabla}'\left\{\vec{\nabla}' \cdot [\varepsilon(\vec{r}') - 1]\vec{E}(\vec{r}')\right\} G(\vec{r}, \vec{r}')\, \mathrm{d}V'$$

As we are dealing with three-dimensional space, any vector

can have three components. As a consequence, when the method of division into N sub-volumes is used, we end up needing to solve $3N$ simultaneous equations.

Perhaps the simplest approach to discretization of the integral is to make the sub-volumes simple cubes or rectangles (e.g. Richmond [97]; Hagmann et al. [98]). This is the basis of the method of moments on which there is a considerable literature. A good discussion of this general area is given by Newman and Kingsley [99].

An improvement that has been proposed is to use tetrahedra rather than cubes because these are better able to fit a curved surface [100, 101]. Hagmann et al. [98], Schaubert et al. [100] and Mendes and Arras [102] also propose improved sets of basis functions, rather than simple constants, which permit the use of larger sub-volumes and, thus, reduce computer demand. It has been shown by Lu and Chew [103] that computational efficiency can be improved by noting that a group of small volumes can be represented by a set of surface sources on their common boundary. This fact is used to continuously replace the internal sources with equivalent larger volumes and results in a slight decrease in computer time.

A logical extension is to allow all the sub-volumes to be spheres. Indeed, in the limit as the radius of each sphere approaches zero, they behave as simple dipoles. This forms the basis of the coupled dipole approximation in which the dipoles are considered as equivalent to the molecules making up the particle.

The coupled dipole method probably began with the paper by Purcell and Pennypacker [104]. It has been explored particularly by Singham and Bohren [105, 106], who developed a method of successive approximations rather than solve a large number of simultaneous equations, which they call the "scattering order method". The range of validity has been extended by Mulholland et al. [107] who included the first magnetic dipole. This enabled the primary sphere diameter to be increased from 0.06 μm to 0.12 μm. Similarly, Okamoto [108] expressed the dipole polarizability of the primary spheres as the first term (a_1) of the Mie series expansion, and achieved calculations for size parameters up to 1.5, or about 0.24 μm in the visible. An algorithm for improving the speed of the calculations has been given by Venizelos et al. [109] Draine and Flateau [110] have reviewed the method.

The iterative approach requires an equivalent medium approximation which allows for the interactive field between the dipoles and alters their polarizability, or refractive index. A number of authors have recently been exploring this. Ku [111] has compared various models and concluded that the one provided by Iskander et al. [112] is the most satisfactory. Wolff et al. [113] prefer the extended Bruggeman theory proposed by Rouleau and Martin [114, 115]. Yet another proposal from Draine and Goodman [116] allows for the radiation reaction of the dipoles and dispersion in the medium.

The most appropriate model may depend upon the volume fraction of the dipole particles. Lumme and Rahola [117] give

$$\frac{m_{\text{eff}}^2 - 1}{m_{\text{eff}}^2 + 2 + \nu(m_{\text{eff}}^2 - 1)} = f_v \frac{m^2 - 1}{m^2 + 2 + \nu(m_{\text{eff}}^2 - 1)}$$

For $\nu = 0$ this reduces to the Maxwell–Garnett equation and for $\nu = 1$ it is equivalent to Bruggeman theory. From numerical calculation these authors conclude that

f_v	ν
0.52	−0.3 to 0.3
0.41	0
0.3	0.3

Lakhtakia and Vikram [118] have also proposed a modified form of the Maxwell–Garnett equation which allows for the finite size of the particles. This takes the form

$$m_{\text{eff}} = m_1 \frac{\left(1 + \frac{2\alpha f_v}{3}\right)^{1/2}}{\left(1 - \frac{\alpha f_v}{3}\right)^{1/2}}$$

where

$$\alpha = \frac{(m_2/m_1)^2 - 1}{1 - \left[(m_2/m_1)^2 - 1\right]\left[\frac{2}{3}(1 - ikam_1)\,e^{ikam_1} - 1\right]}$$

Subscript 1 refers to the surrounding medium and subscript 2 to the particles. The authors claim that the method is suitable for $|kam_j| \leq \pi/5$, where j is 1 or 2, and $0 \leq f_v \leq 0.2$.

Drolen and Tien [119] and Dobbins and Megaridis [120] have explored treating spherical agglomerates approximately as solid spheres with an equivalent refractive index calculated using Maxwell–Garnett theory. Dittman [121] has also proposed a method for agglomerates employing an equivalent refractive index but only including first-order multiple scattering, which is claimed to be sufficient.

The successive approximation method is efficient for small particles but does not converge for large particles. As an example, it is necessary that $x < 3$ for $m = 1.33$. x increases as m decreases. For the full coupled dipole approach very many dipoles may be needed. For example, Goodman et al. [122] found for $m = 1.33 + i0.01$ and $x = 10$ that 3×10^4 were required. The number scales as $(x|m|)^3$. The computational requirements quickly become excessive, even using a Cray-2 [123]. In their review Draine and Flateau [110] show that the method can be accurate for $|m| < 2$ and they discuss a solution technique which permits up to 10^5 dipoles and $x \leq 10$.

A simplifying suggestion has been proposed by Kumar and Tien [124] which allows the internal fields of all the particles to be the same except for a phase term due to their relative positions. This approximation removes the need to solve simultaneous equations and is claimed to have good accuracy.

Methods for improving computer efficiency in solving the

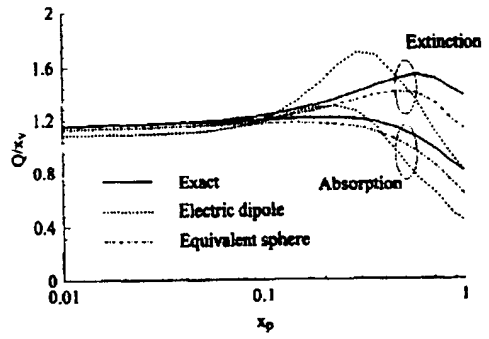

Fig. 8. Ratio of efficiency and volume equivalent size parameter, x_{ve}, for a cluster of 40 primary spheres of size parameter x_p. m = 1.6 + i0.6. (After Mackowski [133].)

simultaneous equations have also been discussed. For example, Flateau et al. [125] showed that for a rectangular array of sub-volumes the matrix has a block-Toeplitz structure. They were able to exploit this to improve the efficiency of the computation. Yung [126] suggested certain reductions from consideration of the requirement of reciprocity. Interestingly, however, Charalampopoulos and Panigrati [127] have raised the possibility that reciprocity may not hold for agglomerates, perhaps as a consequence of multiple scattering.

Bourrely et al. [128] have suggested that computational efficiency can be improved by not using a uniform distribution of dipoles. In their approach the particle was divided into inner and outer regions. The inner region contains larger dipoles with greater separation. Small closely spaced dipoles are only used near the surface. They claim their method to be more accurate, quicker and space-saving, and that it is better at describing the particle shape.

Recent applications of the coupled dipole method include porous particles [113, 129, 130], finite cylinders [131] and particles on a surface [132].

The accuracy of the method has been explored by Mackowski [133] by comparison with exact theory for multiple sphere clusters. Examples for the extinction and absorption efficiencies are illustrated in Fig. 8. The coupled dipole approach tends to underestimate the increase in absorption by a cluster. In a later paper Mackowski [134] showed that the internal field can be non-uniform, leading to errors in the coupled dipole method. However, an electrostatic analysis was explored for the case where the size of the cluster is much less than the wavelength, which was able to resolve the problem. Also, Rouleau [135] compared the calculations for dense clusters of up to 30 spheres against the exact solution. It was concluded that the dipole model was not satisfactory for large particles, and that equivalent refractive index models (such as Maxwell–Garnett) may be preferable.

Michel [136] and Michel et al. [137] have explored scattering by individual irregularly shaped particles using the so-called "strong permittivity fluctuation theory". They begin with an equivalent medium description and then extend it using a perturbation method. Essentially they solve the wave equation in the form

$$\vec{\nabla} \times \vec{\nabla} \times \vec{E}(\vec{r}) - k^2 \varepsilon_{\text{eff}}(\vec{r}) \vec{E}(\vec{r}) = k^2 [\varepsilon(\vec{r}) - \varepsilon_{\text{eff}}(\vec{r})] E(\vec{r})$$

where $\varepsilon(\vec{r}) - \varepsilon_{\text{eff}}(\vec{r})$ is small. The statistical properties were obtained by a Monte Carlo method to generate the clusters. For a cluster of 64 grains each of size parameter $x = 3.3 \times 10^{-5}$, they claim a scattering enhancement of twice that from an effective medium theory alone.

The coupled dipole method and the method of moments have been reviewed and compared by Lakhtakia and Mulholland [138]. They demonstrate that the two methods are equivalent. In a similar vein, Flateau et al. [139] have compared the two techniques for a system of two spheres and have found good agreement for $x \approx 10$.

A method gaining in popularity is the forward difference time domain (FDTD) technique. In this, the electric and magnetic fields are obtained by stepwise integration of the wave equation across the particle. Schlager and Schneider [140] have produced a wide-ranging review and Yang and Lion [141] give a good description of the method.

With advances in computing, new techniques promise radical improvements in speed and handling ability. In this context, Cwik et al. [142] have discussed the application of massively parallel computation to integral equation techniques in light scattering.

Reviews of numerical techniques have been given, for example, by Bates [143], Yaghjian [144], Miller [145] and Bohren and Singham [146].

4. Approximations

Rigorous solutions of the scattering problem, whether analytical or numerical, are complicated and tend to involve considerable computer time and storage for all but the simplest shapes and smallest particles. For certain ranges of size and refractive index, approximations may be used. Not only are these simpler and more readily computable, but they often provide insight into the scattering process.

We shall consider the various approximations roughly in terms of increasing size.

4.1. Rayleigh scattering ($x \ll 1$; $x|m - 1| \ll 1$)

The limitations imposed ensure that the incident electric field is uniform both within and around the particle. It then oscillates as a simple dipole. For incident polarization along the x-direction it can be shown that

$$\vec{E}_{\text{sca}}(\vec{r}) = E_0 \frac{e^{ik_0 r}}{r} k_0^2 \gamma \left(\cos\theta \cos\phi \hat{\theta} - \sin\phi \hat{\phi} \right)$$

where ϕ is the angle between the plane of measurement and

$\hat{x}$. A similar result is obtained for incident polarization along $\hat{y}$, except that ϕ is replaced by $\phi + \pi/2$. For the case of orthogonal measurement planes

$$\begin{pmatrix} E_{\parallel,\mathrm{sca}} \\ E_{\perp,\mathrm{sca}} \end{pmatrix} = \frac{e^{ik_0 r}}{r} k_0^2 \gamma \begin{pmatrix} \cos\theta & 0 \\ 0 & 1 \end{pmatrix} \begin{pmatrix} E_{\parallel,0} \\ E_{\perp,0} \end{pmatrix}$$

From this

$$\begin{pmatrix} \mathfrak{I}_{\parallel,\mathrm{sca}} \\ \mathfrak{I}_{\perp,\mathrm{sca}} \end{pmatrix} = \frac{k_0^4 |\gamma|^2}{r^2} \begin{pmatrix} I_{\parallel,0} \cos^2\theta \\ I_{\perp,0} \end{pmatrix}$$

For unpolarized light

$$\mathfrak{I}_{\mathrm{sca}} = \frac{I_0}{r^2} \frac{1}{2} \left(1 + \cos^2\theta\right) k_0^4 |\gamma|^2$$

The cross-sections are

$$C_{\mathrm{sca}} = \frac{8\pi}{3} k_0^4 |\gamma|^2, \qquad C_{\mathrm{abs}} = -4\pi k_0 \,\mathrm{Re}(i\gamma)$$

For a sphere

$$\gamma = \frac{3V}{4\pi} \frac{m^2 - 1}{m^2 + 2}$$

where V is the volume of the particle. It follows that

$$Q_{\mathrm{sca}} = \frac{8}{3} x^4 \left| \frac{m^2 - 1}{m^2 + 2} \right|^2, \qquad Q_{\mathrm{abs}} = 4x \,\mathrm{Im}\left(\frac{m^2 - 1}{m^2 + 2} \right)$$

For ellipsoids there are three polarizabilities corresponding to the three axes. These are given by

$$\gamma_j = \frac{V}{4\pi} \frac{m^2 - 1}{1 + (m^2 - 1) L_j}$$

The L_j are related through

$$L_1 + L_2 + L_3 = 1$$

In general the L_j are given by complicated integrals. However, simplification occurs for certain situations [1, 2]. For a cloud of randomly oriented ellipsoids

$$\gamma = \frac{1}{3}(L_1 + L_2 + L_3)$$

By comparison with Mie theory, Kerker et al. [147] have suggested that for agreement within 1%, Rayleigh theory can be used for $x|m| \leq 0.2$. For agreement to within 10%, $x|m| \leq 0.5$. Similar work by Ku and Felske [148] suggested that Rayleigh theory was correct to within 1% for all $x \leq 1$ except for soft particles of low absorption ($m_1 < 1.2$; $m_2 < 1$). There seems to be a certain element of contradiction between these two conclusions.

The theory can be extended to slightly larger particles by expanding the scattering coefficients in the form of polynomials in x. Penndorf [149, 150] has provided an expansion for the efficiency factors of spheres, which is useful up to about $x = 1.4$ and $m = 2$ for dielectric spheres. For absorbing material the limit is $x = 0.8$ for $1.25 \leq m_1 \leq 1.75$ and $m_2 \leq 1$. This expansion has also been discussed by Selamet and Arpaci [151]. A series expansion for the field scattered by ellipsoids has been given by Stevenson [152], which appears to be limited to $kb \leq 0.95$ where b is the semi-major axis.

4.2. The Rayleigh–Gans–Debye (RGD) or Born approximation ($|m - 1| \ll 1$; $x|m - 1| \ll 1$)

The two titles of this approximation arise due to different approaches, but they produce the same result. The RGD concept can be understood with the aid of Fig. 9. Because the scatterer is "soft" ($|m - 1| \ll 1$) there is very little reflection of the incident field. Also since ($x|m - 1| \ll 1$) there is very little phase shift inside the particle. As a result of these two constraints, the internal field is approximately the same as the incident field in the absence of the particle.

Since the incident field is divergenceless, the integral equation for the scattered wave becomes

$$\vec{E}_{\mathrm{sca}}(\vec{r}) = k_0^2 \int_{V'} \left(m^2 - 1\right) E_{\mathrm{inc}}(\vec{r}\,') G(\vec{r}, \vec{r}\,') \, dV'$$

For incident polarization along $\hat{x}$ it is found that

$$\vec{E}_{\mathrm{sca}}(\vec{r}) = \hat{x} R_0 k_0^2 \left(m^2 - 1\right) \frac{V'}{4\pi} R(\theta, \phi)$$

and the intensities are

$$\begin{pmatrix} \mathfrak{I}_{\parallel,\mathrm{sca}} \\ \mathfrak{I}_{\perp,\mathrm{sca}} \end{pmatrix} = \frac{k_0^4 V^2 |m^2 - 1|^2}{16\pi^2 r^2} |R(\theta, \phi)|^2 \begin{pmatrix} I_{\parallel,0} \cos\theta \\ I_{\perp,0} \end{pmatrix}$$

Kerker [2] gives values for $R(\theta, \phi)$ for a number of cases. Two examples are: the sphere

$$R(\theta, \phi) = 3 j_1(u)/u$$

and the infinite cylinder at normal incidence

$$R(\theta, \phi) = 2 J_1(u)/u$$

where $u = 2x \sin(\theta/2)$ and j_1 and J_1 are spherical and cylindrical Bessel functions.

The range of validity for spheres has been investigated by Kerker et al. [153], Farone et al. [154] and Heller [155]. For accuracy to better than 10%, $m \leq 1.25$ and $x \to 0$ are required. The maximum value of m decreases as x increases.

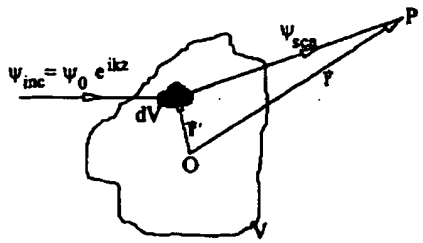

Fig. 9. Illustration of the RGD method. The origin of coordinates is at O and the scattered wave is received at P. The undisturbed incident wave is scattered by the element of volume dV.

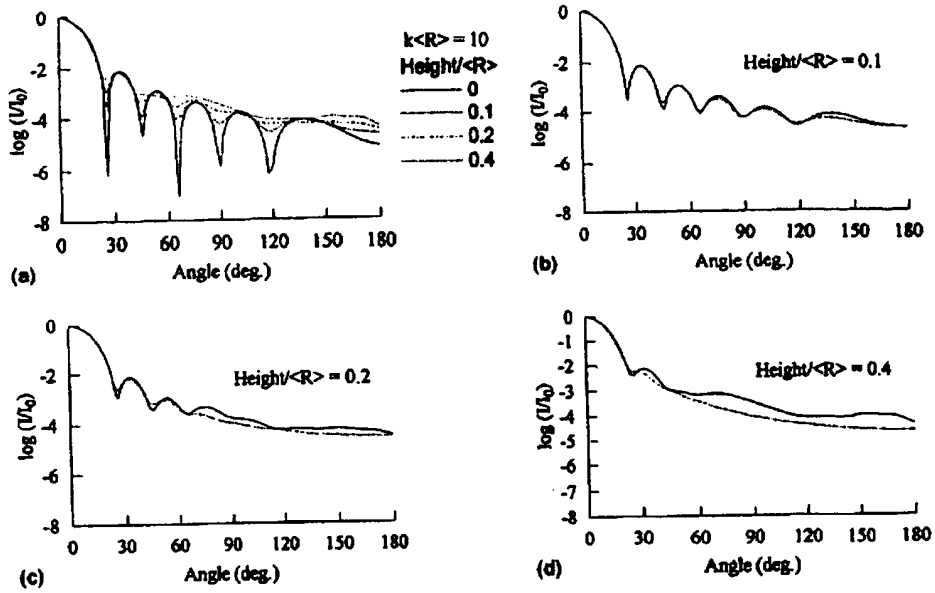

Fig. 10. Scattering by irregular particles in the RGD approximation: (a) influence of height of the irregularity for a mean size parameter of 10; (b)–(d) comparison of scattering by irregular particles (solid line) and a cloud of spheres (dashed line) with the same mean size parameter of 10 and a size distribution equal to the probability distribution of radius. (After Al-Chalabi and Jones [162].)

Latimer and co-workers [156–158] have compared models for ellipsoids, and developed equivalent sphere relations which can be used for $m < 1.5$. Barber and Wang [159] compared RGD with EBCM for a prolate spheroid for $m = 1.05$ and $2x|m - 1| \leq 1.0$. They concluded that errors of up to 20% can occur depending on orientation. The worst case is when the major axis is parallel to the incident electric vector. Best agreement was found for random orientation.

A loose agglomerate of small particles is a candidate for treatment by the RGD method, since it may be argued that the incident wave would propagate through the structure with relatively little change. This approximation removes the need to solve simultaneous equations and is claimed to have good accuracy. The range of validity of such an approximation for a fractal structure was explored by Farias et al. [160, 161]. Fractal structures are discussed later.

A recurring problem in light scattering is the treatment of irregular particles. One method would be to calculate the scattering by a large number of particles individually and then add the results together allowing for random position and orientation. However, since the particles are random in nature, it is preferable to employ a statistical analysis on a cloud directly. This saves considerably on computer effort. Al-Chalabi and Jones [162] performed such an analysis using the RGD approximation. They found that the result depended upon the probability distribution of radius (mean radius and standard deviation) and a correlation function in the surface. As might be expected, increasing height of the irregularities caused increasing smoothing of the scattering polar diagrams and enhanced backscatter. There was also a suggestion that the irregular particles could be treated as a cloud of spheres with a size distribution equal to the probability distribution of radius, provided that the height of the irregularity was not too large. This can be seen in Fig. 10.

A drawback to the RGD approximation is that it does not permit the introduction of polarization effects due to anisotropic particles. Haracz et al. [163] used a modified version in an attempt to overcome this problem. In this, the basic Rayleigh-sized spherical sub-volumes were replaced by ellipsoids, which is equivalent to introducing an anisotropic refractive index. This approach was also used by Jones and Savaloni [164] to explore scattering by finite cylinders at random orientation. Ruppin [76] examined the validity of this calculation by using EBCM. Good agreement was found for axial ratios greater than 10, and, generally, for $m \leq 1.1$ or for $x \leq 1$.

4.3. The Wentzel–Kramers–Brillouin (WKB) approximation

The RGD or Born approximation can be extended in a number of ways. A simple approach, for example, is to allow for the phase shift in the incident wave as it penetrates the particle. For a sphere we may then write

$$\vec{E}(\vec{r}) = \vec{E}_0 \, e^{imk_0(R+z')}$$

where z' is distance along the axis.

The Wentzel–Kramers–Brillouin (WKB) approximation

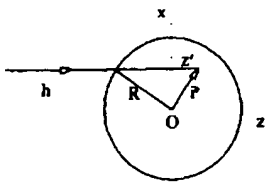

Fig. 11. Illustration of the WKB method.

is similar except that the phase is allowed to vary with distance from the axis according to the particle shape, presuming rectilinear propagation. Klett and Sutherland [165] have noted that this approximation is much improved if allowance is made for internal reflection from the back face of the particle. In this so-called "two-wave" WKB method, the internal field in a sphere for a ray entering a distance h from the axis, as in Fig. 11, would have the form

$$\bar{E}(\bar{r}) = \bar{E}_0\, e^{ik_0(m-1)s}\left\{e^{ik_0mz'} + \frac{m-1}{m+1}\, e^{ik_0m(2s-z')}\right\}$$

where $s = \sqrt{R^2 - h^2}$. Jones et al. [166] have generated error contour charts for the two-wave method. They demonstrated that this was superior to both the RGD and single-wave WKB models. Nonetheless, the range of application is very limited especially at angles greater than 90°.

Further extensions may include allowance for reflection loss on incidence by using the Fresnel equations, and for refraction. The eikonal approximation is similar [167–169]. Similar methods have been employed by Sharma and Somerford [170] to provide simple equations for backscattering by soft obstacles. Roy and Sharma [171] have compared various soft particle approximations.

4.4. Fraunhofer diffraction ($x \gg 1$; $|m - 1| \gg 1$)

This well-known approximation is valid for large obstacles and unpolarized light and scattering close to the forward direction. For a sphere, Hodkinson [172] gives

$$\mathfrak{I}_{sca} = I_0 \frac{\pi^2 D^4}{16\lambda^2}\left[\frac{2J_1(x\sin\theta)}{x\sin\theta}\right]^2 \cdot \frac{1}{2}\left(1 + \cos^2\theta\right)$$

The term in the square bracket is the Airy function. It suggests that the shape of the scattering pattern depends only on size and is independent of refractive index. Indeed, it results in the well-known expression

$$\sin\theta = \frac{1.22\lambda}{D}$$

for the angular position of the first minimum in intensity.

Jones [173] has produced error contour charts comparing Fraunhofer diffraction with Mie theory. For transparent particles the discrepancy is less than 20% for $m > 1.3$ and $x \geq 20$ (≥ 3 μm at visible wavelengths). For absorbing particles, however, errors of less than 20% occur for $m_i > 1.2$ and $x \geq 6$ (≥ 1 μm at visible wavelengths).

For non-absorbing particles of very low refractive index (< 1.1) there is some error even for large particles. This is caused by transmission of the incident wave which interferes with that diffracted, leading to anomalous diffraction. Kusters et al. [174] concluded that serious errors could occur if this effect was not taken into account. However this is simple to do in practice.

It is commonly found that forward scatter is also insensitive to particle shape (e.g. Pollack and Cuzzi [175] and Zerull et al. [176]). This was explored for irregular particles by Jones [177] and Al-Chalabi and Jones [178], who confirmed the lack of sensitivity to shape. As discussed for the RGD approximation, the important parameters were the probability distribution of radius and the correlation function in the surface. The diffraction approach also suggested that the cloud of irregular particles could be modelled as a cloud of spheres with size distribution equal to the probability distribution of radius for small height of irregularity. A diffraction approach to scattering by irregular crystals has been discussed by Muinonen [179].

Complicating factors are introduced by the nature of laser beams and the physical properties of optical components. Diffraction by a particle in a Gaussian beam has been explored by Gréhan et al. [180] and Lock and Hovenac [181]. Good agreement was found between measurement and calculation using the generalized Mie theory. As part of their study the latter authors demonstrated how the Kirchhoff integral can be derived from rigorous theory. In addition, lenses introduce phase changes. This effect has been pursued by Lebrun et al. [182], who applied thin lens theory to provide corrections to the diffraction pattern.

If the concentration is too high, multiple scattering occurs and alters the diffraction pattern so that Fraunhofer theory no longer applies. However, empirical evidence suggests that, in practice, the extinction can be as high as 50% before multiple scattering has to be considered [183, 184].

Various attempts have been made to correct for multiple scattering. A correction at the onset of multiple scattering by use of a first order term from radiative transfer theory has been considered by Schnablegger and Glatter [185].

More complete attempts have been made. The first of these was due to Felton et al. [186] with further development by Hamidi and Swithenbank [187] and Cao et al. [188] The scattering volume was divided into a series of slices, each sufficiently thin that only single scattering occurs within it. The first slice sees only the incident wave and scatters some fraction F according to Fraunhofer diffraction. The second slice sees the incident wave reduced in intensity by F plus the light scattered by the first slice, and so on. By following this procedure through the whole volume, the light distribution at the detector rings is found. The authors provided correction procedures which were claimed to extend the applicable range of the diffraction method to extinctions in excess of 90%.

A different approach has been employed by Hirleman [189] which uses statistics to predict the small-angle light

distribution after many scattering interactions. His results agree well with those of the other authors except at high ring numbers (large angles). Hirleman attributes this to the fact that, in the previous method, a photon scattered out of the system of slices cannot be scattered back in, whereas his method allows for this.

Woodall et al. [190] attempted to get away from plane media by examining the case of a cylinder, which is more suitable to the case of a spray. Their theoretical approach involved the use of the radiative transfer equation and Monte Carlo methods. They found that, due to multiple scattering, the errors in the parameters of a log-normal size distribution could be 25% for the Sauter mean diameter and 50% for the standard deviation for the case of $\tau = 3$.

4.5. Anomalous diffraction ($x \gg 1$; $|m - 1| \ll 1$)

At very low refractive index, the particle transmits light almost without deflection. This then interferes with the diffracted light, producing anomalous diffraction. The scalar diffraction integral equation for a circular aperture becomes:

$$\psi = 2\pi\psi_0 \frac{e^{ik_0 s'}}{s'} \int_0^R K(\theta)\left[1 - e^{ik_0\delta}\right] J_0(k_0\rho \sin\theta)\rho \, d\rho$$

where s' is the distance from the aperture to the screen or detector. $K(\theta)$ is the inclination factor[191] and

$$\delta = 2(m - 1)\sqrt{R^2 - \rho^2}$$

For non-absorbing particles the extinction efficiency is

$$Q_{ext} = 2 - \frac{4 \sin\omega}{\omega} + \frac{4(1 - \cos\omega)}{\omega^2}$$

where $\omega = 2x(m - 1)$.

Chýlek and Klett [192], Streekstra et al. [193] and Fournier and Evans [194] have discussed non-spherical particles. In the latter case, the extinction efficiency for randomly oriented spheroids was checked for aspects ratios between 0.5 and 4 with $1.01 \leq m_1 \leq 2$ and $0 \leq m_2 \leq 1$. More recently, Evans and Fournier [195] have provided an expression for the direct calculation of the average extinction efficiency ($\overline{Q_{ext}}$) for randomly oriented spheroids. Evans and Fournier [196] have provided means of directly calculating the averaged extinction efficiency factor.

Sharma [197] suggests that a more appropriate criterion for validity of anomalous diffraction may be $|m - 1|^2 \ll |m + 1|^2$ as opposed to $|m - 1| \ll 1$. It was found by comparison with Mie theory that anomalous diffraction could work for m as large as 2. In later work Sharma [198] has suggested an improved form for Q_{ext} obtained from expansion of the eikonal method. He proposes

$$S(0)_{II} = C(m)S(0)_{ADA}$$

$$C(m) = 1 + \frac{1}{4}(m + 1)^2(m - 1)(2 - m)^2$$

This is claimed to be valid for $x(m^2 - 1)^2 < 4$.

Stephens [199] performed similar calculations for circular cylinders. He found, surprisingly, that Q_{ext} reduced to the correct form for the limit as $x \to 0$ as well as for $x \to \infty$.

Chýlek and Li [200] have discussed the boundary between the RGD and anomalous diffraction regions where $x \gg 1$ and $x|m - 1| \ll 1$. In particular, they derive expressions for the efficiency factors. For a complex refractive index $m = m_1 + im_2$ they obtain

$$Q_{ext} = 2km_2 \frac{V}{A} + k^2\left[(m_1 - 1)^2 - m_2^2\right]\frac{1}{A}\int\int_A l^2 \, dA$$

$$Q_{abs} = 2km_2 \frac{V}{A} - 2k^2 m_2^2 \frac{1}{A}\int\int_A l^2 \, dA$$

where A is the cross-sectional area and V is the volume. l is the geometric path inside the particle, and

$$V = \int\int_A l \, dA$$

The extension of anomalous diffraction theory to allow for vector properties has been discussed by Bourrely et al. [201]. The method was applied to large spherical particles by an eikonal approximation to Mie theory. Anomalous diffraction by anisotropic scatterers has been considered, for example, by Meeten [202].

There have been a number of interesting recent studies. For example, Maslowska et al. [203] made comparison with the coupled dipole method for calculating scattering by cubes. They found that anomalous diffraction was not satisfactory for certain orientations and that care must be exercised in the application to non-spherical particles. Whitehead et al. [204] applied the technique to liquid crystal drops immersed in a polymer and Khlebtsov [205] to fractal clusters.

4.6. Geometrical optics ($x \gg 1$; $x|m - 1| \gg 1$)

Geometrical optics may be treated by a combination of Fraunhofer diffraction in the forward direction with reflection and refraction at larger angles. Discussions and summaries are given by van de Hulst [1], Kerker [2], Emslie and Aronson [206] and Ungut et al. [207]. The latter authors compared the results with Mie theory for $\theta < 20°$ and found good overall agreement for $x \geq 90$ (≥ 15 μm in the visible) and reasonable agreement for $x \geq 60$ (≥ 10 μm in the visible) at a refractive index of 1.5. However, agreement failed at certain specific sizes due to interference effects.

Glantschnig and Chen[208] produced an approximate geometrical solution in closed form. Agreement with Mie theory was good at small angles for $D \geq 5$ μm in the visible. They also concluded that $\Im_{sca} \propto D^2$ provided

$$x\Delta\alpha \geq 4\pi$$

where $\Delta\alpha$ was the angle subtended by the detector at the scattering centre.

Shipley and Weinmann [209] made comparisons with

Mie theory in the range $200 \leq x \leq 4520$ for $m = 1.333$. They found very good agreement except at angles near grazing incidence and those associated with the rainbow or glory.

There has been considerable discussion on the correct way to calculate efficiency factors. Cohen et al. [210] and Acquista et al. [211] propose

$$\lim_{x\to\infty} Q_{sca} = 1 + \int_0^{2\pi} [|R_1|^2 + |R_2|^2] \cos\theta \sin\theta \, d\theta$$

where R_1 and R_2 are the Fresnel reflection coefficients.

Senior [212] has been able to prove that

$$\lim_{x\to\infty} Q_{ext} = 2$$

for perfectly conducting spheres. Nussenzveig and Wiscombe [213] have given

$$Q_{ext} = 2\left(1 + x^{-2/3}\right)$$

Bohren and Nevitt [214] have produced an equation for Q_{abs} which appears to be accurate over a wide range of sizes and absorption indices. This is

$$Q_{abs} = \frac{4m_1^3}{(m_1+1)^2 - (m_1-1)^2 e^{-\tau}} \times \left\{ \frac{1}{m_1^2} - \frac{2}{\tau^2} e^{-\tau\sqrt{m_1^2-1}} F - (1+\tau) e^{-\tau} \right\}$$

where

$$F = 1 + \frac{\tau}{m_1}\sqrt{m_1^2 - 1}, \qquad \tau = 4xm_2$$

It agrees very well in both the limits $\tau \ll 1$ and $\tau \to \infty$.

Kokhanovsky and Zege [215] have proposed equations for the efficiency factors due to spherical polydispersions. They essentially employ geometrical optics but include the influence of edge effects which are determined by subtracting the pure geometrical optics results from those of Mie theory. In a further paper [216] they provide a general review of approximations for efficiency factors.

There is continuing work on the application of geometrical optics to non-spherical particles. Ravey and Mazeron [217, 218], Hovenac [219], Lock [220, 221] and Macke et al. [222] have produced theories for large spheroids. The latter authors suggest that ray tracing is more effective for spheroids than for spheres and can be used for $x \geq 60$ except for the prediction of polarization effects. Similarly, Mishchenko et al. [223] examined the application to finite cylinders by comparison with the *T*-matrix method and concluded that geometrical optics cannot adequately describe polarization effects.

Bottlinger and Umhauer [224, 225] have considered the applications of ray tracing to individual irregular particles in which they were treated as a set of successive slices. Muinonen et al. [226] also looked at this problem but treated the particles as random structures constructed from log-normal size distributions of height and allowing for the correlation function in the surface.

Other interesting situations considered include inhomogeneous particles [227], hexagonal crystals [228] and ice crystals with inclusions [229].

5. Multiple scattering

5.1. Independent scattering

As we saw in Section 2, if the path length through a particle cloud is greater than or of the order of the optical mean free path, then multiple scattering becomes significant. This can be visualized by imagining streams of photons entering the scattering medium. If the particle concentration is sufficiently low, a photon once scattered has a low probability of being scattered again before leaving the medium provided the depth of the particle cloud is not too large. If the depth or concentration increases then so does the probability of further scattering events. In dense or extensive media a photon may be scattered a very large number of times before eventually emerging.

As described above, the scattering events are independent of each other. It was suggested in Section 2 that a separation of three diameters may be sufficient for this. Provided this condition holds, the individual scattering events may be described by a theory appropriate to a single particle (e.g. Mie theory for a sphere). The only unknown is the amplitude of the incident wave, which must be obtained from a knowledge of the previous scattering events.

Further, if there is a large number of particles randomly positioned in space, then incoherent superposition applies and intensities may be added directly. This is a stochastic process, and, indeed, one way of predicting multiple scattering is the so-called Monte Carlo method [230–239]. As its name implies, this is a technique which uses random numbers to predict the direction of scattered photons, the probability of any direction being given by the appropriate scattering theory. The probability of distance travelled before a further scattering event is determined by the particle concentration, and a random number decides the actual distance.

The Monte Carlo method is straightforward and simple to apply. The major drawback is in the computer time involved. According to Poisson statistics, the error after N scattering events is $\sqrt{N}$, so that the fractional error is $1/\sqrt{N}$. This means that a very a large number of "tries" has to be made if the multiple scattering is to be predicted to any degree of accuracy.

The Monte Carlo method employs successive singular scattering. There have been attempts to tackle this approach analytically. For example, Hottel and Sarofim [240] give expressions for the transmissivity and reflectivity of a plane slab. Similar concepts were employed by Deepak and Green [241] and Zahavi [242]. At sufficiently high concentrations the random scattering process results in

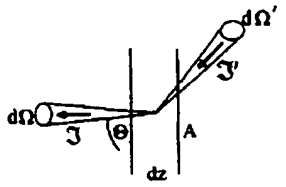

Fig. 12. Illustration of terms in the radiative transfer equation.

photons behaving in a manner similar to diffusion. This was the concept used by Rosseland [243].

Perhaps the most popular method for tackling multiple scattering is the radiative transfer equation with the multi-flux method of solution. This has the advantage of simplicity and the ease of physical understanding if the number of fluxes is small. The simplest is the two-flux method which leads to the Kubelka–Munk [244] equations which are widely used wherever there are reflecting layers. Typical examples are the paint and the food industries to describe thin films, such as of butter. The radiative transfer equation is also used particularly in radiative heat transfer, where an extra term is added to allow for thermal emission.

To obtain the radiative transfer equation for multiple scattering the approach is similar to that in Section 2, except that we have to allow for radiation incident from other directions in the particle cloud being scattered into the direction of the incident beam.

The situation is as in Fig. 12. Radiation of intensity $\Im'$ incident within the solid angle $d\Omega'$ is scattered through the angle Θ' into solid angle $d\Omega$ in the forward direction. The incident intensity, as opposed to irradience, is $\Im$. As previously, the scattering and absorption losses add to

$$dP_1 = -\Im K_{ext}\, dz\, dA\, d\Omega$$

Now, however, we have to add the gain due to in-scatter. For simplicity, we examine a single particle illuminated by the intensity $\Im'$. The power incident is

$$\Im' \frac{\pi D^2}{4}\, d\Omega'$$

From the definition of the phase function, the fraction of this scattered through the angle Θ' into $d\Omega$ is

$$\frac{1}{4\pi} p(\Theta') Q_{sca}\, d\Omega$$

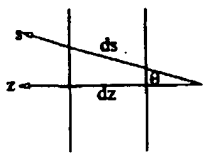

Fig. 13. Illustration of a ray passing at the angle θ through a slab.

For N such particles per unit volume the increase in power is

$$dP_2 = \Im' \frac{\pi D^2}{4}\, d\Omega' \frac{1}{4\pi} p(\Theta') Q_{sca}\, d\Omega\, N\, dV$$

$$= \Im' p(\Theta')\, d\Omega' \frac{K_{sca}}{4\pi}\, dz\, dA\, d\Omega$$

However, this is the contribution from one direction of incidence only. Integrating over all directions and adding the two terms we find the total change in intensity to be (since $dP = d\Im\, dA\, d\Omega$)

$$\frac{d\Im}{dz} = -\Im K_{ext} + \frac{K_{sca}}{4\pi} \int_{4\pi} \Im' p(\Theta')\, d\Omega'$$

We now make a modification to allow for the fact that we may be considering a ray not propagating normally to the faces of the slab. In general it may pass at an angle, as in Fig. 13. Then the path length ds is

$$ds = dz/\cos\theta$$

and we have

$$\cos\theta \frac{d\Im}{dz} = -\Im K_{ext} + \frac{K_{sca}}{4\pi} \int_{4\pi} \Im' p(\Theta')\, d\Omega'$$

Writing $\eta = \cos\theta$, $\omega_0 = K_{sca}/K_{ext}$, where ω_0 is the albedo, and $\tau = K_{ext}x$, where τ is the turbidity, we find

$$\eta \frac{d\Im_\lambda}{d\tau} = -\Im_\lambda + \frac{\omega_0}{4\pi} \int_{4\pi} \Im_\lambda' p(\Theta)\, d\Omega'$$

Kubelka and Munk [244] proposed the pair of equations

$$\frac{dq^+}{dx} = -(K+S)q^+ + Sq^-$$

$$-\frac{dq^-}{dx} = -(K+S)q^- + Sq^+$$

for fluxes travelling in the positive and negative directions. From the radiative transfer equation it can be shown for isotropic scattering ($p(\Theta) = 1$) that $S \equiv K_{sca}$ and $K \equiv 2K_{abs}$. In general there is no such simple relationship. However, relationships have been found for a number of cases (e.g. Bayvel and Jones [5]).

In principle, the multi-flux method can be as accurate as required by taking many fluxes and expanding the phase function such that it resembles real particle scattering (e.g. Mudgett and Richards [245]).

In view of the development of lasers there has been much interest in the transmission and reflection of collimated Gaussian beams and pulses. Examples of the former include the work of Beckett et al. [246], Stotts [247], Look et al. [248], Zege and Kokhanovsky [249] and Ito [250]. Pulse spreading and broadening has been considered, for example, by Prahl et al. [251], van de Hulst and Kattawar [252], Shifrin and Zolotov [253] and Brewster and Yamada [254].

Marquet et al. [255] used radiative transfer theory to predict the intensity profile of a transmitted beam, which they characterized in terms of the maximum and full

width at half the maximum intensity. From this they were able to measure the scattering and absorption coefficients using a CCD array to display the profile.

5.2. Dependent scattering

When the particles approach closer than the limits suggested above there is direct interaction of the electric fields. The scattering by an individual particle is no longer independent since the incident field is modified by the presence of all the others. Also, the scattering becomes at least partly coherent and amplitudes have to be added.

There are essentially two approaches to the problem of dependent scattering. The first is to develop the integral equation formulation in such a way that the volume integration is carried out over the volumes of all the particles present. In its simplest form this is an extension of the coupled dipole approximation discussed in Section 3.2. where the dipoles are formed into groups each of which represents a particle (e.g. Kattawar and Humphreys [256]).

The alternative approach is the boundary condition method. In principle, the method of point matching could be applied to solve the boundary conditions on every sphere. This would be very time-consuming and would suffer from the usual convergence problems associated with this method.

To provide a rigorous solution it is necessary to be able to expand the boundary conditions on any one sphere about the centre of the coordinate system. This was achieved for two spheres, for example, by Levine and Olaofe [257] by the use of bispherical coordinates. More recent studies on two spheres include those by Barton et al. [258] and Fuller [259]. A study of a carbon particle both inside and attached externally to a water drop was studied by Fuller [260, 261] with relevance to absorption by atmospheric aerosol. Mishchenko et al. [91] have applied the T-matrix method to the problem of two spheres.

More generally, a vector addition theorem has been developed which allows this procedure to be carried out for many spheres [262–270]. This approach has also been employed by Quinten and Kreibig [271] in the limit of very small particles, which then becomes equivalent to the coupled dipole approximation. Hamid et al. [272], Popovic and Notaros [273] and Xu [274] have proposed iterative techniques which do not involve matrix inversion and, thus, avoid problems with ill-conditioning.

The suggestion that a separation of three diameters is sufficient to ensure that interaction between scatterers is negligible has been explored by Ivezic and Menguc [275] for two Rayleigh-sized spheres. They found that a separation of three radii was sufficient for interaction not to influence absorption. However, for scattering the separation must be greater than twice the radius divided by the size parameter of the assembly. From their calculations they suggested that the ratio K_{sca}/K_{abs} may be used to indicate the presence of agglomeration as well as the phase function.

Other situations that have been examined include two infinite cylinders [276–278]. An experimental study of the case of two parallel fibres has been undertaken by Padmabandu and Bickel [279]. Arrays of cylinders have been explored by Bever and Allenbach [280]. Cooray and Ciric [281] give an analytical solution for two arbitrarily oriented dielectric spheroids and Sebak [282] discusses TM scattering by two parallel elliptical cylinders. The problem of two spheres has been extended by Hamid et al. [283] to the situation where they are both stratified. Both the full boundary condition solution and an iterative technique were used.

6. General comments on experimental methods

We have seen that the properties of the scattered light depend upon the particle size, shape, orientation, refractive index, and concentration. Thus, in principle, it is possible to use light scattering to measure all of these parameters. This section reviews techniques aimed at measuring such properties of particles. It will be assumed that visible wavelengths are employed, unless it is specifically stated otherwise.

There are two approaches to light scattering measurements:

1. *Integral methods*. In this case large numbers of particles are viewed simultaneously. The scattered intensity is assumed to arise from incoherent superposition. This implies moderate to high concentrations and a significant sample volume. The lower the concentration, the larger the required volume. The resulting intensity comes from integration over space, and a spatial average is obtained. A spatial distribution can only be recovered directly if the total cloud is somewhat larger than the test volume.
2. *Particle counting*. In this group particles are viewed one at a time. This implies moderate to low concentrations and a small sample volume. The higher the concentration, the smaller the volume must be. The size distribution is built up over time and a temporal average is obtained, which differs from the spatial average. This is easy to see. If we imagine two particle sizes with the same concentration but one having twice the velocity, then the faster particles will be counted at twice the rate and their concentration will be apparently doubled. If a spatial average is required then a conversion can only be made if the velocities of the particles are known. If a spatial distribution is needed this must be built up over time by continuously repositioning the test volume.

Particle counting introduces another problem. In the integral techniques it is usually assumed that the particles are uniformly distributed within the test space. Any one small part of the sample volume sees the same size distribution and concentration as any other. It is then unimportant whether the light intensity varies within the test space. (Of course, to ensure that this is so, the test volume must be small in comparison to the scale of any variation within

the particle cloud.) In particle counting the position of the single particle is of paramount importance. A small particle near the centre of a Gaussian beam may yield the same scattered intensity as a large one near the edge. Thus there is a trajectory problem.

There are three ways of overcoming this difficulty. The most obvious is to ensure that there is no variation of intensity within the test volume. This is the "top-hat profile" method. Unfortunately, the methods available for producing such a profile which also retain the coherent structure of the beam throw away much of the available light. The second technique employs deconvolution using previous knowledge of the structure of the test volume. Thirdly, it is often possible to choose a method of measurement involving relative variables (such as an intensity ratio or phase difference) rather than the absolute scattered intensity.

This highlights an important distinction between absolute and relative measurements. The absolute measurement of scattered intensity requires a knowledge of the incident intensity and of the response of the detection system. Thus the light source must be stable or monitored by a separate detector, and there must be no changes in intensity along either the path to the test volume or from there to the detection system. The response must normally be obtained by calibration. A relative measurement has neither of these requirements in general, and is to be preferred if practicable. Typical relative measurements would be intensity ratio, for example at two or more scattering angles (including polar diagram methods or the shape of the forward lobe) or at various wavelengths, polarization ratio, and in laser Doppler methods the visibility and phase difference. Of these the visibility method can present a problem as it relies on an intensity balance between two beams.

The advantage of using scattered intensity lies in its simplicity and its wide dynamic range, which is only limited to be between the noise level of the detection system and saturation. This can be extended by the use of neutral density filters and higher incident light intensity. Relative methods vary both in dynamic range and ease of use. The choice of appropriate technique depends upon the circumstances, but the most widely used are reviewed later.

Finally, it is worth noting some problems which commonly arise in the presence of gases, particularly hot gases. These include:

1. *Density gradients.* The refractive index of a gas is inversely proportional to its temperature and proportional to its pressure. Temperature and pressure gradients give rise to refractive index gradients which deflect the light beam (the "schlieren effect"). The linear displacement is proportional to the gradient and the path length through the medium. This may be considerable in large-scale systems. It can lead to uncertainty in the position of the test space, which may continually be in motion due to turbulence, spreading of the light, yielding uncertainty in incident and scattered intensities, and fluctuations in received intensity. A problem particular to anemometry is that the fringes in the test space may be continually moving, leading to errors in the measured velocity [283].
2. *Gases and particles.* Gases are inevitable in most systems and particles are very common. Their significance to light scattering is twofold: they may interact with the incident and scattered light and they may radiate. The gases most commonly present (i.e. air) do not absorb in the visible and, apart from the effect of density gradients discussed above, they have no relevance unless particles of molecular size are being studied. However if infra-red or ultraviolet wavelengths are employed, for example, this is not so. Particles absorb, scatter and radiate at all wavelengths. The effects of absorption and scattering are to reduce the incident light intensity at the test space and the transmission of scattered light to the exit window. With the path lengths typical of large-scale combustion rigs, for example, these effects can be very significant. They can be avoided by using relative measurements. Thermal radiation adds intensity at all wavelengths. Since the energy is spread over a broad spectrum, its influence can be greatly reduced by the use of narrow pass interference filters. Where appropriate, phase-sensitive detection can also be employed. Relative measurements do not necessarily help overcome the effects of radiation.
3. *Access.* Many practical systems are enclosed and access is limited. This can dictate the technique to be employed. Often there are only two or three ports which severely restricts the possible scattering angles. If there is only one port then the use of backscattering is decreed. An alternative is to develop probes which can be inserted to lead the light in and out, but care must be taken to minimize disturbance to the system. Another problem with access is the presence of windows which inevitably become dirty. This reduces the incident and scattered light and, as before, presses the use of relative methods.

The discussion below begins with integral methods and then moves to particle counting. In both cases the trend is to move from the smaller particles to the larger. Finally, there are sections devoted to the determination of properties other than size, such as refractive index and shape, to specialized techniques like tomography and inertia measurement and the new interest of particles on or near surfaces.

7. Integral methods

7.1. Rayleigh particles

We begin by considering light scattering techniques for measuring the properties of particles which are very small compared with the wavelength, where the Rayleigh approximation holds. The intensity scattered by Rayleigh particles is too weak to detect from individuals, so that integral

scattering methods must be employed. Perhaps the simplest method for absorbing particles, such as soot, is to use ratio of scattering to extinction as proposed by van de Hulst [1]. We saw in Section 4.1 that the scattering is proportional to volume squared while absorption is proportional to volume. Where the volume is very small this means that where absorption exists it dominates. Consequently

$$K_{ext} \cong K_{abs}$$

Since

$$K_{abs} \propto N\overline{D^3}, \qquad K_{sca} \propto N\overline{D^6}$$

where the bar denotes average over all sizes, it follows that

$$\frac{K_{sca}}{K_{ext}} \propto \frac{\overline{D^6}}{\overline{D^3}} = D_{63}^3$$

Thus a size is measured which is biased by the size distribution. The concentration can be recovered from the extinction measurement.

The ratio of scattering to extinction also involves

$$\left|\frac{m^2-1}{m^2+2}\right| \Big/ \mathrm{Im}\left(\frac{m^2-1}{m^2+2}\right)$$

This shows that refractive index can be an important unknown. Its dispersion can also be significant. However, experiments by Bruce et al. [284] have suggested that $Q_{ext} \propto 1/\lambda$ over a wide range of wavelengths. This variation was also found by Choi et al. [285], who measured extinction by the soot in a rich acetylene/air flame and obtained the geometrical properties using a gravimetric technique. They suggested

$$K_{ext} = K_e f_v/\lambda$$

and

$$K_e \approx 8.6 \pm 1.5$$

However, Koylu and Faeth [286] combined extinction measurement with an RGD analysis for aggregates and proposed $Q_{ext} \propto 1/\lambda^{0.83}$.

For non-absorbing particles, van de Hulst [1] recommends the ratio of scattered intensity to equivalent refractive index of the particle cloud. The latter is given by

$$m' = m_0 + \frac{3NV}{2}\left(\frac{m^2-1}{m^2+2}\right)$$

where V is the volume of one particle and m_0 is the refractive index of the surrounding medium. The ratio again yields D_{63}.

7.2. Fractal agglomerates

Small particles dispersed in a fluid are commonly known to aggregate into large randomly branched structures. This is typical behaviour of soot in flames, for example. The method above relied upon $K_{ext} \cong K_{abs}$. However, Ku and Shim [287] point out that since the scattering by particles in an agglomerate is proportional to the square of the number, this assumption may no longer be valid.

Because of the random nature of the agglomerate it has recently become popular to treat them as fractals. In this, the number of individual spheres N inside a cluster with radius of gyration R_g is written

$$N = K_f\left(R_g/r_0\right)^{D_f}$$

where r_0 is the radius of the individual sphere and D_f is the fractal dimension. It is dubious whether the agglomerate is a true fractal, as its properties are not independent of scale. This "self-similarity" is a fundamental property of fractals which does not appear to be satisfied here. Nonetheless, the fractal description is proving to be a very convenient and powerful diagnostic tool.

Quoted values of the fractal dimension vary. Depending upon the material it is usually in the range 1.5 to 2.0. Koylu et al. [288] point out that to fully characterize the agglomerate, the constant K_f must also be known. The specific form suggested for soot is [289]

$$N = 2.27\left(\frac{R_g}{r_0}\right)^{1.82}$$

The authors claim that this is not sensitive to fuel type or flame condition. Sorensen and Feke [290] find $D_f = 1.8$ but $K_f = 1.7$, and claim that the fractal morphology is constant for agglomerates ranging from assemblies of 10 up to 10^8 particles.

The fractal dimension appears to depend upon the history of formation of the aggregate and can yield information on the formation process. Colbeck and Wu [291] found $1.4 \leq D_f \leq 1.96$ for carbonaceous smoke clusters depending upon the history, and $D_f = 1.08$ for magnesium smoke which had the form of chains. Also, Colbeck et al. [292] found that the fractal dimension of carbonaceous smoke increases due to processing in clouds in the presence of water vapour. It rises to $D_f \approx 2$ to 2.5, and the clusters behave more like solid spheres for light scattering.

The scattered intensity from an agglomerate may be obtained from

$$I(q) = I_0 n M_2 \left(\frac{d\sigma}{d\Omega}\right)_0 P(qa)\bar{S}(q)$$

with $(d\sigma/d\Omega)_0$ and $P(qa)$ being the Rayleigh forward scattering differential cross-section and the scattering form factor for the primary particles. M_2 is the second moment of the size distribution and $\bar{R}_g \approx aM_2^{1/D_f}$. $S(q)$ is the structure function and $q = 2k\sin(\theta/2)$.

The fractal dimension can be measured directly by plotting the scattered signal as a function of angle. Provided $q = 2k\sin(\theta/2)$ is sufficiently large, it is found that

$$S(q) \propto q^{-D_f}$$

Sorensen et al. [293] claim that the structure function $S(q)$

has this form provided $qR_g > 1$. However, Bonczyk and Hall [294] state that $q \geq 3$ is required and propose extending the range of angles that can be used by moving to the ultraviolet.

When $qR_g < 1$, the so-called Guinier regime, Sorensen et al. [295] proposed a means of obtaining r_0, N and d. Here

$$S(q) \approx 1 - \frac{1}{3}q^2R_g^2$$

and plotting $S(q)$ against q^2 yields a straight-line plot of slope R_g^2. Plotting the size from scattering extinction (R_{SE}) against R_g results in a set of straight lines of constant r_0 and N. A log–log plot of R_{SE} against R_g gives lines of constant slope $D_f/3$. A network is then established from which the three parameters can be found. However, the authors state that the results are dependent on the assumed form for the correlation function describing the distribution of mass in the agglomerate.

Khlebtsov and Melnikov [296] and Sorensen et al. [297] have explored the structure function in more detail. They find

$$S(q) = \begin{cases} 1 & qR_g < 1 \text{ Rayleigh regime} \\ 1 - \frac{1}{3}\left(qR_g\right)^2 & qR_g < 1 \text{ Guinier regime} \\ \left(qR_g\right)^{-D_f} & qR_g \gg 1 \text{ Power-law regime} \end{cases}$$

(Faeth and Koylu [298] give

$$S(q) = \exp\left(-\left[qR_g\right]^2/3\right)$$

in the Guinier regime, which reduces to the form given above for $1/3[qR_g]^2 \ll 1$.)

Measurements in the Guinier regime can yield the overall size of the agglomerate while the power-law regime contains information on the structure. However, complications arise due to a number of factors, including finite particle size, polydispersity multiple scattering, and the lack of self-similarity.

To allow for finite size, Khlebtsov and Melnikov [296] proposed a modified structure factor of the form

$$S(q) = \frac{1}{M}\left[\frac{(M-1)\sin\left[(D_f-1)\arctan\left(qR_gK\right)\right]}{\left[1+\left(qR_gK\right)^{(D_f-1)/2}\right](D_f-1)qR_gK}\right]$$

where M is the cluster mass and

$$K = \sqrt{\frac{2}{D_f(D_f+1)}}$$

Sorenson et al. [297] take into account the variation of cluster size and suggest

$$S(q) = 1 - \frac{1}{3}q^2\left\langle R_g^2\right\rangle$$

where

$$\left\langle R_g^2\right\rangle = \frac{r_0^2}{K_f^{2/D_f}}\frac{M_2(1+1/D_f)}{M_2}$$

and

$$M_i = \int N^i n(N)\,dN$$

$n(N)$ being the distribution of the number of particles in the clusters.

As implied above, the cluster ceases to behave like a fractal when scales are considered which are too small (of the size of only a few primary particles) or too large (of the order of the cluster size). At the lower (Rayleigh) end, the scattering by a few particles can be calculated directly. At the higher (power-law) end the problem is tackled by the introduction of a cut-off function to the cluster density–density correlation function. If this takes the form $h(r/\xi) = \exp[-(r/\xi)^2]$, where ξ is the characteristic cluster size related to R_g, then Sorenson et al. [297] find

$$S(q) = e^{-(qR_g)^2/D_f}\,{}_1F_1\left(\frac{3-D_f}{2}, \frac{3}{2}; \frac{\left(qR_g\right)^2}{D_f}\right)$$

where ${}_1F_1$ is a confluent hypergeometric function. Fig. 14(a) shows plots of the variation of scattered intensity with $(qR_g)^2$ and Fig. 14(b) illustrates the sensitivity to the cut-off function assuming the form $h = e^{-1.r/\xi)^\beta}$. Fig. 14(c) shows some experimental results for soot in a methane/oxygen flame.

The sensitivity to cut-off function has also been explored by Botet et al. [299] They concluded that the polar diagram is not sensitive to its form, although it does have significance for cross-sections.

A description of light scattering by agglomerates of small particles in terms of their fractal structure has been given by Berry and Percival [300]. They used a mean field theory with scalar analysis. Their results suggested that multiple scattering within the agglomerate was negligible for $D_f < 2$. For $D_f > 2$ it dominates. This was explored further by Nelson [301] who concluded that the mean field approach is valid for assemblies of up to 250 particles. Colbeck et al. [292, 302] reported that the theory of Berry and Percival was in agreement with their experimental results for $D_f < 2$. However, for $D_f > 2$ the mean field theory predicted an increase in Q_{sca} which was not observed. The results were more in agreement with Mie theory for a sphere. Similar conclusions were reached by Khlebtsov [205], who treated the fractal agglomerates as porous spheres in the anomalous diffraction approximation.

The increase for scattering with $D_f < 2$ has also been reported by Dobbins et al. [303]. They suggest that the

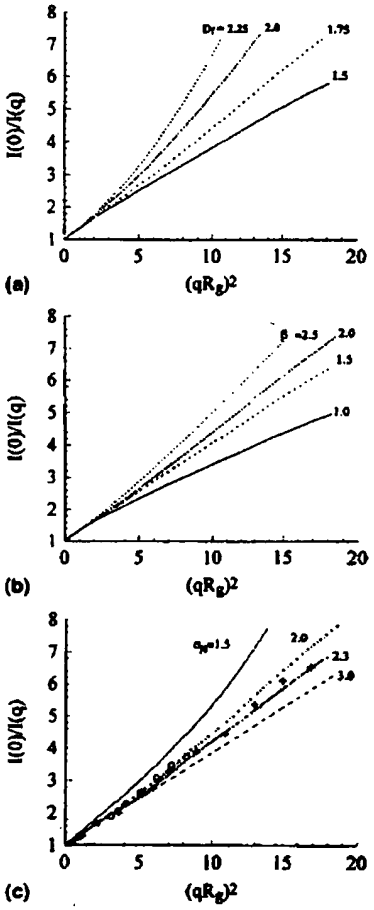

Fig. 14. Scatter diagrams for fractal aggregates: (a) influence of fractal dimension for a structure factor derived from a Gaussian cut-off correlation function; (b) influence of β in the cut-off function for a structure factor derived from a Gaussian cut-off correlation function with $D_f = 1.75$; (c) influence of the width parameter of a zero-order log-normal size distribution function (ZOLD) for a structure factor derived from a Gaussian cut-off correlation function with $D_f = 1.75$. Experimental results are shown for a pre-mixed methane/oxygen flame at height (h) above the burner of 12 mm (O) and 18 mm (+). (After Sorensen et al. [297].)

specific extinction coefficient can be described by

$$\frac{K_{ext}}{c} \approx \frac{6\pi}{\rho\lambda} \mathrm{Im}\left(\frac{m^2-1}{m^2+2}\right) + \frac{4\pi x^3 K_f 2^{D_f}}{\rho\lambda}\left(\frac{3D_f}{16x^2}\right)^{-D_f/2}\left|\frac{m^2-1}{m^2+2}\right|^2$$

An example of the increase in the extinction over that of a volume equivalent sphere is illustrated in Fig. 15.

Because a fractal aggregate with $D_f < 2$ may be a tenuous

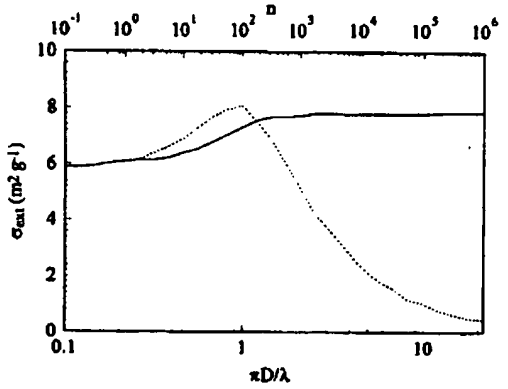

Fig. 15. Specific extinction coefficient against number of primary particles, n, for $x_p = 0.024$, $m = 1.55 - i0.78$, $D_f = 1.75$ and $K_f = 9.0$. The dashed line is the Mie theory prediction for the volume equivalent diameter of the aggregate. (After Dobbins et al. [303].)

structure, it is reasonable to suppose that the incident wave may propagate with little disturbance. This concept led Farias et al. [160, 161] to develop a simplified model based on the RGD approximation. They claim that their model is accurate to within 10% provided that $|m - 1| \leq 1$, the primary particles are within the Rayleigh limit on size and $(m^2 - 1)/(m^2 + 2)$ is not approximated. The method is also said to be satisfactory for some cases with $D_f > 2$, even though the agglomerate is more compact.

Singham and Bohren [304] have pointed to different properties between illumination with unpolarized and polarized light. In the former case the scattering by the agglomerate is insensitive to interactive effects or fractal dimension. For polarized light there is sensitivity to both, and the element M_{34} of the scattering matrix is a strong indicator of the fractal dimension. The agglomeration introduces depolarization into the scattered light. According to Lu and Sorensen

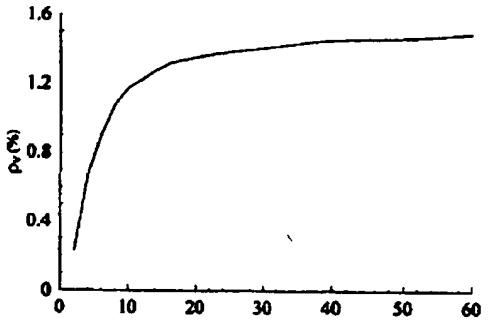

Fig. 16. Depolarization ratio versus number of primary particles per aggregate for linear chains. $m = 1.6 + i0.6$ and $x_p = 0.2$. (After Lu and Sorensen [305].)

[305], the depolarization ratio is given by

$$\rho \approx n^{-0.6}$$

but tends to saturate, as seen in Fig. 16.

A further complication to the simple theory arises due to resonances. Shalaev et al. [306] and Markel et al. [307] suggested that there exist resonances caused by coherent interaction between the particles in the agglomerate. These can cause considerable enhancement of the optical properties. Iskander et al. [308] showed that there is also a resonance when the length of the agglomerate is of the order of the wavelength. At such a point the simple theory could be in error by as much as 50%. The same workers have developed empirical formulas to describe optical absorption by fractal aerosol agglomerates [309].

The agglomerates may be anisotropic due to non-spherical shape. The measurement of shape factors has been explored by Wu and Colbeck [310]. They define the shape factor as

$$\Psi = \frac{\rho}{\rho_0}\left(\frac{D_{ve}}{D_{ae}}\right)^2$$

where ρ is the particle density, ρ_0 is the unit density, D_{ve} is the volume equivalent diameter and D_{ae} is the aerodynamic diameter. It is demonstrated that

$$D_{ae} \approx D_{ve}^{1.5(D_f-1)/D_f}$$

and

$$\Psi \approx D_{ve}^{3/D_f-1}$$

Neimark et al. [311] suggest that, to allow for shape, the fundamental definition of the fractal structure should be adapted. They propose

$$N = \alpha_\gamma\left(L^\gamma W^{1-\gamma}\right)^{D_\gamma}$$

where L is the length and W is the width. Evidently for $\gamma = 1/2$ the length and width have equal influence and $D_\gamma = D_f$, the usual fractal dimension. Similarly, for $\gamma = 1$ length predominates so that $D_\gamma = D_L$ and for $\gamma = 0$ then $D_\gamma = D_W$. For a growing aggregate they define an affinity exponent H through

$$\frac{W}{W_0} = \left(\frac{L}{L_0}\right)^H$$

where W_0 and L_0 are the original or reference values at any time in the growth. Then they show that

$$D_L = \frac{1+H}{2}D_f, \qquad D_W = \frac{1+H}{2H}D_f$$

We note that for $D_L = D_W = D_f$, then $H = 1$. For aggregates growing in a combustion system they find $D_f = 1.75$ and $H = 0.91$.

Any anisotropy, form or intrinsic, results in a rotation of the polarization of the scattered light relative to that incident. For randomly oriented particles there is partial depolarization. This is measured in terms of a depolarization ratio. A scalar theory cannot calculate these effects and a full vector analysis is required. Chen et al. [312] and Markel et al. [313] have tackled this problem.

Wide-ranging reviews of the electromagnetic properties of fractal agglomerates have been given by Charalampopoulos [314], d'Alessio et al. [315], Faeth and Koylu [298] and Shalaev [316].

7.3. Polarization measurement

Anisotropy in particles can be of two types: intrinsic or form. The first of these is a property of the material and is independent of shape. A sphere may exhibit intrinsic anisotropy, for example. Form anisotropy is a property of the shape and is associated with non-spherical particles. A feature of anisotropy, whether it be intrinsic or form, is that it will induce changes in the polarization state of the scattered light relative to that incident. This property can be used to study the nature or extent of the anisotropy.

It is common to refer to vertical (V subscript) and horizontal (H subscript) polarization. Usually the measurement plane is horizontal so that vertical polarization is perpendicular ($\phi = 90°$) and the other is parallel ($\phi = 0°$). Four possibilities exist:

1. The incident polarization is vertical and so is that scattered, then

$$I_{sca} = I_{VV}$$

2. The incident polarization is vertical but that scattered is horizontal, then

$$I_{sca} = I_{HV}$$

3. The incident polarization is horizontal and so is that scattered, then

$$I_{sca} = I_{HH}$$

4. The incident polarization is horizontal but that scattered is vertical, then

$$I_{sca} = I_{VH}$$

For isotropic spheres $I_{HV} = I_{VH} = 0$. It is generally true that $I_{HV} = I_{VH}$ — the reciprocity condition.

The depolarization ratios are defined by

$$\rho_V = I_{HV}/I_{VV}, \qquad \rho_H = I_{VH}/I_{HH}$$

Typically they are found to be of the order 1%.

Measurements of depolarization ratio for flame soot (e.g. Haynes and Wagner [317]) find ρ_V of the order 1% whereas a prolate spheroid assumption would suggest about 4% for long chains at a typical refractive index of $m = 1.56 + i0.56$.

The interactive chain model, however, predicts $\rho_v \leq 1\%$. Thus while Haynes and Wagner concluded that the observed depolarization ratio was due to intrinsic anisotropy and did not display evidence of chain formation, such a conclusion would be dubious with the chain model. Also, Müller-Dethlefs [318] did find evidence in a counterflow diffusion flame for an increase of ρ_v with time.

It must be emphasized, however, that depolarization cannot distinguish between form and intrinsic anisotropy. Some other shape-dependent variable must be employed to do this, such as streaming birefringence (e.g. Jones and Wong [319]).

It can be shown [320] that in the Rayleigh region the ratio I_{vv}/K_{ext} is the same for spheres and spheroids of the same volume. Thus the method of size measurement using the ratio of scattered intensity to extinction is independent of shape.

7.4. Disymmetry and polar diagrams

As the particles become larger, forward scatter increases relative to other angles. A simple measure of this is the disymmetry, defined as the ratio of the scattered intensity at two symmetrical angles. Popularly 45° and 135° are chosen. This yields a monotonic function of size up to $x \approx 2$, or about 0.4 μm in the visible.

More information can be obtained from the complete polar diagram measured for both polarizations. As the particle size increases forward scatter dominates and the polar diagram develops a convoluted lobe structure. For particles larger than about 4 μm and visible light ($x > 20$) the first few lobes around $\theta = 0$ are well represented by Fraunhofer diffraction. According to this, the width of the forward lobe is given by

$$\sin\theta = 1.22\lambda/D$$

while its height is proportional to D^4. Thus this peak becomes increasingly dominant and narrow. The number of lobes in the polar diagram is of the order $x|m|$.

For a polydisperse cloud the lobes due to different sizes occur at different angles. This has the effect of washing out the structure and making it featureless, except close to the forward direction where the strong peak remains.

The polar diagram can be used to measure particle size. However, for single large particles, the structure requires increasing angular resolution which ultimately limits the maximum size that can be determined. For particle clouds structure is not a problem, but the polar diagram may be so featureless that it is difficult to obtain sufficient information to recover a unique size distribution. This is especially so in the presence of experimental error. Further, at most angles the scattering is very sensitive to refractive index, which is an extra problem if this parameter is unknown.

There have been two traditional approaches to recovering the size distribution. In the first a collection of polar diagrams are generated from Mie theory by using a range of parameters in an assumed form of the size distribution function. Typical functions employed are the log-normal and Rosin–Rammler distributions. Brown and Wohletz [321] have proposed the use of the Weibull distribution which naturally arises in fragmenting particle systems. The Rosin–Rammler distribution is one form of the Weibull distribution. The alternative has been to employ a direct inversion scheme, such as that of Phillips and Twomey (see Section 9).

New techniques are continually being explored. For example, Min and Gomez [322] have examined the application of the Fourier transform of the polar diagram to single particles. This results in a frequency and phase corresponding to the number and position of the lobes. In particular, the frequency is found to be a linear function of size for diameters above 10 μm, with additional information being provided by the phase. The calculations suggested that accuracy should be excellent in dilute sprays. If the refractive index is known, the size could be measured to within 1%. Alternatively, an uncertainty of 2% in refractive would result in a sizing error of about 3%. Counting rates up to 30 kHz were possible. The authors confirmed their method on individual particles in the size range 74.75 to 74.95 μm using an angular range from 10 to 17°. This size range is very narrow, suggesting that further study is required.

Glover et al. [323] demonstrate that if a slightly out-of-focus image is taken of a particle, a set of fringes is observed which are regular in the angular range 20 to 70°. These are part of the scattering pattern arising from interference between front-reflected and back-refracted rays. The fringe spacing is directly related to the size through

$$\Delta\theta = \frac{2\pi}{x\left(1 + \frac{1}{m}\right)}$$

where x is the size and m is the real refractive index. A pulsed laser was needed to freeze the fringes, which move with the particle.

A very novel approach due to Ludlow and Everitt [324] reformulates the Mie theory and the RGD approximation in terms of Gegenbauer polynomials, which have the advantage of forming a complete orthogonal set. In consequence the polar diagram can be readily transformed into a set of expansion coefficients via a simple integral over the entire angular range. A plot of these coefficients against order constitutes the Gegenbauer spectrum, which has a number of interesting properties. The spectrum is much simpler in appearance than the original polar diagram and has a distinct cut-off at the order l_{co} given approximately by

$$l_{co} = 2.1x + 0.12$$

where x is the size parameter. An example is shown in Fig. 17, where the C_l are the coefficients of the Gegenbauer expansion. It is not clear how useful this method would be for a polydisperse system.

Polar diagrams have the advantage of being relative. They

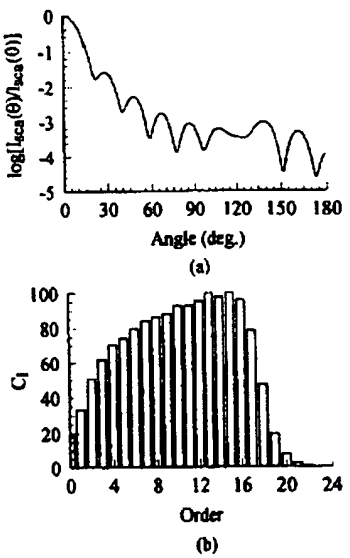

Fig. 17. (a) Angular scattering pattern and (b) Gegenbauer spectrum for $x = 10$ and $m = 1.2$. (After Ludlow and Everitt [324].)

will yield particle size independently of concentration. However, if the concentration needs to be known, then an absolute measurement of scattered intensity is required. Because this is absolute the laser output should be monitored, and the system requires calibration. To do this particles with known scattering cross-section and concentration are needed. A gas is ideal for this purpose. Its concentration may be calculated for given temperature and pressure, and the scattering cross-section is known for many gases. As an example, for oxygen $C_{sca} = 1.05 \times 10^{-31}$ m^2. d'Alessio [320] quotes a number of examples.

7.5. Photon correlation spectroscopy

A drawback of the methods described above is that they rely for their interpretation on a knowledge of the refractive index. A method of sizing based upon mechanical properties would be independent of this. The velocity is such a property.

Small particles (< 1 μm) suspended in a fluid exhibit random Brownian motion as a consequence of molecular bombardment. The more massive, the particle the less significant this effect is. Thus measurement of the random motion can yield size. While a frequency shift is involved due to the Doppler effect, the treatment is essentially dealt with by elastic scattering. For this reason it is sometimes referred to as quasi-elastic light scattering (QELS).

The consequence of the Doppler effect combined with the random motion of the small particles is a broadening of the spectrum of the probing light beam. The application of this diffusional broadening to soot in laminar diffusion flames has been described by Lhuissier et al. [325]

The frequency shifts are small, and while the spectrum can be obtained with a high-resolution spectrometer, an alternative is to find the broadening indirectly via the resulting degradation in coherence. To measure this the scattered signal is compared with itself at increasing delay times, τ. For a single particle size the resulting correlation function decays exponentially, the rate of decay increasing as the linewidth increases—or the particles become smaller. This technique is called photon correlation spectroscopy (PCS). The specific form of the correlation function is

$$S(\tau) = \text{constant} \times \exp\left(-2q^2 D_f \tau\right)$$

where D_f is the diffusion coefficient

$$D_f = \frac{kT}{3\pi\mu D}$$

and k is Boltzmann's constant, T is the temperature and μ is the viscosity of the fluid. Also

$$q = \frac{4\pi}{\lambda} \sin\frac{\theta}{2}$$

In reality there will be a size distribution. The correlation function is then the integral over a series of exponentials. Inverting this to the size distribution is a difficult process, currently the subject of much discussion.

PCS is an established technique for small particles suspended in a stationary liquid, and commercial instruments are available. When used in flowing fluids, however, two complications arise because of the motion. The first is turbulence, which adds an extra random motion to the particles and further broadens the scattered spectrum. The second complication is due to the bulk motion of the gas which carries particles across the test space. The finite transition time is inverted to a characteristic frequency. This effect is the Doppler ambiguity.

A number of authors have explored PCS for measurements on soot in a laminar flow, which removes one of the variables. In this case the correlation function for monodisperse particles takes the form

$$S(\tau) \propto \exp\left(-2q^2 D_f \tau - v^2\tau^2/W_0^2\right)$$

the second term in the bracket being due to the Doppler ambiguity. To minimize this it is necessary to keep v/W_0 as small as possible, v being the velocity and W_0 the beamwidth (i.e. W_0/v is the transit time). Scrivner et al. [326] and Weill et al. [327] have used this method to obtain soot particle size in flames. The latter authors recommend that, for a beamwidth of $W_0 = 250$ μm,

$D \approx 10$ nm: $v < 4.5$ m s^{-1}

$D \approx 100$ nm: $v < 0.5$ m s^{-1}

Weber et al. [328] have discussed the influence of concen-

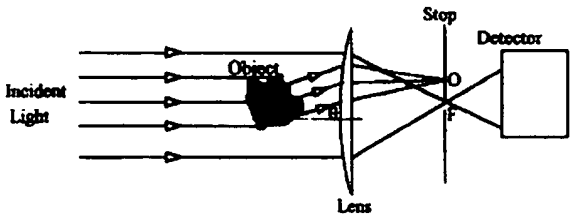

Fig. 18. Illustration of an experiment to measure extinction. Scattered light passes to O and transmitted light to F. A pinhole at F allows the light to pass to the detector.

tration, velocity, particle size and detector aperture on correlation spectroscopy. In general, they conclude that for dilute aerosols with $\tau < W_0/v$ PCS works well, in agreement with the above. However, the method fails for $\tau \geq W_0/v$ and non-dilute systems.

A modified approach to PCS related to photon counting has been proposed by Gonzalez et al. [329] Their technique is based on monitoring the statistical distribution of time intervals between arriving photons. The authors claim that this method can be superior at very low light levels.

If the particles are non-spherical an extra degree of freedom is introduced as they may rotate. The correlation function then has two components which decay at different rates. Rarity [330] was able to separate these by measuring the mutual coherence function between two detectors. In this way he could measure both axes of spheroids. Xie et al. [331] used electron microscopy to measure the size of the primary particles in an agglomerate and then used PCS to provide an equivalent diameter from which the chain length could then be established.

A review of the use of PCS for particle sizing in combustion systems has been given by Bernard [332].

7.6. Spectral extinction

Efficiency factors were reviewed in Fig. 4. For particle sizing the most significant feature is that the extinction efficiency rises monotonically for small x. A reasonable guide is that $x|m-1|<2$. This suggests measuring the extinction as a function of wavelength—the spectral extinction method. Practically, the upper limit is of the order of 1 μm diameter. For larger particles Q_{ext} essentially oscillates around a constant value. The mean extinction then varies as the square of the size. However, the oscillation would make the measurement non-unique, except for strongly absorbing particles where it is damped.

Care must be exercised in measuring extinction. A schematic experiment is indicated in Fig. 18. Light scattered from the cloud arrives at the point O and transmitted light at F. If the true extinction is to be obtained, negligible amounts of scattered light must pass to the detector. It is the function of the stop to ensure that is so. We know that as particle size increases so the scattering becomes more strongly peaked in the forward direction. Thus the accepted angular range becomes ever smaller, as does the aperture ($f\theta$) in the stop. Also, if the transmission is very high, then the measurement may be of a small change in a large background.

If there are temperature gradients and fluctuations of the gas, the transmitted beam is continually in motion. The angular displacement of the beam is proportional to the temperature gradient and the path length through the flame (although positive and negative gradients may offset each other to some extent). The problem associated with this is that either the position of the aperture would have to continually be changed, or a larger aperture be used which would allow in scattered light.

One way of overcoming this difficulty is to use a lens to image the particle cloud onto the detector. In this way deflections are brought back onto the optic axis of the system, and always arrive at the same point. Unfortunately, this also concentrates any emitted light at the aperture. To reduce the significance of this, phase-sensitive detection may be used together with a narrow pass interference filter. Alternatively a high-power laser may be employed.

Since Q_{ext} is very sensitive to refractive index, this parameter needs to be known with reasonable accuracy. Furthermore, the method is most useful for scatterers with refractive index not too different to one, otherwise the measurable size range becomes too restricted. According to Shifrin and Perelman [333] the recommended upper limit is $m = 1.5$. If the particles are suspended in a material other than a gas their refractive index relative to the medium must be used.

At high concentrations multiple scattering becomes important. However, extinction relates to the loss from an infinitesimally small solid angle around the collimated incident beam. The scattering into this is zero. In reality, where a finite aperture is used, there will be some scattering received which will be influenced by multiple scatter. This will be small provided the aperture is sufficiently small. Multiple scattering will not be significant to extinction measurements provided appropriate care is taken to select a suitable aperture.

Where multiple scattering cannot be neglected, a correction factor has been proposed by Szymanski [334]. Here, the

transmissivity has the form

$$T = e^{-K_e}(1 + X)$$

and values for X are provided from near forward radiative transfer theory. The method is found to agree well with experiment.

Walters [335] applied the spectral extinction method to condensing water droplets in steam turbines. A probe was developed with the light source and filters at one end and the detector at the other, and a slit between them through which the droplets passed. The whole probe assembly could be inserted into the turbine chamber. The data were inverted to recover the size distribution using the Phillips–Twomey method (see Section 9).

A method allied to spectral extinction has been applied to obtain mean particle size and concentration in very dense media by Gougeon et al. [336]. This is a double extinction technique and uses the ratio of the extinctions at wavelengths of 0.6328 μm in the visible and 337 μm in the far-infrared. Guidt et al. [337] have validated the technique by making measurements on particles of known size and concentration suspended in a highly viscous gel.

Another feature of the wavelength variation of extinction has been exploited by Winklhofer and Plimon [338] to monitor hydrocarbon fuel in internal combustion engines. Scattering and absorption at two wavelengths is used to discriminate between gaseous fuel and liquid drops. An output wavelength of 3.39 μm from a He–Ne laser was chosen because this coincides with an absorption band in the fuel vapour. In the visible the fuel vapour is almost transparent.

A possible extension to inhomogeneous particles has been considered by Graff et al. [339]. By studying the modifications to the extinction spectrum due to the presence of metallic cores in coated particles, they claim that it may be possible to measure a coating thickness to within 1 nm.

7.7. Fraunhofer diffraction

The Fraunhofer diffraction pattern is very sensitive to size in a simple way, and polydisperse samples can be analysed with good accuracy. Refractive index does not appear in the diffraction equation and comparisons with Mie theory confirm lack of sensitivity to this for sufficiently large particles and small angles. Thus the problem of knowing refractive index not does arise provided a small error in size is acceptable. For larger particles in a size distribution the refractive index begins to affect the higher angles measured. Zhang and Xu [340] predict that errors can be in excess of 10% due to use of the incorrect refractive index. This is roughly in line with the predictions of Jones [173].

A further advantage of Fraunhofer diffraction is that the governing equation is extremely simple, making calculation straightforward. As a consequence of these advantages Fraunhofer diffraction has become a popular and powerful method.

The basic apparatus required is also simple and was illustrated in Fig. 1(b). A parallel beam of monochromatic light, conveniently from a laser, traverses the particle cloud. The transmitted and scattered light are collected by a lens and the intensity is observed in the focal plane. The diffraction pattern is independent of the position of the particle in the beam and only depends on the scattering angle. (The light distribution in this plane is the Fourier transform of that in the test space, where the particle cloud is located, and the lens is often referred to as the "Fourier transform lens".)

The intensity distribution can be measured by traversing a photodetector across the focal plane. This is time-consuming and it is preferable to use a detector array. This may be either linear or, as used by Malvern Instruments, segments of concentric circles. However, as multiple detectors are used, calibration is needed to ensure that their relative response is known [341, 342].

The instrument response can be checked by using particles of known size distribution. An alternative is the use of calibration reticles which have large numbers of discs of well-determined size photographically etched onto glass [342].

The use of diffraction in two-phase flows has been reviewed by Bachalo [343]. The properties of the surrounding fluid can have significant effects, especially if there are density gradients which can cause deflections of the transmitted beam.

Hirleman and Dellenback [344] proposed a method of overcoming this, in which the scattered light passed through a filter composed of an array of birefringent elements that could be made transparent or opaque to a particular polarization by the Faraday effect. The array was switched sequentially to scan the diffraction pattern with rings of any required radii. Transmitted light was collected by a lens and passed to a single detector, so that calibration was not needed provided the response was linear. The centre of the diffraction pattern was determined independently by separating a fraction with a beam splitter and sending this to a position indicator. In this way, allowance could be made for deflections along the light path due, for example, to hot gases.

A similar concept was used by Miles et al. [345], although here conditional sampling was employed. The diffraction pattern was only recorded when the position indicator showed that the beam was central. Tests performed in flowing hot gas indicated that very large errors could occur if conditional sampling was not used. For example, a 45 μm particle was sized as 135 μm without sampling and as 43 μm with sampling.

7.8. Mixtures of small and large particles

The scattered intensity close to the forward direction increases strongly with particle size. At 0° Fraunhofer diffraction gives $I_{sca} \propto D^4$, though at larger angles it becomes more like D^2. This means that the scattering is

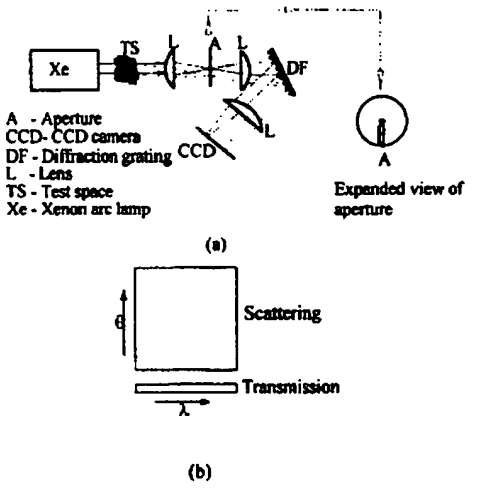

Fig. 19. Illustration of the method of displaying both the angular and wavelength variation of scattered intensity on a CCD camera: (a) apparatus; (b) appearance on screen. (After Card and Jones [347].)

dominated by large particles; one 100 μm particle is equivalent to 10 000 of size 1 μm. Further, small particles no longer satisfy the criteria for Fraunhofer diffraction. Although this limitation can be overcome with the use of Mie theory, there is still a lack of angular information. For these reasons diffraction-based instruments were limited at the lower end until quite recently. The measurement of small particles has been incorporated by combining back-scattering and diffraction [346].

A different approach was used by Card and Jones [347, 348]. This made use of the facts that for large particles scattering is strongly dependent on angle but insensitive to wavelength and vice versa for small particles. A lamp with a continuous spectrum was used as the light source and an optical system devised which was capable of displaying both the angular and wavelength variation on a CCD camera. This is shown in Fig. 19(a). Scattered light passes through the slit in A and the test space is imaged onto the CCD via a diffraction grating. Unscattered light passes through the pinhole to provide a measure of the extinction. The form of the image is as suggested in Fig. 19(b). Evidently, the system is capable of delivering the spectral extinction method, but the authors only used extinction to indicate concentration.

Scatter diagrams for 0.3 μm and 90 μm particles are seen in Fig. 20(a). The expected dependencies on wavelength and angle are clearly demonstrated. Fig. 20(b) shows an example of the scattering by mixtures of these sizes. By comparing the measurements with theory, the volume fraction of the smaller particles could be determined to within less than 1%. Use of the Phillips–Twomey inversion method (see Section 9) indicated that the bimodal size distribution could be recovered satisfactorily.

7.9. Dense particle clouds

We have seen previously the problems which arise when attempting to measure particle size in dense systems because of multiple scattering, and have explored some of the methods used to attempt to correct single-scattering type measurements for this. However, interest is developing in ways of using the multiply scattered light directly. An early proposal was, for example, that of Deepak and Green [241] who predicted the scattering by a radiative transfer approach akin to the Monte Carlo method. In their technique direct transmission and forward scatter at some distance offset from the incident beam were measured.

In LIDAR a laser pulse is transmitted to a target area in the atmosphere and the properties of that region are determined from the reflected signal. The influence of multiple scatter on this have been examined by Benayahu et al. [349] who considered only double scattering, which they claim to be sufficient. Here the direct reflection and backscatter at some offset distance were observed.

A promising concept has been discussed by Zaccanti et al. [350], who examined the influence of multiple scattering on the shape of a transmitted light pulse. They conclude that a time-gated scanning–imaging system should be able to detect absorbing structures inside thick turbid media. However, picosecond pulses are required. The propagation of pulses in dense media has also been examined by Kuga et al. [351]. They find that the speed of propagation of a pulse can be reduced by as much as 50% as a consequence of multiple scattering events. Other studies on pulse spreading and broadening include those of Prahl et al. [251], van de Hulst and Kattawar [252], Shifrin and Zolotov [253] and Brewster and Yamada [254].

An alternative approach is to penetrate the dense medium with a suitable probe. A recent version of this idea is the endoscopic grating velocimeter–granulometer proposed by Cartellier [352].

8. Particle counting

8.1. Measurement of scattered intensity

This leads to the method of measuring the pulse height as individual particles traverse a light beam. Unfortunately, away from the forward direction it is very sensitive to refractive index. Furthermore, it is an absolute measurement which leads to other problems as we shall see later.

The intensity curve may oscillate and, so, not produce a unique value of size. However, the scattered intensity is integrated over the aperture of the collecting lens. Also, if a non-monochromatic light source is used, there is integration over wavelength. The combined effect of these is that

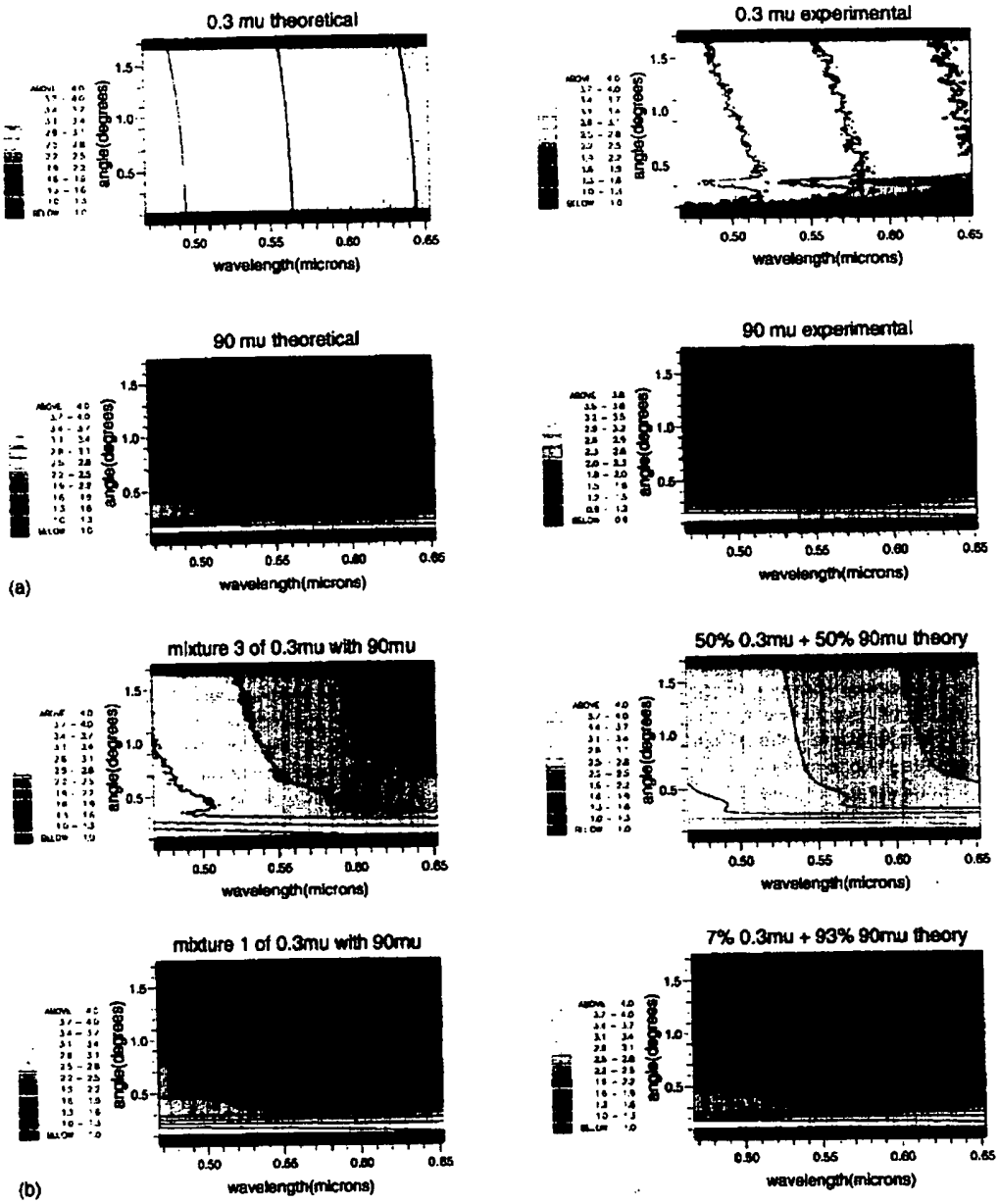

Fig. 20. Diagrams showing the variation of scattered intensity with both angle and wavelength. The shades are representative of the logarithm of intensity, with white being the highest and black the lowest. (a) Pure samples of particles with representative sizes of 0.3 μm and 90 μm. (b) Mixtures of these two sizes. The experimental results are on the left and theoretical ones on the right for the mixtures indicated. (After Card and Jones [347].)

any oscillations tend to be smoothed out and a reasonably monotonic variation of intensity with size is achieved [353].

If the refractive index is known the instrument response can be calculated for spheres. Often, however, it is not known and scattering by non-spherical particles cannot presently be calculated with certainty for other than a few well-defined shapes. However, as mentioned earlier, forward scatter is least sensitive to refractive index and

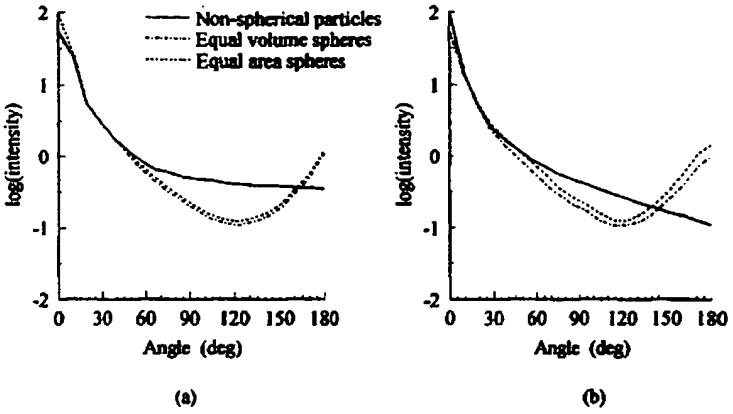

Fig. 21. Comparisons of the scattering patterns of randomly oriented non-spherical particles with equal volume and equal area spheres: (a) cubes; (b) flat plates. (After Pollack and Cuzzi [175].)

shape. For example, Fig. 21 is taken from the work of Pollack and Cuzzi [175] and compares spheres and non-spherical particles. The calculations for the cubes and flat plates were based on a semi-empirical theory which was found to provide reasonable agreement with experiments. The curves clearly demonstrate the advantage of operating close to the forward direction. Unfortunately, it is often necessary in practice to use a considerable aperture in order to collect sufficient scattered light. Much of the advantage is then lost due to the range of angles seen.

While forward scatter confers some advantage, it also raises difficulties. The first is that the unscattered light must be blocked by a stop, which eliminates the use of a small range of angles around $\theta = 0°$. This is unfortunate because scattering is strongest close to this angle. Apart from the loss of intensity, the sensitivity to shape and refractive index is increased. Use of a highly collimated source, such as a laser, minimizes the required stop size but it remains finite. A second problem is that the forward direction is more sensitive to stray light scattered off optical elements and flare from the light source which passes the stop. There is always a balance to be struck, therefore, between a stop small enough to eradicate these sources of noise but which cuts off too much scattered light and a larger one with the opposite consequences.

A third problem with forward scatter is that the detector looks along the incident beam and the test space can be quite long. It is only limited by the depth of field of the optical system. Spatial resolution will be best at 90°, where the test volume is given by the intersection of the incident beam with the depth of field of the detector optics.

Scattering by a single particle is proportional to the incident light intensity and depends upon its position in a non-uniform field: such as the Gaussian form of a laser beam. For systems which rely on received intensity this is a problem since the size will apparently vary with position. Thus the path of a particle is an important unknown. This is the trajectory problem.

Perhaps the most obvious way to tackle this difficulty is to make the incident beam uniform in intensity; the so-called "top-hat" profile (e.g. Gréhan and Gouesbet [354]). For example, the laser may be expanded and only the central portion selected by an aperture. Alternatively, a neutral filter may be constructed with an inverse Gaussian density profile. A holographic method has been used to the same effect [354]. The problem with all such methods is that they throw away much of the available light. A possible way around this problem for one dimension is suggested by Xie et al. [355]. The original Gaussian beam is divided into two halves. Both halves are then rotated to provide their mirror images and they are recombined, as shown in Fig. 22. This yields a reasonable approximation to a one-

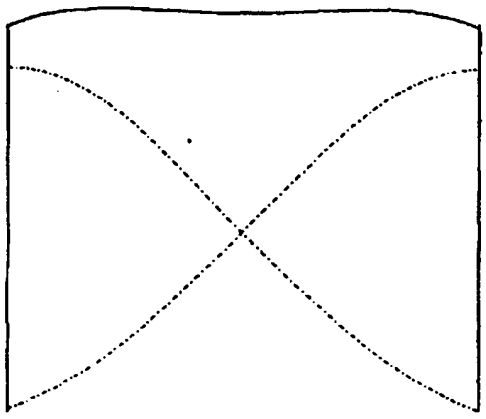

Fig. 22. Illustration of how two half Gaussian curves may be added to provide a "top-hat" profile. The broken curves are Gaussians and the solid line is their sum.

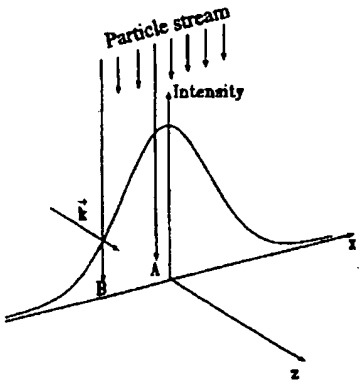

Fig. 23. Cross-section of a Gaussian laser beam.

dimensional "top-hat" profile while retaining all of the light.

Another approach is to mark the centre of the incident beam. Typically this is achieved in one of two ways: either using two beams with the same wavelength but orthogonal polarization or having different wavelengths [356, 357]. One of the beams is expanded and the other is aligned to coincide exactly with its centre. Two detectors are required with filters to select either the polarization state or colour, and signals are only accepted which arise from both beams.

The methods outlined above have the disadvantage that the incident intensity is reduced so that the scattered light is weaker. This need not be a problem with large particles or high-power lasers, but could create problems in marginal situations. There can also be problems with particles skirting the edge of the test space which are only partly illuminated. The latter can be avoided in the two-colour system by accepting only signals with a given ratio of transit times in the two beams, but this restricts the count.

An alternative approach is to invert the light scattering data using known properties of the structure of the test space. A simple technique for this was described by Holve and Self [358]. The principle is illustrated in Fig. 23. It is based on the fact that the incident laser beam has a Gaussian cross-section, so that the illumination of a particle depends upon its trajectory. A small particle following path A will see a higher illumination than one following path B and, consequently, the scattered light will be more intense. Indeed, for the smallest particles the light scattered out from path B may be so weak as to be below the detection limit of the system and they will not be seen. A large particle following path B may scatter the same intensity as a small particle along path A. The biggest signals come from the largest particles following path A.

In the inversion procedure the test space is divided into a number of zones within each of which the incident intensity is approximately constant. The maximum possible pulse height is given only by particles in the largest size class passing through the central zone of maximum brightness. The next class of pulse heights is provided by the largest particles passing through the adjacent zone, which is one step down in brightness, and the next particle size class in the central zone, and so on. In this way the number of pulses of any height is related to the intensities in the test space zones by a triangular scattering matrix. It is assumed that the flux of particles is uniform, such that the size distribution and probability of arrival are independent of the path. Then the matrix can readily be inverted to retrieve the numbers of particles in each size class provided the incident intensities are known; that is, the structure of the test space. This can be obtained by calibration with monodisperse particles. More recently the matrix inversion has been replaced by an integral deconvolution [359], and the structure of the test space calculated from a knowledge of the laser beam and apertures in the apparatus.

In theory there is no upper limit on the particle size. In practice there may be limitations due to finite beamwidth and apertures, and non-linear detector response or saturation. Ultimately it becomes more practical to resort to simpler and more straightforward methods, such as photography, holography or schlieren techniques (e.g. Birch [360] and Harada and Murakami [361]).

Ultimately the smallest measurable size will be limited by noise due to scattering by gas molecules. It is worth mentioning in this context that Ishikawa et al. [362] claim to be able to detect nano-size particles in water by employing photon counting. Their method compares moving averages of the statistically fluctuating signal. A particle is present when the average rises above a threshold set by the average of the background. They were able to size particles in the range 0.067 μm to 0.2 μm.

The operation of particle counters requires the presence of only one particle in the test space at a time. This limits the upper concentration to roughly the reciprocal of the volume of the test space. For example, a spherical volume with diameter 1 mm could accommodate about 10^9 particles per cubic metre. There is, in principle, no lower limit to the concentration but the counting time may become too extended. The particles arrive at random and are subject to Poisson statistics according to which the standard deviation is proportional to the square root of the number of counts. To determine the number of particles of any one size class to within 1% would require that 10 000 were detected.

The size distribution is built up particle by particle so there is no inversion problem. However, a temporal average results. If the spatial average is required this may be recovered if the velocities of the particles are known. Holve and Davis [359] used the known structure of the test space, and measured the time taken for the signal height to change between two fixed fractions of the maximum. Since this is a known distance, the velocity is found. Alternatively, laser Doppler may be employed.

In a combustion system problems arise due to beam fluctuations caused by refractive index gradients in the gas. To avoid this a gating method may be employed in which both

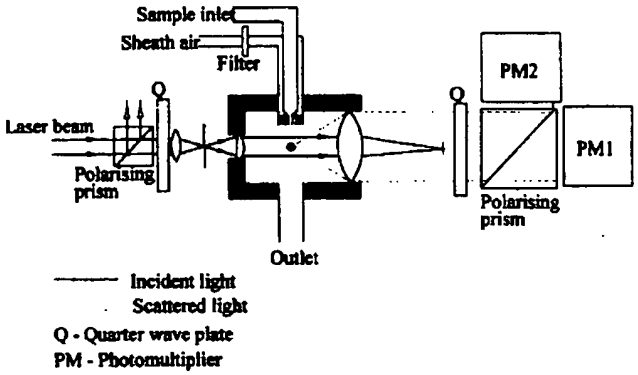

Fig. 24. Schematic diagram of apparatus to discriminate between fibrous and non-fibrous particles. (After Al-Chalabi et al. [367].)

the laser beam centre line and the centre of the sample volume are constrained to coincide before a signal is accepted.

An attempt was made to minimize the influence of non-spherical particles by Hardalupas et al. [363] These authors examined the diffraction patterns of individual particles and rejected any signals where the pattern had a large aspect ratio.

Finally, the measurement of intensity is an absolute method. It is sensitive to changes in incident intensity, due to variation in source output, unclean optical elements or beam blocking by particles along an extended path through a cloud. The scattered light may suffer attenuation for the same reasons.

There is also the need for calibration using particles of known size. Ideally the particles should be spherical of well-defined size. Unfortunately, these are not always readily available at sizes of a few micrometres. Polystyrene latex spheres are popular, but these come in aqueous suspension. To be used in air the suspension must be diluted, sprayed and evaporated to leave behind individual particles.

8.2. *Non-spherical particles*

Recently, attempts have been made to extend the use of particle counting to the characterization on non-spherical particles. Their influence may be detected from the structure of the scattered pulse, the lack of azimuthal symmetry or the polarization states of the scattered light.

The variation in response due to a large particle crossing a smaller beam has been used to provide information on the structure of the particle surface (e.g. Buckle and Bushnell-Watson [364] and Ohba and Isoda [365]). As the beam strikes different facets on the surface the scattered light fluctuates in intensity. A similar concept is the so-called "slit scan" method [366] in which a large particle is scanned by a narrow beam to reveal structure.

Of particular relevance to industrial safety, especially

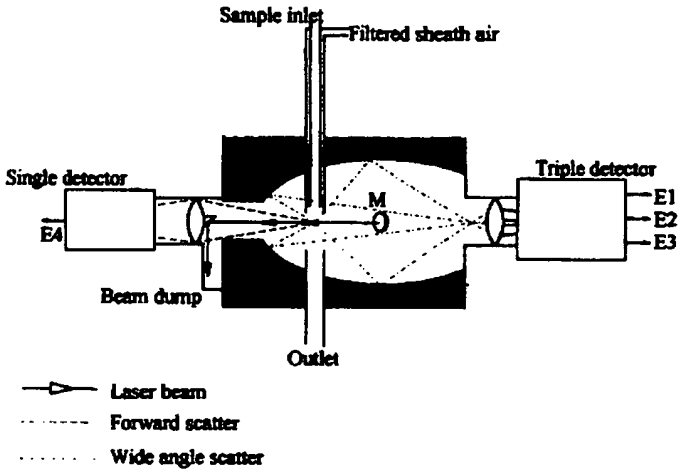

Fig. 25. Schematic diagram of aerosol size and shape monitor. (After Kaye et al. [368].)

with regard to asbestos and mineral wool, is the detection of fibrous materials in the atmosphere. Examples include the polarization method of Al-Chalabi et al. [367] and the anisotropic azimuthal scatter method of Kaye et al. [368] In the former, light from a laser is converted to circular polarization. Light scattered from a spherical particle is similarly circularly polarized, but from a fibre it is elliptically polarized. This change is detected by passing the scattered light through a quarter-wave plate and then to two photomultipliers which observe orthogonal polarizations. An increase in signal at polarization orthogonal to that incident signifies the presence of a fibre. The method is illustrated in Fig. 24. Rood et al. [369] used a similar concept by observing the orthogonal polarized intensities, but from particles sampled through an aligning nozzle onto a slide.

The instrument designed by Kaye et al. [368] is shown in Fig. 25. Here particles are passed through one focus of an ellipsoidal cavity. They are illuminated by a laser beam which enters through a small aperture and is reflected onto the particles by the mirror M. Scattering is observed over a wide range of angles at the second focus. The presence of form anisotropy is indicated by azimuthal asymmetry in the scattering pattern. Originally, three detectors at the vertices of an equilateral triangle were used. A CCD camera has also been employed with the promise of the ability to characterize quite complex shapes [370, 371]. More recently, attempts have been made to compare the observed patterns with theoretical predictions using the RGD approximation [372, 373]. The agreement is encouraging.

Using the original three detectors, Kaye et al. [374] have developed an automated method capable of monitoring up to 10 000 particles per second. The shape factor is obtained from

$$A_f = \frac{40.81}{\bar{E}} \sum_{j=1}^{3} \left(\bar{E} - E_j\right)^2$$

where the three values of E_j are the measurements at each of the detectors and $\bar{E}$ is the average. The mysterious value of 40.81 is to ensure that the maximum value of $A_f = 100$. Of course for spheres, $A_f = 0$.

The same instrument can be used to obtain size from

$$A_b = \sum_{j=1}^{3} E_j + \frac{1}{2} E_4$$

where E_4 is the forward-scattered signal. This measurement can be used to obtain the spherical equivalent size for refractive indices in the range $1.33 \leq m \leq 1.58$.

Similar ideas have been explored by other authors. For example, Sachweh et al. [375] also examined the asymmetry of azimuthal scattering, though at specific angles. Marshall [376] studied the diffraction pattern passing through specially designed filters to the same effect. In a slightly different approach, a fibre detector was developed by Brenci et al. [377] based upon measuring extinction and scattering at two angles.

Other examples of the use of polarization include the study by Belanger et al. [378], who illuminated a mixture of glass fibres and spheres designed to simulate skin or an injection-moulded polymer blend. By using polarized incident light and taking an image of the particles through a crossed polarizer, distinct patterns were observed which were indicative of the structure. Sierra and Mora [379] and Kim and Martin [380] studied the depolarization due to spheroids, in the latter case as a function of wavelength to develop a diagnostic method for interstellar grains. Mishchenko and Hovenier [381] performed a more general analysis for randomly aligned non-spherical particles.

A further application to non-spherical particles was described by Card and Jones [382]. This method used cross-polarization techniques to discriminate between coal and fly ash. The scattered light from the particles was collected at an angle close to the backward direction and analysed for polarization state using two photomultipliers in the same manner as in Fig. 24. By plotting the cross-polarized intensity against particle size, it was found that the two types of particle were readily discriminated. More recently [383] it has been demonstrated that there is a good correlation between the ratio of scattered intensities for the two orthogonal polarizations and the carbon content of the combusted coal particles, as suggested by Fig. 26.

Umhauer and Bottlinger [384] and Sasse [385] have made observations on single irregular particles suspended in an electromagnetic balance. The former authors compared measurements with calculations obtained by applying geometrical optics to slices of the particle in turn. They found that the ratio of the width to height of the scattered spectra was constant. This leads to possible means of eliminating the effects of shape and structure. Sasse [385] and Sasse et al. [386] have examined the phase function and cross-polarization from absorbing particles and means of directly measuring the albedo.

Another method of suspending individual particles was propounded by Doornbos et al. [387] This uses the radiation

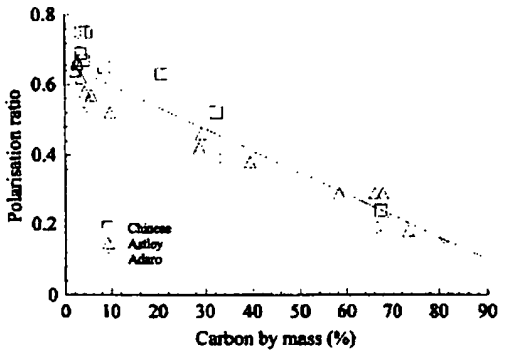

Fig. 26. Variation of mean polarization ratio against percentage of carbon by mass for fly ash from various coals. (After Card and Jones [382].)

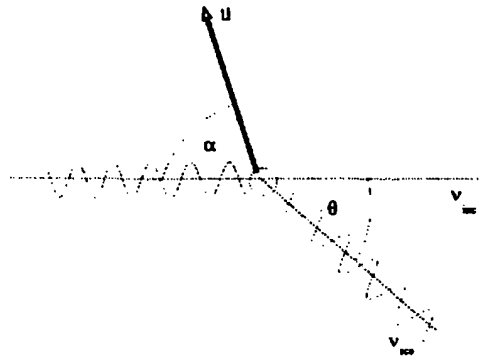

Fig. 27. Illustration of the coordinates for the Doppler shift equation.

pressure from two laser beams to trap single biological cells for optical study. The beams came from two 100 mW diode lasers with output wavelength 780 nm. Particles up to the order of 7 μm could be supported.

An apparatus for measuring all the components of the scattering matrix has been described by Kuik et al. [388] A number of studies have investigated the most suitable elements of this matrix for characterizing non-spherical particles. For example, Mishchenko et al. [91] applied the *T*-matrix method to the problem of two spheres in contact. They concluded that the only distinct manifestations of non-sphericity were that $(M_{22}/M_{11}) \neq 1$, $(M_{33}/M_{11}) \neq (M_{44}/M_{11})$ and non-zero backscattering depolarization ratio. Martin [389] studied slightly non-spherical particles using a perturbation method and obtained solutions for the matrix elements as expansions in spherical harmonics. In particular he found that for a rotationally symmetric particle

$$\frac{M_{13} - iM_{24}}{M_{12} + iM_{34}} = \tan 2\Delta\phi$$

where $\Delta\phi$ is the angle between the azimuthal angle of the particle axis and the direction of the incident polarization.

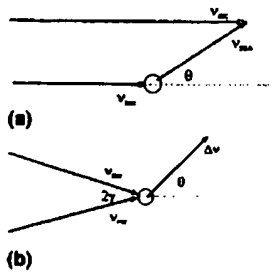

Fig. 28. Determination of the beat frequency in LDA from interference. In (a) the scattered frequency is a function of angle; in (b) it is independent of angle.

8.3. Laser Doppler methods

The need to measure velocity in particle counting suggests the use of optical anemometry. A suitable vehicle for this is the Doppler shift suffered by light deflected by a moving object. In the coordinates of Fig. 27, the scattered frequency seen by a stationary observer at the angle θ is

$$\nu_{sca} = \nu_{inc}\left[1 + \frac{2u}{c}\sin\frac{\theta}{2}\sin\left(\alpha - \frac{\theta}{2}\right)\right]$$

where c is the speed of light. This equation has two implications. First, since $u \ll c$, the change in frequency is very small compared with that of light. Secondly, the scattered frequency varies with angle.

The maximum possible change in frequency is

$$\frac{\nu_{sca} - \nu_{inc}}{\nu_{sca}} = \frac{\Delta\nu}{\nu} = \frac{2u}{c}$$

Thus for a velocity of 10 m s^{-1}, say, we find

$$\frac{\Delta\nu}{\nu} = 7 \times 10^{-8}$$

Such a small change would be difficult to detect directly. However, for a typical optical frequency of 5×10^{13} Hz, then $\Delta\nu = 3.5 \times 10^{6}$ Hz. This is coming into a range which can be readily be detected electronically, and it can be reduced further by appropriate choice of scattering angle. It can be observed by mixing the scattered wave with unscattered light to obtain the beat frequency from their interference, as in Fig. 28(a). The beat frequency varies with angle. Consequently, uncertainty in angle leads to error, and the received frequency can vary across an aperture. Also, it is often required to make measurements at or near the forward direction ($\theta = 0°$) where the beat frequency becomes zero.

These problems can be avoided by the arrangement in Fig. 28(b). Here the particle crosses the interference pattern produced by the intersection of two light beams. Theoretically this can be treated in two ways. Either the Doppler shift can be calculated for the wave scattered from each beam independently and the two waves added to give the beat frequency, or it may simply be considered in terms of a particle crossing a fringe pattern. In the latter case it is easily seen that the received frequency is given by

$$\nu = u/\lambda_f$$

where λ_f is the fringe spacing. The beat frequency treatment yields exactly the same answer. In this crossed beam arrangement the received frequency is independent of scattering angle. Also, the fringe spacing can be measured directly, reducing the error due to angular measurement. The test space is small, being given by the volume of intersection of the two beams, so that spatial resolution is improved.

A consequence of the size of the test space is the maximum allowable concentration. There must be only one par-

ticle at a time in this volume otherwise interference occurs between the scattered signals. For focused laser beams a diameter of 100 μm is reasonable. Then the maximum concentration is of the order 10^{12} m^{-3}. This may be reduced in forward scatter depending upon the achievable depth of field.

The general form of the scattered signal is

$$I_{sca} = A + B\cos(2\pi\nu t + \phi)$$

The frequency ν yields the velocity of the particle. For this reason the technique is referred to as laser Doppler anemometry (LDA). This subject has been reviewed by Durst et al. [390] The amplitudes A and B and the phase are functions of the particle size. Particle sizing techniques have been developed based on the measurement of A, the visibility (B/A) and ϕ.

The most obvious way to measure the size is via the mean intensity A. Such an instrument is a particle counter of the type described in Section 8.1 with added velocity measurement and the advantage of good spatial resolution. Apart from this it suffers from the same problems as the other absolute techniques. The method has been explored, for example, by Yule et al. [391], Ereaut [392], Orfanoudakis and Taylor [393] and Terhaag and Renz [394] using either pointer beams or top-hat beam profiles [354]. The combination with two-colour pyrometry to also obtain temperature has been discussed by Finke et al. [395].

The possible advantage of using the visibility or the phase is that they are relative measurements. They are independent of the instrument provided its response is linear.

8.3.1. Signal visibility

The visibility as a function of particle size can be calculated from Mie theory (e.g. Jones [396] and Eliasson and Dändliker [397]) or using common approximations (e.g. Chu and Robinson [398], Bachalo [399] and Pendleton [400]). A very simple result is that for large particles and collection apertures the visibility in the forward direction ($\theta = 0°$) reduces to

$$V_{sca} = \frac{2J_1(\pi D/\lambda_f)}{\pi D/\lambda_f}$$

where $J_1(z)$ is a Bessel function and λ_f is the fringe spacing in the interference pattern [401–403].

There are several major weaknesses of this method. The equation above shows that the visibility is initially a monotonic function decreasing with size, but then it oscillates. Thus the dynamic range is limited since beyond some point (typically $D \approx \lambda_f$) the size is not uniquely determined. Detailed Mie calculations (e.g. Hong and Jones [404]) also reveal extreme sensitivity to refractive index at even quite small angles away from the forward direction. If this property is not known, then very large errors can ensue. In addition, experiments have shown that the visibility is too shape-sensitive for the method to be employed on anything other than near spheres [405].

For non-absorbing particles the variation of visibility with particle properties and angle increases with the scattering angle until, near the backward direction, measurement is almost impossible [406]. On the other hand, for absorbing particles the visibility becomes unity for all angles greater than about 40° and there is no information. Since in many practical situations access is only available near the backward direction, these are important limitations.

Negus and Drain [407] suggested ways to overcome some of these problems from a study of the effects of aperture type and size and polarization state. In backscatter they were able to obtain a monotonic relationship in the range 0 to 250 μm. Measurement of backscatter was further explored by Azar and Ventrice [408], who produced maps of the real part versus the imaginary part of refractive index to delineate regions in which the visibility method is usable for incident circular polarization. They investigated a range of fringe spacings, aperture sizes and off-axis angles.

The visibility can never be greater than the fringe contrast in the interference pattern. This can be degraded due to unbalanced incident beam intensities. This can be caused by blocking of one beam or unequal blocking on passing through an extended particulate medium. Lack of temporal coherence can also result in the same effect. These phenomena and their significance have been explored, for example, by Yianneskis [409], Kliafas et al. [410, 411] and Lagranja et al. [412].

Also of significance may be refractive index gradients. These introduce two effects. First, phase shifts in the incident beams cause the fringes to move within the test space. Secondly, deflections of the beams cause the test space to wander. In anemometry these lead to false signals and errors in the measurement of velocity. An apparent velocity can be recorded from a stationary particle [413]. A similar problem has been reported by Ancimer and Fraser [414], who also suggest means for minimizing the error.

An interesting alternative to fringes of varying amplitude is fringes of varying polarization. Avery and Jones [415] showed that if the laser Doppler arrangement was modified by passing one beam through a quarter-wave plate and the other through a three-quarter plate, the result was a continual rotation of the plane of polarization across the test space. The period of the rotation was the same as the fringe spacing. Massoli et al. [416, 417] have used this method to measure the ratio of intensities scattered for two orthogonal incident polarizations. They claim to be able to measure drop sizes in sprays of up to several hundred micrometres.

8.3.2. Signal phase

A technique which overcomes many of the problems discussed above is to measure the phase of the scattered signal. This was proposed by Durst and Zaré [418] and came into prominence following the work of Bachalo and Houser [419] and Saffman et al. [420]. A history of the development of phase Doppler anemometer has been given by Hirleman [421].

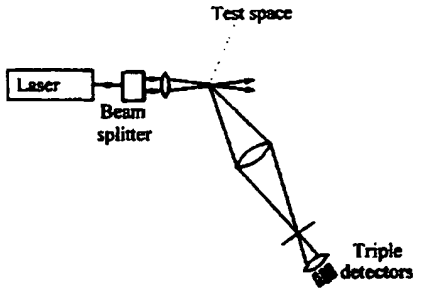

Fig. 29. Schematic diagram of phase Doppler particle analyser. (After Bachalo [424].)

As the particle moves in the test space formed by the two laser beams, the scattered light generates a set of interference fringes which move across the face of any detector. The resulting signal at a fixed point in space oscillates in time as the fringes move past. Because of the way in which the fringe separation varies in space, the phase ϕ varies similarly. This change of phase can be observed by comparing the signals received by two or more spatially separated detectors.

The rate of change of phase with angle generally increases with particle size. Under appropriate conditions it is found that the change is linear with sufficient slope to provide suitable accuracy for particle sizing. It is also linear over a wide range and the dynamic range can be large—typically 0.5–3000 μm. The accuracy at the smaller sizes has been discussed by Sankar et al. [422], who found that for $D < 10$ μm an accuracy of $\pm$ 0.3 μm is possible. Further extension to sub-micrometre particles is considered by Naqwi et al. [423].

There is a limitation, however, because once the phase becomes 2π the wave looks identical to one with a phase of zero. This can partially be overcome by the use of multiple detectors. In the instruments currently available up to three are used, typically as shown in Fig. 29 [424]. The scattering angle is either 30° or 150° out of the plane of the laser beams. The phase difference between the two outer detectors is greater than between either of these with the central one. It can be arranged that while the outer phase difference varies from zero to 6π, the central change is up to 2π. The outer detectors provide good sensitivity to size, while the central detector indicates which of the three cycles is being observed.

A generalized treatment of light scattering out of interferometric devices has been published by Naqwi and Durst [425]. This allows for arbitrary polarization, non-plane waves and Gaussian beams, and for integration over a variety of aperture shapes. Certain polarizations may assist in the production of a linear response by suppressing reflected light. Further analysis by Naqwi et al. [426] has suggested angles and apertures suitable for the measurements of metallic particles as small as 20 nm, transparent particles in the sub-micrometre range and particles with refractive index close to that of the surrounding medium.

The phase Doppler method has the advantage of being intensity-independent provided there is sufficient visibility to yield a measurable signal. It will not suffer from beam blocking nor need particles be restricted to the central zone of high fringe contrast. However, when particle counting, a correction is necessary to allow for the bias towards larger particles because of their larger scattered signal [409].

In the phase Doppler method the fringe spacing can be less than the particle size and the test volume can be kept small. Use of the off-axis angle of 30° also makes the intersection area smaller. Bachalo [427] has reported that concentrations of up to 10^{12} m^{-3} can be used.

The trajectory of the particles through the test space can lead to errors because the sample volume is a function of the particle size, as in all particle counting techniques with non-uniform intensity profiles. Schaub et al. [428] employed an arbitrary beam theory to explore this and found that phases are smaller for trajectories through the edge of the test space away from the receiver, and vice versa. This leads to an artificial apparent broadening of the size distribution. Scattering resonances were found to have a similar effect. The phase errors become particularly significant when the beam-width is not large compared with the particle diameter, as discussed by Albrecht et al. [429, 430]. The signals are only valid for the short period when the beam lies along the particle diameter.

Xu and Tropea [431] have proposed alignment procedures to minimize such errors arising from the Gaussian beam profile. Another suggestion for avoiding trajectory problems when the diameter of the test space is similar to that of the particle is given by Hardalupas and Taylor [432]. This involves the application of validation criteria based upon rejecting signals for which the phase lies outside the expected range in the three-detector system.

An alternative which moves away from the phase Doppler concept has been proposed by Borys et al. [433]. In this a frequency shift is added to one of the laser beams and the Doppler burst moves as the particle travels across the test space. This movement is simply related to the size.

Means of determining particle concentration and flux have been discussed, for example, by Albrecht et al. [429, 430], Qin and Sommerfeld [434] and Sommerfeld and Qin [435]. The difficulty here is that, while the numbers of particles can be counted, there is some uncertainty in the cross-sectional area through which they pass because it is size-dependent. This arises because, as mentioned previously, a large particle near the beam edge will scatter a measurable signal whereas a small one will not. The interpretation is that the larger particles are falling through a larger area. Thus the size and trajectory are also important here.

Tropea et al. [436] have attempted to resolve this difficulty with the design of a dual-mode phase Doppler anemometer. The principle is illustrated in Fig. 30. Two pairs of

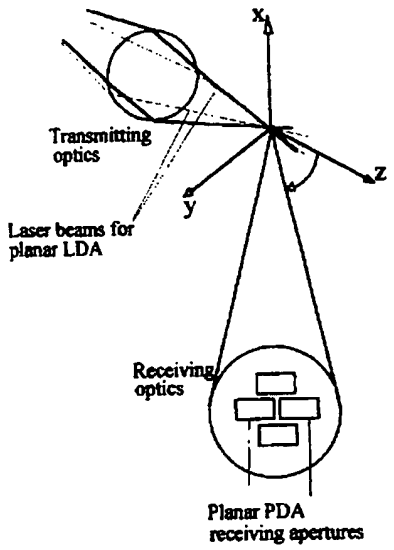

Fig. 30. The optical geometry of the dual-mode PDA. (After Tropea et al. [436].)

laser beams converge onto the test area in orthogonal planes so that two sets of interference fringes are generated at right angles to each other. The two sets could be discriminated, in principle, by using different wavelengths or polarizations. The detection system resides at 30° out of the scattering plane of one set of beams, as in the standard instrument. However, an additional pair of detectors measures the component of a particle's velocity orthogonal to the standard system, thus providing complete information on its trajectory. The effective width of the measurement volume is ascertained from the length of the Doppler burst.

Off-axis measurements raise the questions of shape and refractive index. It would be expected that the method is sensitive to these. Currently the particles must be spherical or nearly so, and the refractive index may need to be known, in order that the instrument response can be calibrated or calculated. Schneider and Hirleman [437] have also pointed out that there may be significant errors in phase due to the presence of refractive index gradients, although the response remains linear. Nonetheless, the inhomogeneity results in a blurring of the recovered size distribution and Köser and Wriedt [438] have proposed an iterative technique for removing this effect.

The influence of shape has been investigated by Doicu et al. [439] using the extended boundary method to solve the problem for spheroids. They find that an eccentricity of 0.05 causes a phase error of 5%.

In two-phase flows small tracer particles are often used to indicate the flow of the gas. An example would be the flow of the gas within and around a liquid spray. It would be convenient to measure both particle sizes with the same optical system but, unfortunately, the scattered signal from the large drops usually swamps that from the seed particles. Friedman and Renksizbulut [440] have avoided this problem by adding an absorbing dye to the large drops to reduce their scattering cross-section.

8.4. Size from the measurement of inertia

In a diverging flow a particle accelerates at a rate dependent upon its inertia. Injecting a particle into a tailored flow pattern and measuring its velocity will yield its size. There are a number of instruments based upon this principle. Such a measurement is purely mechanical and does not depend upon a knowledge of the refractive index. The size recorded is that which determines the mechanics of the interaction between the particle and the carrying fluid. This is the hydraulic or aerodynamic diameter. In many applications in fluid flow this is the required parameter.

An approach proposed by Tate et al. [441] uses a fibre optic probe inserted into the flow. The probe has a hemispherical end which acts as a bluff body causing divergence of the fluid and having a stagnation point a short distance ahead of it where the fluid velocity is zero. Due to its inertia, a particle approaching the probe will not have zero velocity at this point. The more massive the particle, the closer its velocity will be to that at a distance remote from the probe. Hence measurement of the velocity at this point yields the mass and, consequently, the size provided the density is known.

Light is transmitted along the fibre and focused onto the stagnation zone. Reflection from the particle is collected and passed back to a detector where it is mixed with unscattered light. A beat frequency is then observed arising from the Doppler shift.

The minimum measurable particle size is governed by two factors. There must be sufficient light intensity to provide a good signal. Given this, the velocity at the stagnation point must be sufficiently different from zero, which suggests a minimum inertia. Similarly there is a maximum inertia because the velocity must be different from that remote from the probe. Tate et al. [441] claim that a measurable size range in the ratio of ten to one is feasible.

There is some error due to the detection of particles not at the stagnation point arising from the finite depth of field. The upper concentration that can be used is limited by multiple particles in the effective test space.

In turbulent flow there are orthogonal velocity components. This means that a measured particle will not generally be travelling directly towards the probe. Only a component of its velocity will be obtained and it will be judged to be too small. However, results due to Vincent et al. [442] imply that this effect will not be serious in the range of Reynolds number between 3300 and 10^4.

An interesting technique based upon aerodynamic properties has been suggested by Roll et al. [443]. In this particles are optically levitated on a laser beam and their behaviour monitored when the beam is momentarily interrupted. The

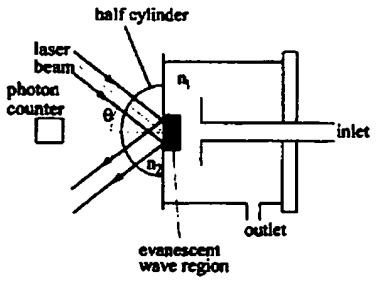

Fig. 31. Use of total internal reflection for the study of particle deposition. The refractive index of the half cylinder (n_2) is greater than that in the chamber (n_1) and the angle of incidence (θ) is greater than the critical angle for total internal reflection. (After Polverari and van de Ven [464].)

method is not restricted to spheres. The authors used it to study the evaporation of single and two-component drops in the size range 10–40 μm.

8.5. Particles on surfaces

A new area which has sparked much interest is scattering by particles on or near surfaces. This has arisen primarily because of the problem of contamination of surfaces in micro-electronic circuit production. There is a need to detect and identify particle contaminants. Recent papers in this area are by Lindell et al. [444], Muinonen et al. [445], Videen [446, 447], Johnson [448, 449], Jakeman [450] and Saiz et al. [451].

Videen et al. [452] have compared four different theories. They all agree in the far field, but approximations break down when the sphere-to-surface distance is less than the wavelength. More recently Videen and co-workers have published a series of papers where they develop a model which only requires the expansion coefficients for the scattered wave of an isolated particle. The particle can be of any shape. The theory treats the particle and its image subjected to three fields, the incident and reflected fields and a term representing the interaction due to the reflection of scattered light [453–455].

Typical further techniques include direct backscatter plus scattering of reflection from a surface [456], the discrete sources model [457], ray tracing [458], image theory [459] and multipole expansion [19]. Some special applications which have been discussed include anisotropic particles [460], cylinders [455], the effects of particle density [461] and sizing metallic particles [462]. While the above have been concerned with metallic surfaces, Liswith et al. [463] have specifically examined scattering by small spheres on silicon and oxidized silicon substrates.

In an interesting variation, Polverari and van de Ven [464] studied the deposition of particles on a transparent surface using frustrated total internal reflection. The incident wave was inside the material, the angle being sufficient for total internal reflection. Particles were deposited on the outside and scattered the evanescent wave which penetrated the surface. The principle is seen in Fig. 31. Since the penetration of the evanescent wave depends upon the angle of incidence, variation of this angle allowed different levels in the particle layer to be observed.

9. Direct inversion to size distribution

To obtain the size distribution for scattering from a cloud of particles, it is necessary to invert the light scattering data. There are two approaches. The first is the "best-fit" method in which the scattering properties are predicted by using presumed size distributions and compared with measurements to find the closest comparison. Commonly, simple two-parameter distributions are assumed such as Rosin–Rammler and log-normal functions. The problem then reduces to the determination of only two numbers. This works well provided that the true distribution is similar to that presumed. However it often breaks down, especially if the true distribution is multi-modal.

The alternative is direct inversion, in which an integral of the form

$$f(x) = \int g(x,y)n(y)\,dy + \varepsilon(x)$$

is solved to obtain $n(y)$. $f(x)$ is the measured function and $\varepsilon(x)$ is due to errors of measurement. $g(x, y)$ is the kernel of the integral and is a known function which may be calculated from an appropriate theory.

Specific forms of the terms in the integral equation are:

1. Fraunhofer diffraction

$$f(x) = I_{sca}(\theta)$$

$$g(x,y) = a^4\left[\frac{2J_1(kR\theta)}{kR\theta}\right]^2$$

$$n(y) = n(D)$$

where $D = 2R$.

2. Spectral extinction

$$f(x) = K_{ext}(\lambda)$$

$$g(x,y) = \frac{\pi D^2}{4}Q_{ext}(D/\lambda)$$

$$n(y) = n(D)$$

3. Photon correlation spectroscopy

$$f(x) = S(\tau)$$

$$g(x,y) = \exp\left(-2k^2D_f\tau\right)$$

$$n(y) = n(D_f)$$

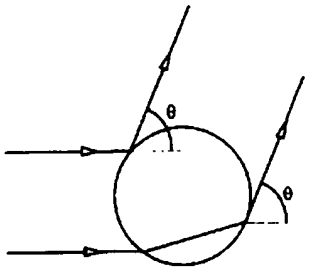

Fig. 32. Ray diagram illustrating the principle of the generation of two pulses by a spherical particle passing through a narrow laser beam. (After Onofri et al. [505, 506].)

In this case the inversion takes the form of a Laplace transform.

We may write the integral equation in matrix form as

$$F_i = G_{ij}N_j + E_i$$

In principle, if there is little or no error ($E_i \rightarrow 0$), the matrix equation may be inverted directly. However, the kernel G_{ij} is ill-conditioned and sensitive both to error and numerical rounding. The art, therefore, is to provide methods of inversion which can deal with noise.

An obvious approach is the method of least squares. Perhaps the most popular such technique is that due to Phillips [465] and Twomey [466]. However, it has the disadvantage that the operator has to adjust an unknown Lagrangian multiplier to achieve an appropriately smooth output curve. Much is left to personal judgement, although Amato et al. [467] discuss ways of selecting the smoothing parameter. In a further development, Shifrin and Zolotov [468] have suggested a means of choosing the most appropriate regularization parameter.

A modified form of the Phillips–Twomey method was used by Ramachandran and Leith [469]. Their results were satisfactory for $0.34 \leq \lambda \leq 0.94\ \mu$m and $0.3 \leq D \leq 2.5\ \mu$m. Ramachandran et al. [470] have further developed the method by the use of computational tomography to enable concentration and size distribution to be obtained as a function of position in an aerosol cloud.

Other methods of direct inversion have been discussed by Bertero et al. [471, 472], Ben-David et al. [473, 474], Viera and Box [475–477], Curry [478], Shimizu and Ishimaru [479], Box and Viera [480], Wolfenberger and Seinfeld [481], Brianzi and Fontini [482], Schnablegger and Glatter [483], Box et al. [484], Dellago and Horvath [485, 486], Ferri et al. [487], Dubovik et al. [488], Gail [489], Bryant and Thomas [490] and Ramachandran and Kandlikar [491]. An interesting variant due to Ligon et al. [492] employs a Monte Carlo technique in which sizes are chosen at random and the sum of the squares of the difference between the predicted and measured scattering parameters is minimized. Benayahu et al. [493] have attempted direct inversion in the presence of double scattering events. The influence of refractive index on the inversion problem in the anomalous diffraction regime has been investigated by Oshchepkov and Dubovik [494].

Recently there seems to have been some renewed interest in fitting the experimental data using presupposed trial functions for the size distribution. Sun and Lewis [495] assumed a log-normal distribution and adjusted the parameters to minimize the sum of the squares using a simplex deconvolution. Amato et al. [496] compared the Twomey method with a multi-modal log-normal distribution and found reasonable agreement.

A lengthy review has been given by Bates et al. [497]. They propose an approach which saves computer time by sacrificing accuracy. Nonetheless, the accuracy is reasonable.

10. Measurement of refractive index

In order to fully characterize particles, their refractive index should be measured as well as size and shape. Not only would this enable particle types to be identified, but proposals are being made to measure temperature directly through the variation of refractive index.

Addition of refractive index increases the number of variables to be measured. For spheres this becomes three—size and the real and imaginary parts of the refractive index. Any one scattering measurement is a function of all three, although close to the forward direction size is by far the dominant parameter. Thus a single measurement can predict a range of possible combinations of the variables lying on one or more surfaces in the variable space. Multiple measurements, in principle, can pinpoint the true values by noting where all the surfaces intersect. This approach was attempted by Avery and Jones [415] for coal, though this was unsuccessful because of the particle irregularity. Similar problems were encountered by Bhattacharya et al. [498].

For more nearly spherical particles, intersecting contours obtained by the visibility method were successful for non-absorbing particles [499]. Later, measurement of the full complex refractive index of absorbing liquid drops was demonstrated by Card and Jones [500], again from the visibility method, although a total of four scattering angles was needed. Takeda et al. [501] have also used contour matching and employed two wavelengths and two angles to provide four measurements. However, only the real part was obtained and dispersion was neglected. Methods involving minimizing the difference between measured and scattered light parameters have also been proposed by Chae and Lee [502] and Schnablegger and Glatter [503].

The possibility of material recognition via refractive index measurement has been proposed by Naqwi et al. [423, 504]. The suggested method involves measuring

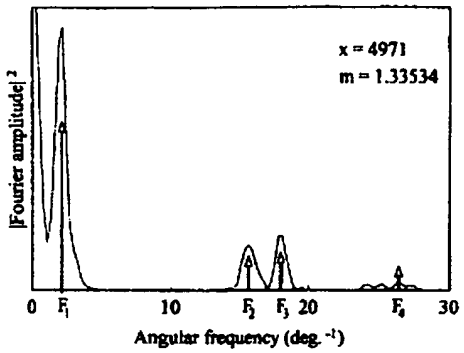

Fig. 33. Magnitude squared of the Fourier transform of the angular scattering diagram near the rainbow. (After van Beeck and Riethmuller [514].)

both phase and frequency of the scattered light. Extra detectors are required and the refractive index comes from the ratios of the phases or frequencies.

Another interesting possibility for the measurement of refractive index and size for the case in which the particle diameter is much larger than the beamwidth, is the so-called dual burst technique [505]. The principle behind this can be understood by considering the behaviour of a single ray as it is traversed by a drop, as in Fig. 32. At any one angle there are two pulses, one due to reflection off the outer surface and one due to refraction. For a given particle size the time delay is a known function of the refractive index. Also, if there is absorption, the height of the pulse due to refraction is reduced. Thus it is possible in principle to measure the full complex refractive index. The authors have performed a full analysis for the case of a narrow Gaussian beam, and have also investigated the prospect of determining inhomogeneity of refractive index by examining concentric spheres [506].

A specific suggestion for refractive index measurement with a view to remote temperature sensing has come from Massoli et al. [507]. They propose that the ratio of scattered intensities at 33° and 60° be measured by using horizontal polarization. This displays a strong monotonic dependence on refractive index, although there is some sensitivity to size. The technique only applies to homogeneous spheres.

Clapp et al. [508] measured the absorption spectrum of an aerosol of water ice in order to obtain the imaginary part of the refractive index. The real part was found by use of the Kramers–Kronig [191] relationship. They quote the full complex refractive index of ice as a function of both temperature and wavelength over the range 2.5 μm to 12.5 μm.

A different approach has been discussed by Taubenblatt and Batchelder [509], essentially employing interferometry. The scattered light is mixed with a reference wave so that both amplitude and phase can be measured. A plot of the extinction against phase shift is found to be sensitive to refractive index. Even for non-spherical particles it is claimed that there is sufficient information for particle discrimination.

An obvious candidate for the measurement of the refractive index of large transparent spheres is to determine the angular position of the rainbow. For spheres which are sufficiently large, this is independent of size. Massoli et al. [507] showed that at optical wavelengths the diameter needed to be greater than about 60 μm.

The position of the primary rainbow is found by geometrical optics as the angle of minimum deviation of a ray which has undergone two internal reflections. There are higher order rainbows associated with multiple internal reflections. The positions of the rainbows are given by Bohren and Huffman [4] as

$$\cos \Theta_n = \sqrt{\frac{m^2 - 1}{n(n+2)}}, \qquad n = 1, 2, 3, \ldots$$

where m is the refractive index.

An attempt to apply the rainbow method to the measurement of refractive index of burning fuel drops, and through this to obtain the temperature, was made by Roth et al. [510]. However, it was soon pointed out that such a drop would have a temperature gradient within it and that this may substantially influence the result of a rainbow measurement. Schneider et al. [511] performed an analysis on this and concluded that errors in the measured temperature would be significant. Kai et al. [25] used the stratified sphere model to indicate the ways in which this position fluctuates and Anders et al. [512] used geometrical optics to the same end. The latter authors suggest that if the surface temperature could be measured independently, then rainbows could be used to find the internal temperature gradient.

Inhomogeneity has also been investigated by Lock et al. [513]. In this case they examined the behaviour of the rainbow for a coated sphere as the thickness of the coating varied. For a coating thickness δ and a drop radius R, the intensity of the rainbow oscillates with thickness provided $\delta/R \leq 10^{-3}$. For $\delta/R \approx 10^{-2}$ the primary rainbow breaks into two separate rainbows.

An interesting technique to measure particle size and to indicate shape has been described by van Beeck and Riethmuller [514]. They take the Fourier transform of the scattering pattern for angles equal to and greater than the rainbow angle. The amplitude spectrum produced has a series of peaks, as indicated in Fig. 33. The positions of the various peaks are given by

$$F_1 = \frac{\sin \tau}{2.3794} \left(\frac{16D^2}{\lambda^2 \cos \tau} \right)^{1/3} \frac{\pi}{180}$$

$$F_2 = \frac{D}{2\lambda} \left(\cos \tau + \cos \frac{\theta}{2} \right) \frac{\pi}{180} - \frac{F_1}{2}$$

$$F_3 = F_1 + F_2$$

where

$$\sin \tau = \sqrt{\frac{m^2 - 1}{3}}$$

The size can be determined either from F_1 or F_2. If the two sizes are not equal, the particle is not spherical.

Some interesting phenomena occur when the beamwidth is of the order or less than the diameter of the particles. For example, Lock [53] demonstrated that a narrow Gaussian beam incident near the edge of a particle can produce rainbows up to ninth order. Chan and Lee [515] observed up to 32 rainbows. They showed that a plot of angular position against order could be used to obtain refractive index.

11. Tomography

With the advent of cheap computing power a new method has become available for the reconstruction of the structure of objects. This is tomography, in which the object is subjected to a test and the response is observed remotely. The test may be the application of a magnetic field, a flux of neutrons or X-rays, as in medical tomography. In scattering a cloud of particles is illuminated by electromagnetic radiation and the scattered intensity is found. The illuminating field may be incident on all points of the object simultaneously, or it may be scanned across. Similarly, the remote response may be measured at all points simultaneously, or the distribution may be built up over time.

The relationship between the detected pattern and the structure of the object leads to a complicated set of mathematical equations. It is for this reason that significant computing power is required.

An early example of the application of tomography to a scattering system was the application to a sooting flame by Jagoda et al. [516]. The problem was simplified by assuming axial symmetry. In this method the cloud is divided into a number of concentric rings each sufficiently narrow that the concentration within it may be considered uniform, as in Fig. 34. The laser beam first passes only through the outer ring along path 1. Since the properties are uniform, the size and concentration are easily determined. The beam next follows path 2. It suffers known extinction as it crosses ring 1 on the way in and out. The extinction due to ring 2 alone is then easily found. Similarly, the light scattered out of ring 2 suffers known extinction as it emerges through ring 1. Thus the size and concentration in ring 2 are found. The process is repeated until the central zone is reached.

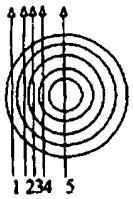

Fig. 34. Illustration of the subdivision of an axially symmetric system into a set of concentric circles.

A more general form of this technique replaces the scanning of the beam and single detector by an expanded beam illuminating the full diameter of the flame and an array of detectors. There is one detector for each ring, as above. For systems which are not axisymmetric the beam–detector assembly can be rotated around the flame and measurements made at a number of angles, as in medical tomography.

More recent applications to scattering include work by Sivanathu and Gore [517] and Menguç and Dutta [518]. In both cases axial symmetry was assumed. In the latter, two beams were used uniformly spaced about the centre of a sooting flame, the comparison of the two yielding an absorption coefficient profile. Bates et al. [519] applied Fourier transform Hadamard tomography to sooting flames and Drescher et al. [520] measured gas concentrations in air. Tomography has been applied to aerosols by Ramachandran et al. [470] and to sprays by Oberlé and Ashgriz [521] using backscatter. A Doppler tomography method has been devised by Wang et al. [522] to map fluid flow velocity.

12. Conclusion

It is now of the order of 100 years since Lorenz [16], Mie [17], Rayleigh [12] and Tyndall [523] laid the foundations of light scattering. Since then the technique has developed into one of the most powerful diagnostic tools for probing the properties of particulate matter.

The primary focus of attention for particle characterization has been the measurement of size. Traditionally this was based on the assumption of a sphere, because of theoretical restrictions, and considerable effort went into developing techniques which were insensitive to shape and (often unknown) refractive index. These were largely successful, and more recent developments have been concerned with extending the dynamic range of the instruments, with regard to both the size and the range of particle concentrations over which they may be employed. The measurement of size is now largely a matter of course, although improvements in instrumentation continue.

Interest has now begun to switch to the determination of other characteristics, such as shape, structure, composition and the distribution of material within a particle cloud. From small beginnings about a decade ago, the rate of publications in this area is accelerating rapidly. Some of the areas of particular interest to combustion include the determination of drop temperature in a spray, the structure of soot agglomerates, the measurement of residual carbon in fly ash and tomography to reveal the structure of a burning spray.

On the theoretical side, there have been massive improvements in numerical methods for the calculation of the scattering properties of non-spherical and non-uniform particles, and in inversion techniques for the direct determi-

nation of particle properties from light scattering data. The new mathematics of fractal analysis has had considerable impact on the understanding of agglomerates of small particles.

Even after a century light scattering continues to be a very vigorous field of study. This is evident from the large and growing number of publications appearing each year. There is every reason to believe that the field will continue to grow with many exciting developments to come. The growing power and speed of computers will inevitably enable the full potential of numerical methods to be realized, so that the properties of particles of complex shape and structure can be calculated for practical values of size and refractive index. They will also assist in the study of the statistical nature of random shapes and multiple scattering interactions, and facilitate direct inversion procedures and tomography. No doubt the extra information generated will lead to new measurement techniques for a wide range of particle properties, especially in those areas where interest has emerged relatively recently such as irregularity, refractive index, composition and structure. General technological development such as new light sources, improved optical fibres, solid-state devices and faster electronics will also have an impact, leading to enhanced and novel instrumentation covering a wider range of operational situations. In the combustion context, this would include the ability to probe hostile environments with increased ease and confidence.

References

[1] van de Hulst HC. Light scattering by small particles. London: Chapman and Hall, 1957 [Reprinted and published by Dover, New York, 1981.]
[2] Kerker M. The scattering of light, New York: Academic Press, 1969.
[3] Jones AR. Progr. Energy Combust. Sci. 1979;5:73–96.
[4] Bohren CF, Huffman DR. Absorption and scattering of light by small particles. New York: Wiley-Interscience, 1983.
[5] Bayvel LP, Jones AR. Electromagnetic scattering and its applications. London: Applied Science Publishers, 1981.
[6] Black DL, McQuay MQ, Bonin MP. Progr. Energy Combust. Sci. 1996;22:267–306.
[7] Jones AR. In: Taylor AMKP, editor. Instrumentation for flows with combustion. London: Academic Press, Ch. 5, 1993.
[8] Saxon DS. Phys. Rev. 1955;100:1771–1775.
[9] Turner L. Appl. Optics 1973;12:1085–1090.
[10] Bowman JJ, Senior TBA, Uslenghi PLE. Electromagnetic and acoustic scattering from simple shapes. Amsterdam: North Holland, 1969.
[11] Morse PM, Feshbach H. Methods of theoretical physics. New York: McGraw-Hill, 1953.
[12] Rayleigh Lord. Phil. Mag. 1881;12:81.
[13] Wait JR. Can. J. Phys. 1955;33:189–195.
[14] Kai L, d'Alessio A. Appl. Optics 1995;34:5520–5530.
[15] Wang RT, van de Hulst HC. Appl. Optics 1995;34:2811–2821.
[16] Lorenz LV. Vidensk. Selsk. Skr. 1890;T6(6).
[17] Mie G. Ann. d. Phys. 1908;25:377.
[18] Lock JA, Yang L. J. Opt. Soc. Amer. 1991;8A:1132–1134.
[19] Johnson BR. J. Opt. Soc. Amer. 1996;13A:326–337.
[20] Perelman AY. Appl. Optics 1996;35:5452–5460.
[21] Kai L, Massoli P. Appl. Optics 1994;33:501–511.
[22] Kai L, d'Alessio A. Part. Part. Syst. Char. 1995;12:119–122.
[23] Kai L, d'Alessio A. Part. Part. Syst. Char. 1995;12:237–241.
[24] Kai L, Min Z, d'Alessio A. Opt. Commun. 1995;116:307–309.
[25] Kai L, Massoli P, d'Alessio A. Part. Part. Syst. Char. 1994;11:385–390.
[26] Bhanti D, Manickavasagam S, Menguc MP. J. Quant. Spectrosc. Radiat. Transf. 1996;56:591–608.
[27] Borghese F, Denti P, Saija R, Sindoni OI. J. Opt. Soc. Amer. 1992;8A:1327–1335.
[28] Borghese F, Denti P, Saija R. Appl. Optics 1994;33:484–493.
[29] Videen G, Ngo D, Chýlek P, Pinnick RG. J. Opt. Soc. Amer. 1995;12A:922–928.
[30] Fuller KA. Opt. Lett. 1993;18:257–259.
[31] Fuller KA. J. Opt. Soc. Amer. 1995;12A:905–915.
[32] Videen G, Ngo D, Chýlek P. Opt. Lett. 1994;19:1675–1677.
[33] Chýlek P, Lesins GB, Videen G, Wong JGD, Pinnick RG. J. Geophys. Res.—Atmos. 1996;101:23365–23371.
[34] Lock JA, Hovenac EA. J. Opt. Soc. Amer. 1991;8A:1541–1552.
[35] Lai HM, Leung PT, Poon KL, Young K. J. Opt. Soc. Amer. 1991;8A:1553–1558.
[36] Asano S, Yamamoto G. Appl. Optics 1975;14:29–49.
[37] Kurtz V, Salib S. J. Imaging Sci. 1993;37:43–60.
[38] Martin RJ. J. Mod. Optics 1993;40:2467–2494.
[39] Farafonov NG, Voshchinnikov VV, Somsikov VV. Appl. Optics 1996;35:5412–5426.
[40] Voshchinnikov VV. J. Quant. Spectrosc. Radiat. Transf. 1996;55:627–636.
[41] Tam WG, Corriveau R. J. Opt. Soc. Amer. 1978;68:763–767.
[42] Gouesbet G, Maheu B, Gréhan G. In: Gouesbet G, Gréhan G, editors. Optical particle sizing: theory and practice. New York: Plenum Press, 1988:27–42.
[43] Gouesbet G, Gougeon P, Le Toulouzan JN, Thioye M. In Gouesbet G, Gréhan G, editors. Optical particle sizing: theory and practice. New York: Plenum Press, 1988:371–384.
[44] Gouesbet G, Gréhan G, Maheu B. J. Opt. Soc. Amer. 1990;7A:998–1007.
[45] Chevaillier JP, Fabre J, Gréhan G, Gouesbet G. Appl. Optics 1990;29:1293–1298.
[46] Lock JA, Gouesbet G. J. Opt. Soc. Amer. 1994;11A:2503–2515.
[47] Lock JA, Gouesbet G. J. Opt. Soc. Amer. 1994;11A:2516–2525.
[48] Ren KF, Gréhan G, Gouesbet G. J. Opt. Soc. Amer. 1994;11A:2072–2079.
[49] Lock JA. Appl. Optics 1995;34:559–570.
[50] Ren KF, Gréhan G, Gouesbet G. Part. Part. Syst. Char. 1990;9:144–150.
[51] Gouesbet G. Part. Part. Syst. Char. 1995;12:242–256.
[52] Guilloteau F, Gréhan G, Gouesbet G. Appl. Optics 1992;31:2942–2951.
[53] Lock JA. J. Opt. Soc. Amer. 1993;10A:693–706.

[54] Hodges JT, Gréhan G, Gouesbet G, Presser C. Appl. Optics 1995;34:2120–2132.
[55] Gouesbet G, Letellier C, Gréhan G, Hodges JT. Opt. Commun. 1996;125:137–157.
[56] Lock JA. J. Opt. Soc. Amer. 1995;12A:929–938.
[57] Gouesbet G, Lock JA, Gréhan G. Appl. Optics 1995;34:2133–2143.
[58] Gouesbet G. Appl. Optics 1996;35:1543–1555.
[59] Gouesbet G. J. Opt. Soc. Amer. 1996;13A:2434–2440.
[60] Lock JA, Hodges JT. Appl. Optics 1996;35:6605–6616.
[61] Onofri F, Gréhan G, Gouesbet G. Appl. Optics 1995;34:7113–7124.
[62] Lewin L. IEEE Trans. 1970;MTT-18:1041–1047.
[63] Joo KS, Iskander MF. IEEE Trans. 1990;AP-38:1483–1490.
[64] Ludwig AC. Comp. Phys. Commun. 1991;68:306–314.
[65] Skarapoulos NC, Ioannadou MP, Chrissoulidis DP. J. Opt. Soc. Amer. 1994;11A:1859–1866.
[66] Al-Rizzo HM, Tranquilla JM. Appl. Optics 1995;34:3502–3521.
[67] Waterman PC. Proc. IEEE 1965;53:805–812.
[68] Barber P, Yeh C. Appl. Optics 1975;14:2864–2872.
[69] Wiscombe WJ, Mugnai A. Appl. Optics 1988;27:2405–2421.
[70] Killinger RT, Zerull RH. In: Gouesbet G, Gréhan G, editors. Optical particle sizing: theory and practice. New York: Plenum Press, 1988:419–429.
[71] Mugnai A, Wiscombe WJ. Appl. Optics 1989;28:3061–3073.
[72] Iskander MF, Lakhtakia A, Durney CH. Proc. IEEE 1982;70:1361–1362.
[73] Iskander MF, Chen HY, Penner JE. Aerosol Sci. Technol. 1989;10:172–180.
[74] Iskander MF, Chen HY, Duong TV. IEEE Trans. 1989;EMC-31:157–163.
[75] Schneider JB, Peden IC. IEEE Trans. 1988;AP-36:1317–1321.
[76] Ruppin R. J. Phys. D 1990;23:757–763.
[77] Kuik F, de Haan JF, Hovenier JW. Appl. Optics 1994;33:4906–4918.
[78] Barton JP. Appl. Optics 1996;35:532–541.
[79] Barber PW, Hill SC. In: Gouesbet G, Gréhan G, editors. Optical particle sizing: theory and practice. New York: Plenum Press, 1988:43–53.
[80] Mishchenko MI, Travis LD. Opt. Commun. 1994;109:16–21.
[81] Mishchenko MI. J. Opt. Soc. Amer. 1991;8A:871–882.
[82] Mishchenko MI. Appl. Optics 1993;32:4652–4666.
[83] Mishchenko MI, Travis LD. Appl. Optics 1994;33:7206–7225.
[84] Khlebtsov NG. Appl. Optics 1992;31:5359–5365.
[85] Mishchenko MI. Astrophys. J. 1991;367:561–574.
[86] Mishchenko MI, Travis LD, Mackowski DW. J. Quant. Spectrosc. Radiat. Transf. 1996;55:537–575.
[87] Barton JP, Alexander DR. J. Appl. Phys. 1991;69:7973–7986.
[88] Khaled EEM, Hill SC, Barber PW. IEEE Trans. 1993;AP-41:295–303.
[89] Khaled EEM, Hill SC, Barber PW. Appl. Optics 1994;33:3308–3314.
[90] Mishchenko MI, Mackowski DW. Opt. Lett. 1994;19:1604–1606.
[91] Mishchenko MI, Mackowski DW, Travis LD. Appl. Optics 1995;34:4589–4599.
[92] Wang ZL, Hu C, Liu WG. J. Phys. D 1994;27:447–451.
[93] Wang YM, Chew WC. IEEE Trans. 1993;AP-41:1633–1639.
[94] Peltoniemi JI. J. Quant. Spectrosc. Radiat. Transf. 1996;55:637–647.
[95] Newton RG. Scattering theory of waves and particles. New York: McGraw-Hill, 1966.
[96] Saxon DS. In: Kuriyan JG, editor. Proc. UCLA Conf. Radiation and Remote Probing of the Atmosphere. Los Angeles, CA: NASA, 1974:227–308.
[97] Richmond JH. IEEE Trans. 1966;AP-14:460–464.
[98] Hagmann MJ, Gandhi OP, Durney CH. IEEE Trans. 1978;AP-26:743–748.
[99] Newman EH, Kingsley K. Comp. Phys. Commun. 1991;68:1–18.
[100] Schaubert DH, Wilton DR, Glisson AW. IEEE Trans. 1984;AP-32:77–85.
[101] Schaubert DH, Meany PM. IEEE Trans. 1986;AP-34:587–595.
[102] Mendes L, Arras E. IEEE Trans. Magnetics 1991;27:4295–4298.
[103] Lu CC, Chew WC. IEEE Trans. 1995;AP-43:500–507.
[104] Purcell EM, Pennypacker CR. Astrophys. J. 1973;186:705–714.
[105] Singham SB, Bohren CF. J. Opt. Soc. Amer. 1988;5A:1867–1872.
[106] Singham SB, Bohren CF. Appl. Optics 1989;28:517–522.
[107] Mulholland GW, Bohren CF, Fuller KA. Langmuir 1994;10:2533–2546.
[108] Okamoto H. Opt. Rev. 1995;2:407–412.
[109] Venizelos DT, Lon W, Charalampopoulos TT. Appl. Optics 1996;35:542–548.
[110] Draine BT, Flateau PJ. J. Opt. Soc. Amer. 1994;11A:1491–1499.
[111] Ku JC. J. Opt. Soc. Amer. 1993;10A:336–342.
[112] Iskander MF, Chen HY, Penner JE. Appl. Optics 1989;28:3083–3091.
[113] Wolff MJ, Clayton GC, Martin PG, Schulte RE. Astrophys. J. 1994;423:412–425.
[114] Rouleau F, Martin PG. Astrophys. J. 1993;414:803–814.
[115] Rouleau F, Martin PG. Astrophys. J. 1993;416:707–718.
[116] Draine BT, Goodman J. Astrophys. J. 1993;405:685–697.
[117] Lumme K, Rahola J. Astrophys. J. 1994;425:653–667.
[118] Lakhtakia A, Vikram CS. Opt. Eng. 1993;32:1996–1998.
[119] Drolen BL, Tien CL. J. Quant. Spectrosc. Radiat. Transf. 1987;37:433–448.
[120] Dobbins RA, Megaridis CM. Appl. Optics 1991;30:4747–4754.
[121] Dittman R. Part. Part. Syst. Char. 1996;13:97–103.
[122] Goodman JJ, Draine BT, Flateau PJ. Opt. Lett. 1991;16:1198–1200.
[123] Perrin JM, Sivan JP. Astron. Astrophys. 1991;247:497–504.
[124] Kumar S, Tien CL. ASME J. Heat Transf. 1990;112:178–185.
[125] Flateau PJ, Stephens GL, Draine BT. J. Opt. Soc. Amer. 1990;7A:593–600.
[126] Yung YL. Appl. Optics 1978;17:3707–3709.
[127] Charalampopoulos TT, Panigrati PK. J. Phys. D 1993;26:2075–2981.

[128] Bourrely C, Chiappetta P, Le Maire T, Torresani B. J. Opt. Soc. Amer. 1992;9A:1336–1340.
[129] Henning Th, Stognienko R. Astron. Astrophys. 1993;280:609–616.
[130] Kozasa T, Blum J, Okamoto H, Mukai T. Astron. Astrophys. 1993;276:278–288.
[131] Buitenhuis J, Dhont JK, Lekkerkerker HNW. J. Coll. Interf. Sci. 1994;162:19–24.
[132] Taubenblatt MA, Tran TK. J. Opt. Soc. Amer. 1993;10A:912–919.
[133] Mackowski DW. J. Opt. Soc. Amer. 1994;11A:2851–2861.
[134] Mackowski DW. Appl. Optics 1995;34:3535–3545.
[135] Rouleau F. Astron. Astrophys. 1996;310:680–698.
[136] Michel B. J. Opt. Soc. Amer. 1995;12A:2471–2481.
[137] Michel B, Henning Th, Stognienko R, Rouleau F. Astrophys. J. 1996;468:834–840.
[138] Lakhtakia A, Mulholland GW. J. Res. Nat. Bur. Stand. 1993;98:699–716.
[139] Flateau PJ, Fuller KA, Mackowski DW. Appl. Optics 1993;32:3302–3305.
[140] Schlager KS, Schneider JB. IEEE Antennas Prop. Mag. 1995;37(4):39–57.
[141] Yang P, Lion KN. J. Opt. Soc. Amer. 1996;13A:2072–2085.
[142] Cwik T, van de Geijn R, Patterson J. J. Opt. Soc. Amer. 1994;11A:1538–1545.
[143] Bates RHT. IEEE Trans. 1973;MTT-23:605–623.
[144] Yaghjian AD. Trans. IEEE 1980;AP-30:113–128.
[145] Miller EK. IEEE Trans. 1988;AP-36:1281–1305.
[146] Bohren CF, Singham SB. J. Geophys. Res. 1991;D96:5269–5277.
[147] Kerker M, Scheiner P, Cooke DD. J. Opt. Soc. Amer. 1978;68:135–137.
[148] Ku JC, Felske JD. J. Quant. Spectrosc. Radiat. Transf. 1984;31:569–574.
[149] Penndorf R. J. Opt. Soc. Amer. 1962;52:797–800.
[150] Penndorf R. J. Opt. Soc. Amer. 1962;52:896–904.
[151] Selamet A, Arpaci VS. Int. J. Heat Mass Transf. 1989;32:1809–1820.
[152] Stevenson AF. J. Appl. Phys. 1953;24:1143–1151.
[153] Kerker M, Farone WA, Matijevic E. J. Opt. Soc. Amer. 1963;53:758–759.
[154] Farone WA, Kerker M, Matijevic E. In: Kerker M, editor. Electromagnetic scattering. Oxford: Pergamon Press, 1963:55–71.
[155] Heller W. In: Kerker M, editor. Electromagnetic scattering. Oxford: Pergamon Press, 1963:107–120.
[156] Latimer P. J. Coll. Interf. Sci. 1975;53:195–200.
[157] Latimer P, Barber P. J. Coll. Interf. Sci. 1978;63:310–316.
[158] Latimer P. Appl. Optics 1980;19:3039–3041.
[159] Barber P, Wang DS. Appl. Optics 1978;17:797–803.
[160] Farias TL, Carvalho MG, Koylu UO. Trans. ASME—J. Heat Transf. 1995;117:152–159.
[161] Farias TL, Koylu UO, Carvalho MG. Appl. Optics 1966;35:6560–6567.
[162] Al-Chalabi SAM, Jones AR. J. Phys. D 1995;28:1304–1308.
[163] Haracz RD, Cohen LD, Cohen A. J. Appl. Phys. 1985;58:3322–3327.
[164] Jones AR, Savaloni H. Part. Part. Syst. Char. 1989;6:110–118.
[165] Klett JD, Sutherland R A. Appl. Optics 1992;31:373–386.
[166] Jones AR, Koh J, Nasaruddin A. J. Phys. D 1996;29:39–42.
[167] Alvarez-Estrada RF, Calvo ML, del Egido PJ. Optica Acta 1980;27:1367–1378.
[168] Sharma SK, Roy TK, Somerford DJ. J. Phys. D 1988;21:1685–1691.
[169] Sharma SK, Roy TK, Somerford DJ. J. Mod. Opt. 1988;35:1213–1224.
[170] Sharma SK, Somerford DJ. J. Mod. Optics 1994;41:1433–1444.
[171] Roy A, Sharma SK. J. Mod. Optics 1996;43:2225–2237.
[172] Hodkinson JR. Appl. Optics 1966;5:839–844.
[173] Jones AR. J. Phys. D 1977;10:L163–L165.
[174] Kusters KA, Wijers JG, Thoenes D. Appl. Optics 1991;30:4839–4847.
[175] Pollack JB, Cuzzi JN. In: Schuerman DW, editor. Light scattering by irregularly shaped particles. New York: Plenum Press, 1980:113–125.
[176] Zerull RH, Killinger RT, Giese RH. In: Gouesbet G, Gréhan G, editors. Optical particle sizing: theory and practice. New York: Plenum Press, 1988:603–609.
[177] Jones AR. In: Gouesbet G, Gréhan G, editors. Optical particle sizing: theory and practice. New York: Plenum Press, 1988:301–310.
[178] Al-Chalabi SAM, Jones AR. Part. Part. Syst. Char. 1994;11:200–206.
[179] Muinonen KO. Appl. Optics 1989;28:3044–3050.
[180] Gréhan G, Gouesbet G, Guilloteau F, Chevaillier JP. Opt. Commun. 1992;90:1–6.
[181] Lock JA, Hovenac EA. Amer. J. Phys. 1993;61:698–707.
[182] Lebrun D, Belaid S, Özkul C, Ren KF, Gréhan G. Opt. Eng. 1996;35:946–950.
[183] Negus C, Azzopardi BJ. Report AERE-R9075, Harwell Laboratory, UKAEA, 1972.
[184] Yumanchi T, Ohyama Y. Bull. Jap. Soc. Mech. Eng. 1982;25:1931–1937.
[185] Schnablegger H, Glatter O. Appl. Optics 1995;34:3489–3501.
[186] Felton PG, Hamidi AA, Aigal AK. ICLASS IVA/4/1-11, Inst. Energy, London, 1985.
[187] Hamidi AA, Swithenbank J. In: Gouesbet G, Gréhan G, editors. Optical particle sizing: theory and practice. New York: Plenum Press, 1988:321–334.
[188] Cao J, Brown DJ, Rennie AG. J. Inst. Energy 1991;64:26–30.
[189] Hirleman ED. In: Gouesbet G, Gréhan G, editors. Optical particle sizing: theory and practice. New York: Plenum Press, 1988:135–146.
[190] Woodall CM, Peters JE, Buckius RO. Atom. Sprays 1995;5:197–211.
[191] Born M, Wolf E. Principles of optics. Oxford: Pergamon Press, Oxford, 1977.
[192] Chýlek P, Klett JD. J. Opt. Soc. Amer. 1991;8A:274–281.
[193] Streekstra GJ, Hoekstra AG, Heethar RM. Appl. Optics 1994;33:7288–7296.
[194] Fournier GR, Evans BTN. Appl. Optics 1991;30:2042–2048.
[195] Evans BTN, Fournier GR. Appl. Optics 1994;33:5796–5804.
[196] Evans BTN, Fournier GR. Appl. Optics 1996;35:3281–3285.
[197] Sharma SK. J. Mod. Optics 1992;39:2355–2361.
[198] Sharma SK. Opt. Commun. 1993;100:13–18.
[199] Stephens GL. Appl. Optics 1984;23:954–959.
[200] Chýlek P, Li J. Opt. Commun. 1995;117:389–394.

[201] Bourrely C, Le Maire T, Chiappetta P. J. Mod. Opt. 1991;38:305–315.
[202] Meeten GH. J. Coll. Interf. Sci. 1982;87:407–415.
[203] Maslowska A, Flateau PJ, Stephens GL. Opt. Commun. 1994;107:35–40.
[204] Whitehead JB, Žumar S, Doane JW. J. Appl. Phys. 1993;73:1057–1065.
[205] Khlebtsov NG. J. Mod. Optics 1993;40:2221–2235.
[206] Emslie AG, Aronson JR. Appl. Optics 1973;12:2563–2572.
[207] Ungut A, Grehan G, Gouesbet G. Appl. Optics 1981;20:2911–2918.
[208] Glantschnig WJ, Chen S-H. Appl. Optics 1981;20:2499–2509.
[209] Shipley ST, Weinmann JA. J. Opt. Soc. Amer. 1978;68:130–134.
[210] Cohen A, Acquista C, Cooney JA. Appl. Optics 1980;19:2264–2265.
[211] Acquista C, Cohen A, Cooney JA, Wimp J. J. Opt. Soc. Amer. 1980;70:1023–1025.
[212] Senior TBA. Appl. Optics 1983;22:1796–1797.
[213] Nussenzveig HM, Wiscombe WJ. Phys. Rev. Lett. 1986;45:1490–1494.
[214] Bohren CF, Nevitt TJ. Appl. Optics 1983;22:774–775.
[215] Kokhanovsky AA, Zege EP. Appl. Optics 1995;34:5513–5519.
[216] Kokhanovsky AA, Zege EP. J. Aerosol Sci. 1997;28:1–21.
[217] Ravey JC, Mazeron P. J. Opt. 1982;13:273–282.
[218] Ravey JC, Mazeron P. J. Opt. 1983;14:29–41.
[219] Hovenac EA. Appl. Optics 1991;30:4739–4746.
[220] Lock JA. Appl. Optics 1996;35:500–514.
[221] Lock JA. Appl. Optics 1996;35:515–531.
[222] Macke A, Mishchenko MI, Muinonen K, Carlson LBE. Opt. Lett. 1995;20:1934–1936.
[223] Mishchenko MI, Travis LD, Macke A. Appl. Optics 1996;35:4927–4940.
[224] Bottlinger M, Umhauer H. J. Aerosol Sci. 1991;21(S1):S145–S149.
[225] Bottlinger M, Umhauer H. Appl. Optics 1991;30:4732–4738.
[226] Muinonen K, Nousiainen T, Fast P, Lumme K, Peltoniemi JI. J. Quant. Spectrosc. Radiat. Transf. 1996;55:577–601.
[227] Kim H, Ling H. IEEE Trans. 1992;AP-40:517–525.
[228] Zhang JY, Xu LS. Appl. Optics 1995;34:5867–5874.
[229] Macke A, Mishchenko MI, Cairns B. J. Geophys. Res.—Atmos. 1996;101:23311–23316.
[230] Kattawar GW, Plass GN. Appl. Optics 1968;7:415–419.
[231] Kattawar GW, Plass GN. Appl. Optics 1968;7:699–704.
[232] Kattawar GW, Plass GN. Appl. Optics 1968;7:869–878.
[233] Kattawar GW, Plass GN. Appl. Optics 1968;7:1519–1527.
[234] Bucher EA. Appl. Optics 1973;12:2391–2400.
[235] van de Hulst HC. Multiple light scattering, vols 1 and 2. New York: Academic Press, 1980.
[236] Bruscaglioni P, Zaccanti G, Wei Q. Appl. Optics 1993;32:6142–6150.
[237] Bicout D, Brosseau C, Martinez AS, Schmitt JM. Phys. Rev. E 1994;49:1767–1770.
[238] Code AD, Whitney BA. Astrophys. J. 1995;441:400–407.
[239] Bergougnoux L, Misguich-Ripault J, Firpo JL, André J. Appl. Optics 1996;35:1735–1741.
[240] Hottel HC, Sarofim AF. Radiative transfer. New York: McGraw-Hill, 1967.
[241] Deepak A, Green AES. Appl. Optics 1970;9:2362–2371.
[242] Zahavi E. Appl. Optics 1979;18:1627–1631.
[243] Rosseland S. Astrophysik und Atom—Theoretisches Grundlage. Berlin: Springer-Verlag, 1931:41–44.
[244] Kubelka P, Munk F. Z. Tech. Phys. 1931;12:593.
[245] Mudgett PS, Richards LW. Appl. Optics 1971;10:1485–1502.
[246] Beckett P, Foster PJ, Hutson V, Moss RL. J. Quant. Spectrosc. Radiat. Transf. 1974;14:1115–1125.
[247] Stotts B. J. Opt. Soc. Amer. 1977;67:815–819.
[248] Look DC, Nelson HF, Crosbie AL, Dougherty PL. ASME J. Heat Transf. 1978;100:480–485.
[249] Zege EP, Kokhanovsky AA. Appl. Optics 1994;33:6547–6554.
[250] Ito S. Appl. Optics 1995;34:7106–7112.
[251] Prahl SA, van Gemert MJC, Welch AJ. Appl. Optics 1993;32:559–568.
[252] van de Hulst HC, Kattawar GW. Appl. Optics 1994;33:5820–5829.
[253] Shifrin KS, Zolotov IG. Appl. Optics 1995;34:552–558.
[254] Brewster MQ, Yamada Y. Int. J. Heat Mass Transf. 1995;38:2569–2581.
[255] Marquet P, Bevilacqua F, Depeursinge C, de Haller EB. Opt. Eng. 1995;34:2055–2603.
[256] Kattawar GW, Humphreys TJ. In: Schuerman DW, editor. Light scattering by irregularly shaped particles. New York: Plenum Press, 1979:177–190.
[257] Levine S, Olaofe GO. J. Coll. Interf. Sci. 1968;27:442–457.
[258] Barton JP, Ma W, Schaub SA, Alexander DR. Appl. Optics 1991;30:4706–4715.
[259] Fuller KA. Appl. Optics 1991;30:4716–4731.
[260] Fuller KA. J. Opt. Soc. Amer. 1994;11A:3251–3260.
[261] Fuller KA. J. Opt. Soc. Amer. 1995;12A:881–892.
[262] Bruning JH, Lo YT. IEEE Trans. 1971;AP-19:378–390.
[263] Borghese F, Denti P, Toscano G, Sindoni OI. Appl. Optics 1979;18:116–120.
[264] Borghese F, Denti P, Saija R, Toscano G, Sindoni OI. J. Opt. Soc. Amer. 1984;1A:183–191.
[265] Fuller KA, Kattawar GW, Wang RT. Appl. Optics 1986;25:2521–2529.
[266] Fuller KA, Kattawar GW. Opt. Lett. 1988;13:90–92.
[267] Wittman RC. IEEE Trans. 1988;AP-36:1078–1087.
[268] Hamid AK, Ciric IR, Hamid M. Can. J. Phys. 1990;68:1157–1165.
[269] Mackowski DW. Proc. Roy. Soc. 1991;A433:599–614.
[270] Ioannidou MP, Skarapoulos NC, Chrissoulidis DP. J. Opt. Soc. Amer. 1995;12A:1782–1789.
[271] Quinten M, Kreibig U. Appl. Optics 1993;32:6173–6182.
[272] Hamid AK, Ciric IR, Hamid M. IEE Proc.—H 1991;138:565–572.
[273] Popovic BD, Notaros BM. IEE Proc.—H 1993;140:36–42.
[274] Xu YL. Appl. Optics 1995;34:4573–4588.
[275] Ivezic Z, Menguc MP. Int. J. Heat Mass Transf. 1996;39:811–822.
[276] Tsuei TG, Barber PW. Appl. Optics 1988;27:3375–3381.
[277] Yousif HA, Kohler S. J. Opt. Soc. Amer. 1988;5A:1085–1096.
[278] Yousif HA, Kohler S. J. Opt. Soc. Amer. 1988;5A:1097–1104.
[279] Padmabandu GG, Bickel WS. J. Opt. Soc. Amer. 1991;8A:1706–1712.

[280] Bever SJ, Allebach JP. Appl. Optics 1992;31:3524–3532.
[281] Cooray MFR, Ciric IR. IEEE Trans. 1991;AP-39:680–684.
[282] Sebak A. Can. J. Phys. 1991;69:1233–1241.
[283] Hamid AK, Ciric IR, Hamid M. Can. J. Phys. 1992;70:696–705.
[284] Bruce CW, Stromberg TF, Gurton KP, Mozer JB. Appl. Optics 1991;30:1537–1546.
[285] Choi MY, Mulholland GW, Hamins A, Kashiwagi T. Combust. Flame 1995;102:161–169.
[286] Koylu UO, Faeth GM. Trans. ASME—J. Heat Transf. 1996;118:415–421.
[287] Ku JC, Shim KH. ASME J. Heat Transf. 1991;113:953–958.
[288] Koylu UO, Xing Y, Rosner DE. Langmuir 1995;11:4848–4854.
[289] Koylu UO, Faeth GM, Farias TL, Carvalho MG. Combust. Flame 1995;100:621–633.
[290] Sorensen CM, Feke GD. J. Aerosol Sci. 1996;25:328–337.
[291] Colbeck I, Wu Z. J. Phys. D 1994;27:670–675.
[292] Colbeck I, Appleby L, Hardman EJ, Harrison RM. J. Aerosol Sci. 1990;21:527–538.
[293] Sorensen CM, Cai J, Lu N. Appl. Optics 1992;31:6547–6557.
[294] Bonczyk PA, Hall RJ. Langmuir 1992;8:1666–1670.
[295] Sorensen CM, Cai J, Lu N. Langmuir 1992;8:2064–2069.
[296] Khlebtsov NG, Melnikov AG. J. Coll. Interf. Sci. 1994;163:145–151.
[297] Sorensen CM, Lu N, Cai J. J. Coll. Interf. Sci. 1995;174:456–460.
[298] Faeth GM, Koylu UO. Combust. Sci. Technol. 1995;108:207–229.
[299] Botet R, Rannou P, Cabane M. J. Phys. A 1995;28:297–316.
[300] Berry MV, Percival IC. Optica Acta 1986;33:577–591.
[301] Nelson J. J. Mod. Opt. 1989;36:1031–1057.
[302] Colbeck I, Hardman EJ, Harrison RM. J. Aerosol Sci. 1989;20:765–774.
[303] Dobbins RA, Mulholland GW, Bryner NP. Atmos. Envir. 1994;28:889–897.
[304] Singham SB, Bohren CF. Langmuir 1993;9:1431–1435.
[305] Lu N, Sorensen CM. Phys. Rev. E 1994;50:3109–3115.
[306] Shalaev VM, Botet R, Jullien R. Phys. Rev. B 1991;44:12216–12225.
[307] Markel VA, Shalaev VM, Stechel EB, Kim W, Armstrong RL. Phys. Rev. B 1996;53:2425–2436.
[308] Iskander MF, Chen HY, Penner JE. Atmos. Envir. 1991;25A:2563–2569.
[309] Chen HY, Iskander MF, Penner JF. Appl. Optics 1991;30:1547–1551.
[310] Wu Z, Colbeck I. Europhys. Lett. 1996;33:719–724.
[311] Neimark AV, Koylu UO, Rosner DE. J. Coll. Interf. Sci. 1996;180:590–597.
[312] Chen HY, Iskander MF, Penner JF. J. Mod. Optics 1991;37:171–181.
[313] Markel VA, Muratov LS, Stockman MI, George TF. Phys Rev. B 1991;43:8183–8195.
[314] Charalampopoulos TT. Progr. Energy Combust. Sci. 1992;18:13–45.
[315] d'Alessio A, Minutolo P, Gambi G, d'Anna A. Ber. Bunsen. Ges. 1993;97:1574–1582.
[316] Shalaev VM. Phys. Rep. 1996;272:61–137.
[317] Haynes BS, Wagner HG. Ber. Bunsen. Ges. 1980;84:585–592.
[318] Müller-Dethlefs K. Ph.D. thesis, Imperial College, University of London, 1979.
[319] Jones AR, Wong W. Combust. Flame 1975;24:139–140.
[320] d'Alessio A. In: Siegla DC, Smith GW, editors. Particulate carbon formation during combustion. New York: Plenum Press, 1981:207–259.
[321] Brown WK, Wohletz KH. J. Appl. Phys. 1995;78:2758–2763.
[322] Min SL, Gomez A. Appl. Optics 1996;35:4919–4926.
[323] Glover AR, Skippon SM, Boyle RD. Appl. Optics 1995;34:8409–8421.
[324] Ludlow IK, Everitt J. Phys. Rev. E 1995;51:2516–2526.
[325] Lhuissier N, Gouesbet G, Weill ME. Combust. Sci. Technol. 1989;67:17–36.
[326] Scrivner SM, Taylor TW, Sorensen CM, Merklin JF. Appl. Optics 1986;25:291–296.
[327] Weill ME, Lhuissier N, Gouesbet G. Appl. Optics 1986;25:1676–1683.
[328] Weber R, Rambau R, Schweiger G, Lucas K. J. Aerosol Sci. 1993;24:485–499.
[329] Gonzalez F, Saiz JM, Moreno F, Valle PJ. J. Phys. D 1992;25:357–361.
[330] Rarity JG. In: Gouesbet G, Gréhan G, editors. Optical particle sizing: theory and practice. New York: Plenum Press, 1988:217–228.
[331] Xie GW, Patel S, Wong FCH, Shaw DT. Aerosol Sci. Technol. 1995;22:219–235.
[332] Bernard JM. J. Quant. Spectrosc. Radiat. Transf. 1988;40:321–330.
[333] Shifrin KS, Perelman AY. Opt. Spectrosc. 1963;15:434–439.
[334] Szymanski WW. J. Aerosol Sci. 1992;5:425–433.
[335] Walters PT. Appl. Optics 1980;19:2353–2365.
[336] Gougeon P, Le Toulouzan JN, Gouesbet G, Thenard C. J. Phys. E 1987;20:1235–1242.
[337] Guidt JB, Gouesbet G, le Toulouzan JN. Appl. Optics 1990;29:1011–1022.
[338] Winklhofer E, Plimon A. Opt. Eng. 1991;30:1262–1268.
[339] Graff A, Ostender F, Quinten M. J. Aerosol Sci. 1996;27:313–324.
[340] Zhang H-J, Xu G-D. Powder Technol. 1992;70:189–192.
[341] Dodge LG. Opt. Eng. 1984;23:626–630.
[342] Hirleman ED, Oechsle V, Chigier NA. Opt. Eng. 1984;23:610–619.
[343] Bachalo WD. Int. J. Multiphase Flow 1994;20(S):261–295.
[344] Hirleman ED, Dellenback PA. Appl. Optics 1989;28:4870–4878.
[345] Miles BH, Sojka PE, King GB. Appl. Optics 1990;29:4563–4573.
[346] Wedd MW. Private communication. Malvern: Malvern Instruments, 1995.
[347] Card JBA, Jones AR. Part. Part. Syst. Char. 1996;13:137–142.
[348] Card JBA, Jones AR. Meas. Sci. Technol. 1996;7:1643–1652.
[349] Benayahu Y, Baram A, Ben-David A, Cohen A. J. Opt. Soc. Amer. 1992;9A:1633–1637.
[350] Zaccanti G, Bruscaglioni P, Ismaeli A, Carraresi L. Appl. Optics 1992;31:2141–2147.
[351] Kuga Y, Ishimaru A, Rice D. Phys. Rev. B 1993;48:13155–13158.

[352] Cartellier A. Appl. Optics 1992;31:3493–3505.
[353] Durst F, Umhauer H. In: Proceedings LDA Symposium, Copenhagen. Lyngby: Technical University of Denmark, 1975:430–456.
[354] Gréhan G, Gouesbet G. Appl. Optics 1986;25:3527–3538.
[355] Xie GW, Scott P, Shaw DT, Zhang YM. Opt. Lett. 1991;16:861–863.
[356] Wang JCR, Hencken KR. Appl. Optics 1986;25:635–657.
[357] Hess CF, Li F. In: Gouesbet G, Gréhan G, editors. Optical particle sizing: theory and practice. New York: Plenum Press, 1988:271–282.
[358] Holve DJ, Self SA. Appl. Optics 1979;18:1632–1645.
[359] Holve DJ, Davis GW. Appl. Optics 1985;24:998–1005.
[360] Birch KG. Optica Acta 1968;15:113–127.
[361] Harada Y, Murakami T. Appl. Optics 1991;30:4921–4929.
[362] Ishikawa M, Kanebako M, Akiyama K. Optik 1990;84:59–63.
[363] Hardalupas Y, Morikita H, Taylor AMKP. Meas. Sci. Technol. 1995;6:717–726.
[364] Buckle ER, Bushnell-Watson YM. J. Coll. Interf. Sci. 1985;105:529–538.
[365] Ohba K, Isoda S. Presented at Int. Symp. Optical Part. Sizing, Rouen, France, Paper 10, 1987.
[366] Bhandari R, Kerker M. J. Stat. Phys. 1988;52:1263–1283.
[367] Al-Chalabi SAM, Jones AR, Savaloni H, Wood R. Meas. Sci. Technol. 1990;1:29–35.
[368] Kaye PH, Eyles NA, Ludlow IK, Clark JM. Atmos. Envir. 1991;25A:645–654.
[369] Rood AP, Walker EJ, Moore D. Aerosol Sci. Technol. 1992;17:1–8.
[370] Kaye PH, Hirst E, Clark JM, Micheli F. J. Aerosol Sci. 1992;23:597–611.
[371] Hirst E, Kaye PH, Guppy JR. Appl. Optics 1994;33:7180–7186.
[372] Hirst E, Kaye PH, Buckley KM, Saunders SJ. Part. Part. Syst. Char. 1995;12:3–9.
[373] Hirst E, Kaye PH. J. Geophys. Res.—Atmos. 1996;101:19231–19235.
[374] Kaye PH, Alexander-Buckley K, Hirst E, Saunders S, Clark JM. J. Geophys. Res.—Atmos. 1996;101:19215–19221.
[375] Sachweh BA, Dick WD, McMurry PH. Aerosol Sci. Technol. 1995;23:373–391.
[376] Marshall MS. Opt. Eng. 1996;35:832–837.
[377] Brenci M, Guzzi D, Mancaglia AG, Pierraccini M. Sensors Actuators 1995;A48:23–27.
[378] Belanger C, Cielo P, Patterson WI, Favis BD, Utrachi LA. Polym. Eng. 1994;34:1589–1597.
[379] Sierra AQ, Mora AVD. Appl. Optics 1995;34:6256–6262.
[380] Kim SH, Martin PG. Astrophys. J. 1995;444:293–305.
[381] Mishchenko MI, Hovenier JW. Opt. Lett. 1995;20:1356–1358.
[382] Card JBA, Jones AR. Combust. Flame 1991;86:394–402.
[383] Card JBA, Jones AR. Combust. Flame 1995;101:539–547.
[384] Umhauer H, Bottlinger M. Appl. Optics 1991;30:4980–4986.
[385] Sasse C. Rev. Sci. Instrum. 1993;64:864–869.
[386] Sasse C, Muinonen K, Piironen J, Dröse G. J. Quant. Spectrosc. Radiat. Transf. 1996;55:673–681.
[387] Doornbos RMP, Schaeffer M, Hoekstra AG, Sloot PMA, de Grooth BG, Greve J. Appl. Optics 1996;35:729–734.
[388] Kuik F, Stammes P, Hovenier JW. Appl. Optics 1991;30:4872–4881.
[389] Martin RJ. J. Mod. Optics 1995;42:157–169.
[390] Durst F, Melling A, Whitelaw JH. Principles and practice of laser doppler anemometry, 2nd ed. London: Academic Press, 1981.
[391] Yule AJ, Chigier NA, Atakan MS, Ungut A. J. Energy 1977;1:220–228.
[392] Ereaut P. Ph.D. thesis, University of Sheffield, 1983.
[393] Orfanoudakis NG, Taylor AMKP. Combust. Sci. Technol. 1995;108:255–277.
[394] Terhaag U, Renz U. Part. Part. Syst. Char. 1996;13:150–185.
[395] Finke JR, Swank WD, Jeffery CL, Mananso CA. Meas. Sci. Technol. 1993;4:559–565.
[396] Jones AR. J. Phys. D 1974;7:1369–1376.
[397] Eliasson B, Dändliker R. Optica Acta 1974;21:119–149.
[398] Chu WP, Robinson DM. Appl. Optics 1977;16:619–626.
[399] Bachalo WD. Appl. Optics 1980;19:363–370.
[400] Pendleton JD. Appl. Optics 1982;21:684–688.
[401] Farmer WM. Appl. Optics 1972;11:2603–2612.
[402] Farmer WM. Appl. Optics 1974;13:610–622.
[403] Fristrom RM, Jones AR, Schwar MJR, Weinberg FJ. In: Proc. 7th Faraday Symp., Chem. Soc., London, 1973:183–197.
[404] Hong NS, Jones AR. J. Phys. D 1976;9:1839–1848.
[405] Hong NS. Ph.D. thesis, Imperial College, University of London, 1977.
[406] Roberds DW. Appl. Optics 1977;16:1861–1868.
[407] Negus C, Drain LE. J. Phys. D 1982;15:375–402.
[408] Azar M, Ventrice CA. J. Aerosol Sci. 1995;26:1009–1017.
[409] Yianneskis M. Powder Technol. 1987;49:261–269.
[410] Kliafas Y, Taylor AMKP, Whitelaw JH. Exp. Fluids 1987;5:159–176.
[411] Kliafas Y, Taylor AMKP, Whitelaw JH. ASME J. Fluids Eng. 1990;112:142–148.
[412] Lagranja JL, Garcia-Palacin JI, Aisa LA. Opt. Eng. 1994;33:2449–2460.
[413] Hong NS, Jones AR, Weinberg FJ. Proc. Roy. Soc. 1977;A353:77–85.
[414] Ancimer RJ, Fraser RA. Meas. Sci. Technol. 1994;5:83–92.
[415] Avery RK, Jones AR. J. Phys. D 1982;15:1373–1384.
[416] Massoli P, Beretta F, d'Alessio A. Appl. Optics 1989;28:1200–1205.
[417] Massoli P, Beretta F, d'Alessio A. Combust. Sci. Technol. 1990;72:271–282.
[418] Durst F, Zaré M. In: Proceedings LDA Symposium, Copenhagen. Lyngby: Technical University of Denmark, 1975:403–429.
[419] Bachalo WD, Houser MJ. Opt. Eng. 1984;23:583–590.
[420] Saffman M, Buchhave P, Tanger H. In: Adrian, Durão, Durst, Mishina, Whitelaw, editors. Laser anemometry in fluid mechanics—II. Lisbon: LADOAN, 1984:85–104.
[421] Hirleman ED. Part. Part. Syst. Char. 1996;13:59–67.
[422] Sankar SV, Weber BJ, Kamemoto DY, Bachalo WD. Appl. Optics 1991;30:4914–4920.
[423] Naqwi A, Durst F, Kraft G. Appl. Optics 1991;30:4903–4913.
[424] Bachalo WD. In: Gouesbet G, Gréhan G, editors. Optical particle sizing: theory and practice. New York: Plenum Press, 1988:283–289.
[425] Naqwi A, Durst F. Appl. Optics 1993;32:4003–4018.

[426] Naqwi AA, Menon R, Fingerson LM. Expt. Fluids 1996;20:328–334.
[427] Bachalo WD. Presented at 2nd Int. Conf. Laser Anemometry Advances and Applications, Strathclyde, Scotland, Paper 14, 1987.
[428] Schaub SA, Alexander DR, Barton JP. Appl. Optics 1994;33:473–488.
[429] Albrecht HE, Borys M, Fuchs W. Exp. Fluids 1993;16:61–69.
[430] Albrecht HE, Borys M, Wenzel M. Part. Part. Syst. Char. 1996;13:18–26.
[431] Xu TH, Tropea C. Meas. Sci. Technol. 1994;5:969–975.
[432] Hardalupas Y, Taylor AMKP. Exp. Fluids 1994;17:253–258.
[433] Borys M, Kroger W, Fuchs W. Tech. Messen 1996;63:14–21.
[434] Qin HH, Sommerfeld M. Exp. Fluids 1992;13:393–404.
[435] Sommerfeld M, Qin HH. Exp. Fluids 1995;18:187–198.
[436] Tropea C, Xu TH, Onofri F, Gréhan G, Hangen P, Stieglmeier M. Part. Part. Syst. Char. 1996;13:165–170.
[437] Schneider M, Hirleman ED. Appl. Optics 1994;33:2379–2388.
[438] Köser O, Wriedt T. Appl. Optics 1996;35:2537–2543.
[439] Doicu A, Schabel S, Ebert F. Part. Part. Syst. Char. 1996;13:79–88.
[440] Friedman JA, Renksizbulut M. Part. Part. Syst. Char. 1995;12:225–231.
[441] Tate AHJ, Seville JPK, Singh A, Clift R. In: Gas cleaning at high temperatures, I. Chem. E. Symp. Ser. 99, 1986:89–100.
[442] Vincent JH, Emmett PC, Mark D. In: Liu BYH, Piu DYH, Fissan H, editors. Aerosols. Amsterdam: Elsevier, 1984.
[443] Roll G, Kaiser T, Schweiger G. J. Aerosol Sci. 1996;27:105–117.
[444] Lindell IV, Sihvola AH, Muinonen KO, Barber PW. J. Opt. Soc. Amer. 1991;8A:472–476.
[445] Muinonen KO, Sihvola AH, Lindell IV, Barber PW. J. Opt. Soc. Amer. 1991;8A:477–482.
[446] Videen G. J. Opt. Soc. Amer. 1991;8A:274–281.
[447] Videen G. J. Opt. Soc. Amer. 1993;10A:110–117.
[448] Johnson BR. J. Opt. Soc. Amer. 1992;9A:1341–1351.
[449] Johnson BR. J. Opt. Soc. Amer. 1994;11A:2055–2064.
[450] Jakeman E. J. Phys. D 1994;27:198–210.
[451] Saiz JM, Valle PJ, Gonzalez F, Moreno F, Jordan DL. Opt. Eng. 1994;33:1261–1270.
[452] Videen G, Turner MG, Iafelice VJ, Bickel WS, Wolfe WL. J. Opt. Soc. Amer. 1993;10A:118–126.
[453] Videen G. Opt. Commun. 1995;115:1–7.
[454] Videen G. Opt. Commun. 1996;128:81–90.
[455] Videen G, Ngo D. J. Opt. Soc. Amer. 1997;14A:70–78.
[456] Bruno WM, Bessey JS, Whitesmith PM, Burke PE. Appl. Optics 1996;35:2292–2303.
[457] Eremin Yu, Orlov N. Appl. Optics 1996;35:6599–6604.
[458] Saiz JM, Gonzalez F, Moreno F, Valle PJ. J. Phys. D 1995;28:1040–1046.
[459] Chao JC, Rizzo FJ, Elshafiey I, Lin YJ, Upda L, Martin PA. J. Opt. Soc. Amer. 1996;13A:338–344.
[460] Borghese F, Denti P, Saija R, Fucile E, Sindoni OI. J. Opt. Soc. Amer. 1995;12A:530–540.
[461] Gonzalez F, Saiz JM, Valle PJ, Moreno F. Opt. Eng. 1995;34:1200–1207.
[462] Moreno F, Saiz JM, Valle PJ, Gonzalez F. App. Phys. Lett. 1996;68:3087–3089.
[463] Liswith ML, Bawolek EJ, Hirleman ED. Opt. Eng. 1996;35:858–869.
[464] Polverari M, van de Ven T. J. Coll. Interf. Sci. 1995;173:343–353.
[465] Phillips DL. J. Assoc. Comp. Mach. 1962;9:84–97.
[466] Twomey S. J. Assoc. Comp. Mach. 1963;10:97–101.
[467] Amato U, Carfora MF, Cuomo V, Serio C. Appl. Optics 1995;34:5442–5452.
[468] Shifrin KS, Zolotov IG. Appl. Optics 1996;35:2114–2124.
[469] Ramachandran G, Leith D. Aerosol Sci. Technol. 1992;17:303–325.
[470] Ramachandran G, Leith D, Todd L. J. Opt. Soc. Amer. 1994;11A:144–154.
[471] Bertero M, de Mol C, Pike ER. In: Gouesbet G, Gréhan G, editors. Optical particle sizing: theory and practice. New York: Plenum Press, 1988:55–61.
[472] Bertero M, Boccacci P, de Mol C, Pike ER. J. Aerosol Sci. 1989;20:91–99.
[473] Ben-David A, Herman BM, Reagan JA. Appl. Optics 1988;27:1235–1242.
[474] Ben-David A, Herman BM, Reagan JA. Appl. Optics 1988;27:1243–1254.
[475] Viera G, Box MA. Appl. Optics 1985;24:4525–4533.
[476] Viera G, Box MA. Appl. Optics 1987;26:1312–1327.
[477] Viera G, Box MA. Appl. Optics 1988;27:3262–3274.
[478] Curry BP. Appl. Optics 1989;28:1345–1355.
[479] Shimizu K, Ishimaru A. Appl. Optics 1990;29:3428–3433.
[480] Box MA, Viera G. J. Opt. Soc. Amer. 1990;A7:1015–1018.
[481] Wolfenberger JK, Seinfeld JH. J. Aerosol Sci. 1990;21:227–247.
[482] Brianzi P, Fantini M. Inverse Problems 1991;7:355–368.
[483] Schnablegger H, Glatter O. Appl. Optics 1991;30:4889–4896.
[484] Box GP, Sealy KM, Box MA. J. Atmos. Sci. 1992;49:2074–2082.
[485] Dellago C, Horvath H. J. Aerosol Sci. 1993;24:129–141.
[486] Dellago C, Horvath H. J. Aerosol Sci. 1993;24:143–154.
[487] Ferri F, Bassini A, Paganini E. Appl. Optics 1995;34:5829–5839.
[488] Dubovik OV, Lapyonok TV, Oshchepkov SL. Appl. Optics 1995;34:8422–8436.
[489] Gail GP. Appl. Optics 1995;34:7787–7792.
[490] Bryant G, Thomas JC. Langmuir 1995;11:2480–2485.
[491] Ramachandran G, Kandlikar M. J. Aerosol Sci. 1996;27:1009–1112.
[492] Ligon DA, Chen TW, Gillespie JB. Appl. Optics 1996;35:4297–4303.
[493] Benayahu Y, Ben-David A, Fastig S, Cohen A. Appl. Optics 1995;34:1569–1578.
[494] Oshchepkov SL, Dubovik OV. J. Phys. D 1993;26:728–732.
[495] Sun F, Lewis JWL. Appl. Optics 1995;34:8437–8446.
[496] Amato U, di Bello D, Esposito F, Serio C, Pavese G, Romano F. J. Geophys. Res.—Atmos. 1996;101:19231–19235.
[497] Bates RHT, Smith VA, Murch RD. Phys. Rep. 1991;201:185–277.
[498] Bhattacharya SP, Wall TF, Gupta RP. Int. Commun. Heat Mass Transf. 1996;23:809–821.
[499] Atakan M S, Jones AR. J. Phys. D 1982;15:1–13.

[500] Card JBA, Jones AR. Part. Part. Syst. Char. 1991;8:267–273.
[501] Takeda K, Yoshitoshi I, Munakata C. Meas. Sci. Technol. 1992;3:27–32.
[502] Chae S-K, Lee H-OS. Aerosol Sci. Technol. 1993;18:403–417.
[503] Schnablegger H, Glatter O. J. Coll. Interf. Sci. 1993;158:228–242.
[504] Naqwi A, Durst F, Lin X. Appl. Optics 1991;30:4949–4959.
[505] Onofri F, Girasole T, Gréhan G, Gouesbet G, Brenn G, Domnik J, Xu TH, Tropea C. Part. Part. Syst. Char. 1996;13:112–124.
[506] Onofri F, Blondel D, Gréhan G, Gouesbet G. Part. Part. Syst. Char. 1996;13:104–111.
[507] Massoli P, Beretta F, d'Alessio A, Lazzaro M. Appl. Optics 1993;32:3295–3301.
[508] Clapp ML, Miller RE, Worsnop DR. J. Phys. Chem. 1995;99:6317–6326.
[509] Taubenblatt MA, Batchelder JS. Appl. Optics 1991;30:4972–4979.
[510] Roth N, Anders K, Frohn A. In: Proc. 2nd Int. Cong. Opt. Part. Sizing, Arizona State University, Tempe, AZ, 1990:306–315.
[511] Schneider M, Hirleman ED, Salaheen H, Chowdhury DQ, Hill SC. In: Proc. 3rd Int. Congress Opt. Part. Sizing, Keis University, Yokohama, Japan, 1993:323–326.
[512] Anders K, Roth N, Frohn A. Part. Part. Syst. Char. 1996;13:125–129.
[513] Lock JA, Jamison JM, Liu CY. Appl. Optics 1994;33:4677–4689.
[514] van Beeck JPAJ, Riethmuller ML. Appl. Optics 1996;35:2259–2266.
[515] Chan CW, Lee WK. J. Opt. Soc. Amer. 1996;13B:532–535.
[516] Jagoda IJ, Prado G, Lahaye J. Combust. Flame 1980;37:261–274.
[517] Sivanathu YR, Gore JP. J. Quant. Spectrosc. Radiat. Transf. 1993;50:483–492.
[518] Menguç MP, Dutta P. Trans. ASME—J. Heat Transf. 1994;116:144–151.
[519] Bates SC, Carangelo R, Knight K, Serio M. Rev. Sci. Instrum. 1993;64:1213–1221.
[520] Drescher AC, Gadgil AJ, Price PN, Nazaroff WW. Atmos. Envir. 1996;30:929–940.
[521] Oberlé C, Ashgriz N. Atom. Sprays 1995;5:45–73.
[522] Wang XJ, Milner TE, Nelson JS. Opt. Lett. 1995;20:1337–1339.
[523] Tyndall J. Phil. Mag. 1869;37:384–394.

This Page is Inserted by IFW Indexing and Scanning Operations and is not part of the Official Record

BEST AVAILABLE IMAGES

Defective images within this document are accurate representations of the original documents submitted by the applicant.

Defects in the images include but are not limited to the items checked:

- ☐ BLACK BORDERS
- ☐ IMAGE CUT OFF AT TOP, BOTTOM OR SIDES
- ☐ FADED TEXT OR DRAWING
- ☐ BLURRED OR ILLEGIBLE TEXT OR DRAWING
- ☐ SKEWED/SLANTED IMAGES
- ☐ COLOR OR BLACK AND WHITE PHOTOGRAPHS
- ☐ GRAY SCALE DOCUMENTS
- ☐ LINES OR MARKS ON ORIGINAL DOCUMENT
- ☒ REFERENCE(S) OR EXHIBIT(S) SUBMITTED ARE POOR QUALITY
- ☐ OTHER: _____

IMAGES ARE BEST AVAILABLE COPY.
As rescanning these documents will not correct the image problems checked, please do not report these problems to the IFW Image Problem Mailbox.